DYNAMICAL PROPERTIES OF POINT DEFECTS IN METALS

ABSTRACT

By

SEVERINE S. POHLONG

A Thesis

SUBMITTED IN FULFILMENT OF THE REQUIREMENT
FOR THE DEGREE OF
DOCTOR OF PHILOSOPHY

To

DEPARTMENT OF PHYSICS
NORTH - EASTERN HILL UNIVERSITY
SHILLONG - 793 022
INDIA
1996

SUMMARY

DYNAMICAL PROPERTIES OF POINT DEFECTS IN METALS

The study of dynamics of irradiation-produced point defects: self-interstitial atoms (SIAs) and vacancies is of fundamental importance in understanding of various physical properties of irradiated metals. Of special interest, is the vibrational frequency spectra of the defect and a few of its neighbours. The presence of point defects in crystal is reflected on the vibrational frequency spectra, which are different from those of the ideal lattice atoms. The present thesis discusses the dynamical properties of self interstitials and vacancies in cubic metals. A semi-empirical potential, called the embedded atom method (EAM) potential in fcc metals has been determined. The local frequency spectra of SIAs in Cu, which is a typical fcc metal, is discussed on the basis of this new potential. The local frequency spectra of SIAs and vacancies in bcc metals are also discussed on the basis of the Johnson and Wilson (JW) potentials [1].

Chapter I contains a brief introduction to the thesis emphasising the generation of the EAM potentials in fcc metals and also various physical properties of the solid containing point defects. The advent of new potentials like EAM potentials or N-body potentials replaces the empirical pair potentials and helps to calculate many properties of metals where the electronic contribution plays important role. Regarding the vibrational frequency spectra of SIAs, a number of characteristic defect modes: the low-frequency resonance modes and the high-frequency localized modes are discussed. The effect of resonance modes on some thermodynamic properties and elastic constants of the defect metals are pointed out. The local frequency spectra of the first and second neghbours of a vacancy do not show the presence of characteristic modes but the frequency spectra of the first neighbours shift towards the lower frequency region of the spectrum. Formation entropy of a vacancy is also discussed.

In chapter II we have generated the EAM potentials for fcc metals. These potentials are based on the electron density functional theory developed by Daw and Baskes [2]. The EAM potential consists of two parts: (i) the embedding function, which is the energy required to embed an atom in the field of the other atoms and (ii) the pair part, from the repulsion of atomic cores, which is of the Morse form. The new potential can explain various types of perfect crystal properties as well as defect properties in metals like vacancies, crack-tips, alloys, surfaces etc. In the present work the embedding function has been chosen from the one used by Banerjea and Smith [3]

$$F(\rho) = F(\rho_e)\left[1 - \eta \ln\left(\frac{\rho}{\rho_e}\right)\right]\left(\frac{\rho}{\rho_e}\right)^{\eta} \qquad (1)$$

where ρ is the electron density at a lattice site which is due to the contribution from all other atoms, except the particular atom at the lattice site. The pair part is

$$\Phi(r) = D\left[e^{-2\alpha(r-r_o)} - 2e^{-\alpha(r-r_o)}\right] \qquad (2)$$

The different potential parameters γ, D, α, r_o are fitted to elastic constants, vacancy formation energy, cohesive energy and lattice constant, in a third neighbour model. The generation of the EAM potentials becomes complete when all the potential parameters are obtained. The generated potentials are then used to discuss the divacancy binding energy, the low-indexed plane surface energies and phonons for six fcc metals : Cu, Ag, Au, Ni, Pd and Pt. The obtained phonons in the present study are in good agreement with experimental phonons in Cu, Ag and Ni but in the case of Au, Pd and Pt the agreement is not so good. The obtained phonons are then used to discuss the density of state and thermal displacement of an atom in Cu.

In chapter III we have introduced the density of states, the Greens fucntion and the local density of states. The density of state $Z(\omega)$ is given by

$$Z(\omega) = \frac{1}{3N} \sum_{k\sigma} \delta(\omega_{k\sigma} - \omega) \qquad (3)$$

where $\omega_{k\sigma}$ are phonons frequencies and N is the number of atoms in

the solid. The density of state is also expressed in terms of Green's function as [4]

$$Z(\omega) = \frac{2M\omega}{3N\pi} \mathrm{Im} \sum_{l\alpha} G_{\alpha\alpha}(l,l;\omega) \qquad (4)$$

where $G_{\alpha\alpha}(l,l;\omega)$ is the diagonal element of the same site Green's functions of the lattice. The local density of state of an atom at site l in the α-direction is

$$Z_{\alpha}(l,\omega) = \frac{2M\omega}{\pi} \mathrm{Im} G_{\alpha\alpha}(l,l;\omega) \qquad (5)$$

The total spectrum of the lattice is the sum of local frequency spectra of all atoms in the lattice. The concept of the local density of states is quite useful in the study of defect dynamics because the vibrational behaviour of the defect and its neighbours are affected most so that the local density of states of the defect site show the excitations of some characteristic defect modes : the low-frequency resonance modes and the high-frequency localized modes.

The local density of states are quite useful in calculating the various properties of of the defect crystals. The change in various thermodynamic quantities of a crystal can be expressed in terms of the local density of states easily. The mean square thermal displacement is expressed as

$$\langle u_{\alpha}^{2} \rangle = \int_{0}^{\infty} \frac{Z_{\alpha}(l,\omega)}{M_{\alpha}^{2}} \varepsilon(\omega,T)\,d\omega \qquad (6)$$

where $\varepsilon(\omega,T) = \frac{\hbar\omega}{2} \coth\left(\frac{\hbar\omega}{2kT}\right)$.

The vacancy formation entropy can be expressed in term of a change in the frequency spectra and is give by :

$$S_{lV}^{F} = k\int_{o}^{\infty} \sigma(\omega,T)\,\Delta Z(\omega)\,d\omega = k\int \sum_{d} (Z(d,\omega) - Z(\omega))\sigma(\omega,T)\,d\omega \qquad (7)$$

where $\sigma(\omega,T) = 1 - \ln\left(\frac{\hbar\omega}{kT}\right)$, and d stands for neighbours of vacancy.

In Chapter IV the local density of states of <100>-dumbbell has been discussed in fcc metals, using Green's function method, with copper as a typical example. The EAM potential has been used to calculate the ideal lattice force constants and the force constants changes in the defect space, using a second neighbour force model . The defect space is divided into different irreducible representations and many characteristic modes have been obtained at different frequencies in Thz: the resonance modes are E_g(2.74), A_{2u}(5.56) and E_u(3.12); the localized modes are A_{1g} (11.08). Eg(12.94), E_u(13.16). But when the experimental phonons based force constants are used in the calculations of the ideal lattice Green`s functions, and the EAM potential is used to calculate the defect lattice force constants,the resonant frequencies are E_g(1.62), E_u(2.20) and the localized modes are A_{1g}(7.30,14.06), A_{2u}(7.36). The use of EAM potential in the dynamic-defect calculations has been done for the first time and could reproduce the defect modes. The presence of low frequency resonance modes also explains the reduction in shear moduli and the long-range migration of the SIAs at low temperatures.

In Chapter V we have calculated the local density of states of <110>-dumbbell in bcc metals: α-Fe, Mo and W using the Green's function method. Two sets of force constants have been used to calculate the ideal lattice green's function (i) from the (JW) potentials and (ii) from the experiments based phonons. The force constant changes in the defect space have been calculated from the JW potentials. In both the cases many characteristics defect modes have been obtained at different frequencies when the JW potentials are used consistently the resonance modes occur at : $B_{1g}(1.68)$, $B_{1u}(2.18)$, $B_{2u}(2.70)$, $B_{3u}(0.59)$ and the localized modes at $A_g(11.32)$, $B_{1g}(11.32)$, $B_{2u}(11.70)$, $B_{3u}(16.88)$ for α-Fe; similarly the resonance modes $B_{2g}(2.16)$, $B_{1u}(3.28)$, $B_{2u}(2.64)$, $B_{3u}(2.16)$ and the localized modes at $A_g(9.70, 16.28)$, $B_{1g}(9.38,15.62)$, $B_{1u}(15.86)$, $B_{2u}(9.58)$, $B_{3u}(13.72)$ for Mo; also the resonance modes $B_{2g}(1.14)$, $B_{1u}(2.28)$, $B_{2u}(1.82)$, $B_{3u}(1.38)$ and the localized modes at $A_g(8.04,13.92)$, $B_{1g}(8.14)$, $B_{2g}(13.54)$, $B_{1u}(13.72)$, $B_{2u}(8.30)$, $B_{3u}(11.76)$ for W. When the experimental phonons are used, the resonance modes are: for α-Fe, $B_{1g}(2.42)$, $B_{2g}(1.86)$, $B_{1u}(3.08)$, $B_{2u}(3.26)$, $B_{3u}(1.88)$ and the localized

modes at A_g(9.37,10.99), B_{1g}(10.94), B_{2u}(11.24), B_{3u}(9.46,16.10); for Mo the resonance modes B_{1g}(1.39,7.995), B_{2g}(2.73), B_{1u}(3.55), B_{2u}(3.11), B_{3u}(2.59) and the localized modes at A_g(8.26, 12.77), B_{2g}(12.17), B_{1u}(12.38), B_{2u}(8.07), B_{3u}(10.965); for W the resonance modes B_{2g}(1.98), B_{1u}(2.78), B_{2u}(2.18), B_{3u}(1.86) and the localized modes at A_g(7.30,12.12), B_{1g}(7.34), B_{2g}(11.84), B_{1u}(12.00), B_{2u}(7.46), B_{3u}(10.40).

The obtained local frequency spectra are then utilized to calculate the mean square thermal displacements of the dumbbell, in all the three metals and with both sets of force constants used. The results show an increase in thermal displacements as compared to that of the host atom, especially in the case of α-Fe. This is the result of low-frequency resonance modes. The resonance modes also explain the long range migration of SIAs at low temperatures.

In Chapter VI we have calculated the local frequency spectra of the first and second neighbours of vacancies in α-Fe, Mo and W using the same Green's function's method and following the same

procedures regarding the force constants and force constant changes as done in the case of SIAs. It has been found that there is a significant shift of the density of states towards the lower frequency in the spectra of the first neighbours as found by Hatcher *et al* [5] in Cu, whereas the spectra of second neighbours resemble those of the respective host spectra in the case of Mo and W but in the case of α-Fe the second neighbours' spectra shift towards the higher frequencies when the lattices are allowed to undergo relaxation. The vacancy formation entropy also are calculated from the local frequency spectra in all the three metals for the case of relaxed lattices and also for unrelaxed lattices. The values of the vacancy formation entropy for relaxed lattice when the JW potentials are used consistently are : α-Fe (1.559k), Mo(2.25k), W(3.199k), but when the experimental based phonons are used, we get α-Fe(1.485k), Mo(1.94k) and W (2.446k). In the case of unrelaxed lattices the values are: α-Fe(2.043k), Mo(1.61k), W(1.921k) when JW potential is used and they are α-Fe(1.646k), Mo(1,69k), W(2.143k) when experimental phonons are used. In general, the obtained values of formation entropy are comparable to those obtained by others.

References :

[1] R.A. Johnson and W.D. Wilson *Interatomic Potentials and simulation of lattice defects* ed. P.C. Gehlen, J.R. Beeler and R.I.Jaffee (New York: Plenum, 1971).

[2] M.S.Daw and M.I.Baskes *Phys. Rev. Lett.* 50 1285 (1983); *Phys. Rev. B* 29 6443 (1984).

[3] A.Banerjea and J.R.Smith *Phys. Rev. B* 37 6632 (1988).

[4] P.N.Ram, *Radiation Effects and Defects in Solids*. 118, 1 (1991).

[5] R.D. Hatcher, R. Zeller and P.H. Dederichs, *Phys.Rev.B.* 19, 5083 (1978).

DYNAMICAL PROPERTIES OF POINT DEFECTS IN METALS

By

SEVERINE S. POHLONG

A Thesis

SUBMITTED IN FULFILMENT OF THE REQUIREMENT
FOR THE DEGREE OF
DOCTOR OF PHILOSOPHY

To

DEPARTMENT OF PHYSICS
NORTH - EASTERN HILL UNIVERSITY
SHILLONG - 793 022
INDIA
1996

CERTIFICATE

I certify that the thesis entitled " Dynamical Properties of Point Defects in Metals " by Mr S.S. Pohlong for the degree of Doctor of Philosophy (Physics) of North Eastern Hill University, Shillong, embodies the records of original research works carried out by him under my supervision. He has been duly registered and the thesis presented is worthy of being considered for the award of Ph.D. degree.

This work has not been submitted to any other university or institute for any degree.

P.N. Ram 23.10.96

Prof. P.N. Ram

(Supervisor)

पूर्वोत्तर पर्वतीय विश्वविद्यालय
प० प० विवि० परिसर, शिलांग-७९३०२२ (मेघालय)
Phone :
Grams : NEHU
North-Eastern Hill University
NEHU Campus, Shillong - 793022 (Meghalaya)

PRE-PHD COURSE GRADE CERTIFICATE

THIS IS TO CERTIFY THAT MR SEVERINE S. POHLONG SECURED THE GRADES MENTIONED BELOW IN THE FOLLOWING PRE-PHD COURSES

COURSE	GRADE
SOLID STATE PHYSICS (Department level)	A
HIGH ENERGY PHYSICS (Department level)	A
COMPUTER COURSE (School level)	O
FRENCH LANGUAGE (University level)	O

DATED 6/11/96

SHILLONG

PROF. & HEAD

Professor & Head
Department of Physics
North Eastern Hill University
Shillong-793022

TO MY

PARENTS

BROTHERS

AND

SISTER

ACKNOWLEDGEMENT

I wish to express my sicere thanf and gratitude to my supervisor Prof P M Ram for having introduced and guided me in the field of Lattice Dynamics in solids necessary Computer Programmings and Solid State Physics Course worf and for his constant helps and encouragements at various stages of my research worf I would like to thanf Dr M K Parida Dr I K Sinha and Mr P B Jingran for offering us the Course worfs the Head of Physics Department Prof C S Shastry for encouraging me to carry out this worf in the Department of Physics and teachers like Prof P Shukla Prof VSI Rao Dr BM Jyrwa and others for their helps Further I would like to thanf all the members of the Computer Centre NEHU for their computational helps and constant encouragements especially the Director Dr S M Rai Miss Baphimon Kynjah Mr P P Dey and others

I wish to thanf all my friends who have extended their helps and moral encouragements to complete this worf especially Dr J M Blah with whom I have been together for a long time Paul Sansan and others whose names are not mentioned here

Thanf God for all these achievements

Severine S Pohlong

CONTENTS

page

CHAPTER I

CHAPTER II

CHAPTER III

LISTS OF TABLES :

LISTS OF FIGURES :

CHAPTER I

INTRODUCTION

A perfect crystal is a solid where each lattice point is occupied by a basis and such a crystal can be realized only at absolute zero. Due to various factors, a solid deviates from pertect crystallinity and becomes an imperfect solid. Any form of imperfections introduced into a solid is called a defect. A defect may be in the form of configurational disorder which may be caused by the presence of thermal energy in the crystal or by exposure of the crystal to some form of radiations. If a defect is confined to a point only, it is called a point defect : viz., vacancies, substitutional impurity, and interstitials. A vacancy is formed when an atom is missing from a lattice site, a substitutional impurity is due to the presence of a foreign atom at the lattice site and the interstitial is the atom which occupies a position in between lattice sites or interstice of a crystal and if the interstitial atom is coming from one of the host atoms, it is called self-interstitial; vacancies and self-interstitials are known as intrinsic point defects. A typical feature of point defects is that they violate only a

short range order within the crystal. Besides point defects, there are some other defects : viz., line defects, e.g., dislocations and other extended defects like surfaces etc. In this thesis we are concerned only with the properties of the intrinsic point defects in cubic metals.

The presence of defects in solids changes their properties drastically, i.e., many important properties of the solids are controlled by the defects rather by the nature of the host. For example, when a pure semiconductor is doped with impurities, it exhibits a remarkable increase in the electrical conductivity contributed by the impurity atoms than by the host atom and which leads to various transistor actions; the colour and luminescence of many crystals arise from the presence of impurities or imperfections; atomic diffusion may be accelarated enormously by impurities or imperfections; mechanical and plastic properties of a material are usually controlled by imperfections; further, when a trace of Cr^{+++} ions are added to Al_2O_3 crystal makes the latter to acquire laser property. These are few examples illustrating the importance of defects in solids which play a very important

role in the advancement of Science and technology. When a substitutional impurity is present in a solid, besides the change in mass, force constants and phonon's spectra, there is a drastic change in the local vibrational frequency spectrum of the impurity which is different from spectrum of the host. The appearance of some characteristic modes within the band frequency called resonance modes and other sharp modes occuring above the band called localized modes play vital role in the properties of the defective solid. Both resonance and localized modes appear in the form of some resonant peaks; resonance modes are produced when the defect is vibrating with some vibrational frequencies which are already present in the host whereas the localized modes produced by the defect can not propagate in the crystal and thereby become localized in nature. The vibrational properties of substitutional impurity has been studied extensively by a large number of workers in a number of impurity-host systems in different types of solids as discussed in many reviews [1-5].

Compared to substitutional impurities the theory of vibrational properties of intrinsic point defects is less

developed. However, of late the situation is changing and the study of the properties of SIAs in metals have been carried out extensively, especially in the case of fcc metals regarding their structures, energies and dynamics. In order to study the dynamical properties of the defect, the stable structure of the SIAs in different metals should be ascertained. The split-interstitial or dumbbell configuration seems to be the most stable in cubic metals. In this configuration the lattice is shared by two atoms placed symmetrically about it and aligned along one of the primary axes in the lattice. The axis of the dumbbell lies along <100> for fcc metals and along <110> for bcc metals. In fcc metals the <100>-split configuration was found to be the most stable configuration by various computer simulation studies [6-9] and different experimental techniques : diffuse X-ray scattering [10-13], elastic after effect and internal friction [14,15], magnetic-after effect [16] and change in elastic constants [17-19]. The <110>-split configuration has been found to be the most stable for many bcc metals in various experimental studies [12,19,20-28] and computer simulation studies [29-33].

In the study of the vibrational properties of intrinsic point defects in metals, the quantity which is very important and affected most by the presence of the defects (SIAs and vacancies) is the local frequency spectrum of the defect. The most characteristic feature of the defect spectra consists in the appearance of resonant type peaks corresponding to defect modes, the low-frequency resonance modes and the high-frequency localized modes as in the case of substitutional impurities mentioned earlier. Further, the presence of defects produces a distortion in the lattice around the defect site which extends over a few neighbours. The distortion results in the alteration in the positions of the atoms in the defect space which gives rise to a change in force constants. The change in force constants results in important changes in the frequency spectrum of the solid reflected through local frequency spectra of the defects and their neighbours. From the local density of states of the defect and its neighbours, many important physical properties of a defective solid can be calculated.

From the theoretical point of view, there are many methods through which the vibrational spectrum of the defect and the host atom can be calculated. Some of the methods which can be employed are: Green's function method [34-36], cluster method, molecular dynamics [6,8] and recursion method [37-39]. The latter two methods are suited only to calculate the local frequency spectrum of the defect and detailed calculations of physical properties of the defect crystal is not possible. On the other hand the Green's function method has been widely used to calculate the various important physical properties of the defect crystal. In fact the physical properties are expressed in terms of the defect lattice Green's functions. The Green's function method basically involves a form of perturbation expansion of the defect Green's function in terms of the perfect lattice Green's function. Due to its simplicity and effectiveness the Green's function method will be used in the present work to calculate the local density of states of the defect in the case of SIAs and the neighbours in the case of vacancies. The imaginary part of the same site Green's functions gives the local density of states of the atom concerned. In order to calculate the defect lattice

Green's function and also some other properties of the defect, a proper choice of suitable potentials is necessary. In the earlier studies of the dynamics of point defects in metals, different types of empirical pair potentials have been used. These pair potentials were able to explain many physical properties of the defects in cubic metals, though most of the time the focus of attentions has been the fcc metals. The early works in metals using empirical potentials has been reviewed by Johnson [30,40]. Dederichs *et al* [42-44] have used Born-Mayer potential, Morse potential and modified Morse potential to discuss the various static and dynamical properties of point defects in fcc metals [42-44]. For bcc metals the spline fit potentials [40] have been found to be more suitable. Especially the Johnson and Wilson (JW) potentials are found to be suitable for static [33,45] and dynamic [46-48] properties of point defects in bcc metals. However, it is obvious that the empirical pair potentials are adequate in modelling the interatomic interactions in metals, especially the many body effects causing deviation from Cauchy relation $C_{12} = C_{44}$. However,with the advent of new semi-empirical approaches like embedded atom method (EAM) [49,50] and N-body

potentials [51], the situation has changed and many more properties of metals including properties of point defects have been discussed using these potentials [52,53]. However, these potentials have not been utilized for the discussion of dynamical properties of point defects in metals. One of the aims of the present work has, therefore been to use these new potentials to discuss the dynamical properties of intrinsic point defects in metals.

In any dynamical study of point defects , apart from force constants changes the important information needed is the perfect crystal phonons. In case of metals the perfect lattice phonons are usually obtained on the basis of Born-von Karman models fitted to measured phonon dispersion in neutron scattering experiments. In such cases the force constant changes are adjusted in an adhoc way on the basis of some other experimental measurements or they are determined with the help of empirical pair potentials. Altenatively, the pair potentials are obtained for individual metals through an empirical fit of some well known experimental quantities e.g., elastic constants. Once empirical pair potentials are determined they may be used both for perfect

crystal description as well as for calculating force constant changes near the defects. The use of empirical pair potentials have been quite common in the study of vibrational properties of metals containing point defects.

Extensive studies have been carried out regarding the properties of <100>-dumbbell interstitials in fcc metals [42-44,46,54-67], especially with the local density of states of the dumbbell and other related properties. The occurrence of some typical defect modes : the low-frequency resonance modes and high-frequency localized modes in the local frequency spectrum of the <100>-dumbbell plays vital role to explain various important quantities related to the defect crystal. The occurrence of resonance modes have been confirmed by different experimental techniques in Cu and Al [68-70], though in some cases the evidence of resonance mode in Al is absent. This demands a rigorous theoretical investigation of the dynamics of the SIAs, especially the local frequency spectrum of the defect and its neighbours. Using the local density of states of the dumbbell, many thermodynamical properties can be calculated, of which the

detailed account has been given in reviews [46,54,59,64]. Following the earlier works by Ram, we are using the Green's function method to study the dynamical behaviour of the <100>-dumbbell in fcc metals with the application of the EAM potentials to calculate the force constants of the ideal lattice and also the force constant changes in the vicinity of the defect to calculate the defect lattice Green's function. The EAM potentials consist of the embedding function and the Morse form of potential as a pair part. This is to extend the utility of these potentials in the dynamical studies of point defects in metals which have not been used so far.To examine the suitability of the potentials, Green's functions for the ideal lattice is also calculated from force constants fitted to experimental phonons in Cu [71].

As far as the dynamics of bcc metals metals are concerned, comparatively, less attention has been paid. Extensive study of the dynamics of <110>-dumbbell in bcc metals is still lacking, though the symmetry, structure and position of the dumbbell are known at least in α-Fe, Mo and W. Recently Ram [47] has

calculated the local frequency spectrum of the <110>-dumbbell in Mo by using the Green's function method and have found the occurrence of the low-frequency resonance modes and high-frequency localized modes as in the case of fcc metals. This work was later on extended by Blah *et al* [48] to calculate the local frequency spectra of the neighbours of the defect and it was found that the same resonance and localized modes occur as found in dumbbell spectrum but the amplitudes of vibration of atoms is much reduced. In this work we want to extend the calculation of the local frequency spectra of the <110>-dumbbell to α-Fe and W to have a better outlook of the behaviour of the normal bcc metals. In this context the JW potentials which was used to calculate the force constant changes in the vicinity of the defect are also used to calculate the ideal lattice Green's functions and as such the calculation of local density of states of the dumbbell is repeated for Mo also. Following the earlier works [47,48] in Mo, the ideal lattice Green's functions are also calculated from the force constants obtained from the experimental phonons fit to the Born-von Karman model for Mo [72], W [74] also. Then there are two sets of calculations of the

defect Green's functions (i) from the consistent use of the JW potentials and (ii) from the experimental phonons. The local density of states of the dumbbell are then used to calculate the mean-square displacements of the dumbbell in both the cases for all the three metals.

The discovery of the low-frequency resonance modes of SIAs is one of the important developments in the field of studies of radiation damage in metals. Dederichs [42-44] has explained the occurrence of resonance modes in terms of highly compressed atomic arrangement in the lattice around the interstitial. In general the distance between the interstitial and its neighbours is considerably smaller than the nearest-neighbour distance in the ideal lattice and consequently there is a strong repulsion between the atoms in the defect space leading to very high force constants compared to the ideal lattice nearest-neighbour force constants and as such the occurrence of high-frequency localized modes is understandable but the simulteneous occurrence of the defect characteristic modes can not be understood so clearly .The ocurrence of resonance modes within the in-band frequency spectra

have facilitated the explanation of most intriguing behaviour of the interstitials e.g., their high mobility at low temperatures [44,46,54,55]. The resonance modes are quite important in understanding the various physical properties of the irradiated metals. They explain the large experimentally observed changes in elastic constants [63]. Further, the resonance modes explain some important thermal properties of the irradiated metals, e.g., the increase in the specific heat and the large increase in thermal displacements [59,60]. The large thermal displacements associated with the low-frequency resonance modes result in sharp reduction in Debye-Waller factor as has been found out in the Mossbaeur measurements of irradiated metals by Vogl *et al* [75,76] and Marangos *et al* [77,78]. The presence of the resonance modes also lead to drastic changes in phonon dispersion curves as commented by Wood and Mostoller [57] and Schober *et al* [56].

Besides the study of the dynamics of SIAs in cubic metals, the dynamics of vacancies are also important in understanding the properties of irradiated metals. Though less attention has been paid to the study of vacancy but it is equally

important in the study of radiation damage in metals. The presence of a vacancy changes the whole atmosphere in its neighbourhood though the most affected atoms are the first and second neighbours of the vacancy. To a first order approximation, we can view a problem where all the neighbours of the vacancy are in their own respective positions as in the case of an ideal lattice. This is the case of an unrelaxed lattice. The different atoms interact among themselves but there is a zero coupling between the vacancy and its neighbours. But in a more realistic situation, when a vacancy is created, the neighbouring atoms readjust themselves by occupying new positions in order to attain minimum energy configuration.This is the case of a relaxed lattice. The works on static relaxation round the vacancy have shown that there is an inward relaxation of the first neighbours and an outward relaxation of the second neighbours [33,79]. The relaxation of the neighbouring atoms of the vacancy alters the force constant matrix between the different pair of atoms in the defect space, besides the missing force constants between the vacant site and its neighbours. All these result in the modification of the local

density of states of the neighbours with the possible appearance of characteristic defect modes: the resonance modes and localized modes.

In this context, Land and Goodman [80] carried out an investigation on the vibrational effects of vacancies in cubic metals with short ranged forces using molecular approximation and their result for Cu showed the appearance of modes just above the maximum frequency of the crystal which may be regarded as a local mode. On the other hand Hatcher *et al* [81] have used the Green's function method to discuss the vibrational behaviour of vacancy in Cu and α-Fe and have found that no local mode appear. Apparently, more work is needed to understand the vibrational behaviour of vacancies in metals. Another aspect which plays an role in the study of the dynamics of vacancies is the choice of appropriate potential suitable in the distorted region round the vacant site. Hatcher *et al* [81] have pointed out that the Morse potential seems to work well for fcc metals while for a typical bcc metal α-Fe, a spline fit type of potential due to Chang and Graham [82,83] works well.

From our experience with the studies of SIAs and their neighbours in bcc metals : α-Fe, Mo and W, the JW potentials give reasonable description of the dynamical properties of these metals when the defect is modelled with interaction up to second neighbours [see Chapter V]. Therefore the JW potential is used in the study of the local frequency spectra of the first and second neighbours of the vacancy in α-Fe, Mo and W using Green's function method both for relaxed lattice as well as for unrelaxed lattice. As in the case of SIAs, the JW potentials are used to calculate the perfect lattice Green's functions and the changes in force constants in the vicinity of the defect to obtain the local frequency spectra and also the scaled force constant changes when the ideal lattice Green's functions are calculated from the force constants based on the experimental phonons fit to the Born-von Karman models for α-Fe [73], Mo [72] and W [74]. The obtained local density of states are then used to calculate the formation entropy of the vacancy and the mean-square thermal displacements of the first and second neighbours in the case of relaxed lattice.

The thesis has been organized as follows :

Chapter II contains the generation of a new potential for fcc metals based on the electron density functional theory called EAM potential together with the Morse form for a pair part contribution. The different parameters of the embedding function and the Morse part are determined by fitting to experimental values : elastic constants, cohesive energy, vacancy formation energy and the lattice constant. The obtained potential parameters are then used to calculate the unrelaxed divacancy formation energy and unrelaxed surface energy. As a further application, of the EAM potentials, phonons are also calculated for six fcc metals : Cu, Ag, Au, Ni,Pd and Pt and results are compared with the experimental values.

Chapter III contains the the Green's function formulation to calculate the local density of states of the defect and its neighbours. Firstly, the Green function for ideal lattice is presented and with the change in force constant matrix due to

defect, the expression for the defect lattice Green's functions is also presented. The imaginary part of the same site Green's functions give the local density of states of the atoms concerned. The local frequency spectra are then applied to calculate few thermodynamical properties like, thermal displacements, formation entropy etc.

Chapter IV contains the application of the EAM potentials to calculate the local frequency spectrum of <100>-dumbbell in fcc metals with Cu as a typical example. Low-frequency resonance modes and high-frequency localized modes appear in the local frequency spectrum of the dumbbell. The calculation is repeated with the ideal lattice Green,s function calculated from the force models based on experimental phonons while the force constants near the interstitial are calculated with the help of the EAM potentials. The calculations show that the EAM potential is effective in the dynamical studies of point defects in fcc metals.

Chapter V contains the calculation of the local density of states of <110>-dumbbell in α-Fe, Mo and W, using the Green's function method. The JW potentials have been used to calculate the force constant changes as well as the ideal lattice Green's functions. The ideal lattice Green's functions are also calculated from the force constants based on the experimental phonons. The local frequency spectra of the defect in all the metals show appearance of resonance and localized modes. The local frequency spectra of the defect are then used to calculate the mean-square thermal displacements of the dumbbell in all the three metals. The presence of low-frequency resonance modes provides answers to decrease in shear moduli and long range migration of the SIAs.

Chapter VI contains the calculation of the vibrational spectra of the first and second neighbours of vacancy in α-Fe, Mo and W by using Green's function method again. The JW potentials have been used to calculate the force constant changes in the defect space and the ideal lattice Green's functions. In addition, the ideal lattice Green's functions are also calculated

from the experimental phonon-based force constants. The local density of states are utilized to calculate the formation entropy of the vacancy for all the three metals when the lattice is relaxed as well as when it is unrelaxed. In the case of relaxed lattice calculation the mean-square displacements of the first and second neighbours are also presented. The results are discussed in the light of the available experimental results.

CHAPTER II

2. Analytic Embedded Atom Method Potentials for FCC metals

2.1. Introduction

Many problems in solid state physics and material sciences require a detailed understanding of the energetics and structure of nonuniformities in metals and alloys. Due to the lower symmetry and long-range strains generally found around defects and surfaces, the study of this problem requires techniques that can handle a large number of atoms. Historically the problems have been addressed with various pair-potential models of the energetics of the constituents of the solids [40,41,84]. This process is certainly useful in many circumstances. However there are some significant problems associated with the application of the pair potentials when the local environment is substantially different from the uniform bulk. This includes such problems as surfaces, grain boundaries, internal voids, fracture etc. However, the pair potentials have been used sucessfully to treat

inert impurities, such as He in metals [85], still the potentials are not apllicable to chemically active impurities. It has been demonstrated [85] in particular that the energy of a hydrogen atom in a transition-metal cluster cannot be represented by pair interactions, whereas the energy of He atom can be represented.

Daw and Baskes [49,50] have proposed an alternative to the pair-potential approach based on density functional ideas, called the embedded atom method (EAM). This new approach provides a framework for a general picture of metallic bonding an approximate expression for energy of an arbitrary arrangement of atoms in a metallic system. This new method has been applied to several problems with good results. The applications to bulk pure metals include the migration of chemically active impurities in metals [50], structure of liquid metals, dislocation propagation, fracture properties, grain boundaries, phonon spectra [86-89]. It has been applied to surfaces and shown to provide realistic values for both the surface energies and geometries including the prediction of the (1x2)surface reconstruction of Pt(110) [90]. Furthermore this approach has been applied sucessfully to

segregation phenomena in Ni-Cu alloys [91-92]. The accuracy of computer simulation studies of metallic crystals has greatly increased with the replacement of widely used empirical pair potentials [40,41,84] by these semi-empirical potentials based on density functional theory using the effective medium [93] or quasi-atom approach [94]. Ever since the introduction of EAM by Daw and Baskes [49,50], the method has been widely used for a variety of problems ranging from perfect lattice phonons to highly distorted defect structures. A closely related model (N-body potential) has been developed by Finnis and Sinclair [51] for bcc metals based on a second-moment approximation to tight binding theory.

As is clear from the work of Daw and Baskes [49,50] and of Foiles *et al* [52], there is tedious numerical fitting to obtain the parameters and functions required for the model and all results must be obtained by detailed computation. Although once the parameters and functions are determined for a particular metal, the same set can be used for the study of various properties of the metal including those which were really

intractable by pair potential approach, nevertheles the use of these potentials and functions is not very straight forward or convenient, since one has to have a detailed table for embedding functions for various values of electronic charge density which would be quite cumbersome.

In this background Johnson [94] introduced a simple nearest-neighbour analytic model for fcc metals providing much needed ease and simplicity in their use for computational studies of such metals. However, the main problem with Johnson's analytic model is that the anisotropy ratio A(=C/C') is constrained to be equal to 2 whereas the experimental values range from 1.22 for aluminium to 3.19 for copper. Oh and Johnson [95] have extended the model beyond the nearest neighbour interaction and have applied it to fcc and hcp metals. However, with this extension the embedding functions have to be determined numerically with the help of the equation of state of expanded or compressed perfect lattice given by Rose *et al* [96]. A choice of exponential form for total charge density has enabled Mei *et al* [97] to obtain a closed analytic form of the embedding function. They

have obtained potential parameters for fcc metals using a third neighbour model and have tested the potential in the molecular dynamic study of thermodynamic properties of copper. However, it is not clear whether the embedding function obtained by Mei *et al* [97] has the right functional behaviour as a function of charge density which is seen in first principle studies [98,99]. Unfortunately Mei *et al* have not discussed this aspect of the embedding function obtained by them which very much depends on the choice of the pair potential function. In any case, the analyticity of the embedding function which depends on the exponential form of the total electron density seen by an atom in the lattice, is not fully exploited in this model with its tie-up with the pair potential expression.

On the other hand, Banerjea and Smith [100] have found that in a wide range of situations e.g., cohesion in solids, chemisorption and diatomic molecules, the host electron density, to a good approximation, is a simple exponential function of the interparticle separation. Based on this fact these authors have suggested a universal form for the embedding function : a

universal electron density-distance relation yields a universal embedding energy-electron density relation [100]. This form of embedding function is found to have the right functional behaviour obtained from effective medium theory. This type of embedding function has been used by Johnson and Oh [101] to obtain EAM potentials for bcc metals. Evidently, it is of considerable interest to use the universal form of embedding energy to determine the EAM potentials for fcc metals. In the present work, therefore, we have used the same universal embedding energy-density relation together with a pair potential of the Morse form to obtain potential parameters for six fcc metals. Especially, we have used a third neighbour model to evaluate the potential parameters for fcc metals : Cu, Ag, Au, Ni, Pd, and Pt by fitting them to elastic constants : Voigt average shear elastic constant, G_V, C44, and the Cauchy pressure, (C12 - C44)/2, vacancy formation energy, cohesive energy and the lattice constant. The obtained parameters have been employed to calculate unrelaxed divacancy binding energy and unrelaxed surface energies. The obtained results are well within the range of experimental values. Further, we have calculated phonons based

on the present potentials. The calculated phonon dispersion, frequency spectrum and the mean square displacement are in agreement with the available experimental and calculated results.

2.2. Theory

In the EAM the energy of each atom is computed from the energy needed to embed the atom in the local electron density provided by the other atoms of the metals. This electron density is approximated by the linear superposition of atomic electron densities contributed by a other atoms in a cluster surrounding the atom under consideration. This electron density is a slowly varying function of position. By making the simplification that this background electron density is constant, the energy of this atom is the energy associated with the electron density of the atom plus the constant background. This defines an embedding energy as a function of the background electron density and the atomic species. In addition, there is an electrostatic energy contribution due to the core-core overlap. This idea has been developed by Daw and Baskes [49,50] who showed that these ideas

lead to an approximation for the total energy of the form

$$E_{tot} = \sum_{i} F_i(\rho_i) + \frac{1}{2} \sum_{\substack{j,i \\ (j \neq i)}} \phi_{ij}(r_{ij}), \qquad (2.1)$$

where $\phi_{ij}(r_{ij})$ is the two-body central potential between atoms i and j separated by a distance r_{ij}, $F_i(\rho_i)$ is the embedding energy of an atom at the ith lattice site with total electron density ρ_i resulting from the superposition of electron densities of neighbouring atoms :

$$\rho_i = \sum_{j \neq i} f_j(r_{ij}), \qquad (2.2)$$

where $f_j(r_{ij})$ is the spherically averaged atomic electron density due to jth atom at site i. For a monoatomic crystal, equations (2.1) and (2.2) reduce to

$$E_{tot} = NE \qquad (2.3)$$

with $$E = F(\rho) + \frac{1}{2} \sum_{m} \phi(r^m) \qquad (2.4)$$

and $$\rho = \sum_{m} f(r^m), \qquad (2.5)$$

where N is the number of atom in the crystal and r^m is the distance of mth atom from a particular atom taken as origin.

In order to apply the EAM the functions f, ϕ and F must be given. The standard fitting procedure to determine these functions is : (i) to choose specific functional forms of f and ϕ (ii) to fit the parameters of the given f and ϕ to experimental data and finally (iii) to determine the embedding function F, using Smith and Banerjea scheme of total universal binding energy relation (UBER) [100].

The crucial point in the implementation of the EAM is the choice of the embedding function $F(\rho)$ and the pair potential $\phi(r)$. For the embedding function we take the universal form suggested by Banerjea and Smith [100] :

$$F(\rho)=F(\rho_e)\left[1 - \gamma \ln\left(\frac{\rho}{\rho_e}\right)\right]\left(\frac{\rho}{\rho_e}\right)^{\gamma}, \qquad (2.6)$$

where $F(\rho_e)$ is the value of embedding energy at equilibrium

electron density ρ_e and the quantity γ is defined by

$$\frac{1}{\gamma} = \frac{1}{\rho_e}\left[\frac{\Delta F}{\left[\frac{d^2F(\rho)}{d\rho^2}\right]_{\rho_e}}\right]^{1/2}, \qquad (2.7)$$

where $\Delta F = -F(\rho_e)$ is the depth at the embedding energy minimum. Though parameter γ is related to the scaling lengths occuring in universal binding energy relation (UBER) and the scaled charge density-distance relation [100], equation (2.7) will be used to determine γ, since the embedding function and its double derivative at equilibrium charge density $\left[F(\rho_e),\ F''(\rho_e)\right]$ are easily related to unrelaxed vacancy formation energy and certain combination of elastic constants (see below) and with this choice of embedding function we find that the condition

$$\left.\frac{dF}{d\rho}\right|_{\rho=\rho_e} = F'(\rho_e) = 0 \qquad (2.8)$$

is automatically satisfied, i.e., we work in in the framework of the so called normalized form of EAM [94,101,102] : an EAM model

remains invariant under a transformation in which a linear term in the electron density is added to the embedding function and an appropriate subtraction is made from the two-body potential and when this transformation is carried out with $F'(\rho_e)=0$, the two body potential becomes an effective two-body potential. For a small deviation of electron density at atomic sites in any atomic configuration the change in crystal energy is dominated by the effective two-body potential alone and as such this effective potential provides a good approximation for the calculation of defect energies. The single vacancy is a defect where the deviation of the electron density from the perfect crystal at the equilibrium is small enough and a Taylor series expansion of $F(\rho)$ about equilibrium electron density ρ_e can be terminated after second order term. Therefore, apart from the effective two-body potential term the unrelaxed formation energy contains only terms in $F''(\rho_e)$ in the present model. In EAM the unrelaxed vacancy formation energy is

$$E_{1V}^{F} = \sum_{m} \left[F\left(\rho_e - f(r_e^m) \right) - F(\rho_e) \right] - \frac{1}{2} \sum_{m} \phi(r_e^m). \qquad (2.9)$$

Expanding the first term and using equation (2.8) we get

$$E_{1V}^{F} = \frac{1}{2} F''(\rho_e) \sum_{m} \left[f(r_e^m) \right]^2 - \frac{1}{2} \sum_{m} \phi(r_e^m). \qquad (2.10)$$

As $F''(\rho_e)$ is much smaller than $F(\rho_e)$ in the present model the unrelaxed vacancy formation energy may be approximated to [101,103]

$$E_{1V}^{F} = - \frac{1}{2} \sum_{m} \phi(r_e^m). \qquad (2.11)$$

Using the cohesive energy

$$-E_C = F(\rho_e) + \frac{1}{2} \sum_{m} \phi(r_e^m), \qquad (2.12)$$

we find that

$$F(\rho_e) = - (E_C - E_{1V}^{F}). \qquad (2.13)$$

Now using the equations for elastic constants C_{11}, C_{12} and C_{44} given by Daw and Baskes [49] and Johnson [95] we can write

$$F''(\rho_e) = \frac{9\Omega(C_{12}-C_{44})}{\left[\sum_m r^m f'(r^m)\right]^2} . \qquad (2.14)$$

To obtain the equilibrium electron density and $F''(\rho_e)$ we must choose an expression for the atomic electron density f(r). The experience [103,104] tells us that simple exponential or a variation of it represents the atomic density quite well. However, with the choice of embedding function given by equation (2.6) an exponential representation for the total electron density is implied and, therefore, an exponential form for f(r) may not be a suitable choice. In the interest of simplicity we have chosen a power law for atomic electron density

$$f(r) = f_e\left[\frac{r_{ie}}{r}\right]^{\beta} \qquad (2.15)$$

which also provides immense analytic convenience [101]. The parameter β can be fitted to atomic electron density calculations or treated as an adjustable parameter. Using atomic electron density given by equation (2.15) the expression for $F''(\rho_e)$ is simplified to

$$F''(\rho_e) = \frac{9\Omega(C_{12}-C_{44})}{\beta^2 \rho_e^2} \quad . \tag{2.16}$$

Substituting for $F(\rho_e)$ and $F''(\rho_e)$ in equation (2.7) the parameter γ is then given by

$$\frac{1}{\gamma} = \beta \left[\frac{E_C - E_{1V}^F}{9\Omega(C_{12}-C_{44})} \right]^{1/2} \quad . \tag{2.17}$$

Thus in the present model the parameters defining the universal form of the embedding energy are determined by the crystal properties, namely the Cauchy pressure, cohesive energy and the vacancy formation energy. The only adjustable parameter β is determined with the help of known atomic electron densities obtained from the Hatree Fock calculation by Clementi [105], where the total density is given by

$$f(r) = N_s f_s(r) + (N - N_s) f_d(r) \tag{2.18}$$

where, N_s and N are the numbers of electron in the s-state and N the total number of electrons in the outermost orbit, when the contribution is considered from the electrons in the outermost shell only. The spherically averaged s- and d- like densities are computed as

$$f_s(r) = \left| \sum_i C_i R_i(r) \right|^2 / 4\pi$$

$$R_i(r) = \frac{(2\zeta_i)^{(n_i + 1/2)}}{[(2n_i)!]^{1/2}} r^{n_1 - 1} e^{-\zeta_i r} \qquad (2.19)$$

n_1, ζ_i and C_i are taken from the Clementi tables calculations with double Zeta functions. The same procudure follows for the case of $f_d(r)$. Various values of ζ from equation (2.15) are used to fit with equation (2.18). The overall fit determines the value of ζ.

We next consider the pair potential function $\phi(r)$ which is taken to be of Morse form in the present model

$$f(r) = D \left[e^{-2\alpha(r-r_o)} - 2e^{-\alpha(r-r_o)} \right], \qquad (2.20)$$

where the parameters D, r_o and α define the depth , distance to the minimum and a measure of the curvature near the minimum, respectively.

The parameters α, r_o and D are determined by fitting to the elastic constants : the Voight average shear modulus G_V =(C11 - C12 + 3C44)/5 and C44 and by using the equilibrium condition for the perfect lattice. Taking a third neighbour model, i.e., both the charge density f(r) and the two-body potential $\phi(r)$ are cut off at a distance between third and fourth neighbours, the Voigt average shear modulus G_V and C_{44} are given by

$$15\Omega G_V = 6r_{1e}^2 \phi''(r_{1e}) + 3r_{2e}^2 \phi''(r_{2e}) + 12r_{3e}^2 \phi''(r_{3e}), \qquad (2.21)$$

$$2\Omega C_{44} = r_{1e}^2 \phi''(r_{1e}) - r_{1e}\phi'(r_{1e}) + 2r_{3e}^2 \phi''(r_{3e}) - 2r_{3e}\phi'(r_{3e}) \qquad (2.22)$$

where r_{ie} are the ith neighbour equilibrium distances and ϕ' and

$\ddot{\phi}$ refer to the first and second derivatives. The equilibrium condition for the perfect lattice is given by

$$6r_{1e}\dot{\phi}(r_{1e}) + 3r_{2e}\dot{\phi}(r_{2e}) + 12r_{3e}\dot{\phi}(r_{3e}) = 0. \qquad (2.23)$$

Using the relation between the elastic cvonstants

$$5G_V = C_{11} - C_{12} + 3C_{44}$$

and equation (2.20), the expression for D is

$$D = \frac{(C_{11} - C_{12} + 3C_{44})}{(2\alpha r_e)^2 \left[e^{2\alpha r_e}\left\{ 2e^{-2\alpha r_e} + 2e^{-2\sqrt{2}\alpha r_e} + 12e^{-2\sqrt{3}\alpha r_e} \right\} - e^{\alpha r_e}\left\{ e^{-\alpha r_e} + e^{-\sqrt{2}\alpha r_e} + 6e^{-\sqrt{3}\alpha r_e} \right\} \right]} \qquad (2.24)$$

while equation (2.23) results into

$$e^{\alpha r_o} = \frac{2e^{-\alpha r_e} + \sqrt{2}e^{-\sqrt{2}\alpha r_e} + 4\sqrt{3}e^{-\sqrt{3}\alpha r_e}}{2e^{-2\alpha r_e} + \sqrt{2}e^{-2\sqrt{2}\alpha r_e} + 4\sqrt{3}e^{-2\sqrt{3}\alpha r_e}} \qquad (2.25)$$

$$C_{11} = \frac{1}{9} F''(\rho_e)\beta^2 r_e^2 +$$

$$D\alpha r_e e^{2\alpha r_o}\left\{ (2\alpha r_e + 1)e^{-2\alpha r_e} + (12\alpha r_e + 2\sqrt{3})e^{-2\sqrt{3}\alpha r_e} \right\} -$$

$$D\alpha r_e e^{2\alpha r_o}\left\{ (\alpha r_e + 1)e^{-\alpha r_e} + (6\alpha r_e + 2\sqrt{3})e^{-\sqrt{3}\alpha r_e} \right\} +$$

$$D\alpha^2 r_e^2 \left[2e^{-2\alpha(r_e - r_o)} - e^{-\alpha(r_e - r_o)} \right] +$$

$$D\alpha r_e \left[e^{-2\alpha(r_e - r_o)} - e^{-\alpha(r_e - r_o)} \right] +$$

$$4D\alpha^2 r_e^2 \left[2e^{-2\alpha(\sqrt{2}r_e - r_o)} - e^{-\alpha(\sqrt{2}r_e - r_o)} \right] +$$

$$2D\alpha\sqrt{2}r_e \left[e^{-2\alpha(\sqrt{2}r_e - r_o)} - e^{-\alpha(\sqrt{2}r_e - r_o)} \right] +$$

$$6D\alpha^2 r_e^2 \left[2e^{-2\alpha(\sqrt{3}r_e - r_o)} - e^{-\alpha(\sqrt{3}r_e - r_o)} \right] +$$

$$2D\alpha\sqrt{3}r_e \left[e^{-2\alpha(\sqrt{3}r_e - r_o)} - e^{-\alpha(\sqrt{3}r_e - r_o)} \right]. \qquad (2.26)$$

Using explicit forms for the embedding energy equation (2.26) and pair potential equation (2.20) including atomic charge density equation (2.15) and equations (2.24) and (2.25) the three elastic constants are obtained as

$$\Omega C_{12} = \frac{1}{9} F''(\rho_e)\sigma_e^2\beta^2 +$$
$$D\alpha r_e e^{2\alpha r_o}\left\{ (2\alpha r_e + 1)e^{-2\alpha r_e} + (12\alpha r_e + 2\sqrt{3})e^{-2\sqrt{3}\alpha r_e}\right\} -$$
$$D\alpha r_e e^{2\alpha r_o}\left\{ (\alpha r_e + 1)e^{-\alpha r_e} + (6\alpha r_e + 2\sqrt{3})e^{-\sqrt{3}\alpha r_e}\right\} \quad (2.27)$$

$$\Omega C_{44} = D\alpha r_e e^{-\alpha r_o}\left\{ (2\alpha r_e + 1)e^{-2\alpha r_e} + (12\alpha r_e + 2\sqrt{3})e^{-2\sqrt{3}\alpha r_e}\right\}$$
$$-D\alpha r_e e^{2\alpha r_o}\left\{ (\alpha r_e + 1)e^{-\alpha r_e} + (6\alpha r_e + 2\sqrt{3})e^{-\sqrt{3}\alpha r_e}\right\}. \quad (2.28)$$

With the embedding function given by equation (2.6) and the Morse form for the pair potential the EAM potential is completely defined and is analytic providing much simplicity and convenience in use almost similar to pair potentials which is of vital importance in detailed computer simulation. With the normalized form of the embedding function we have seen that the vacancy formation energy is approximated by the effective pair potential only. However, with the inclusion of embedding function the vacancy formation energy in the present model is given by

$$E_{1V}^{F} = 12F\left\{\rho_e - f(r_{1e})\right\} + 6F\left\{\rho_e - f(r_{2e})\right\} + 24F\left\{\rho_e - f(r_{3e})\right\} - 42F(\rho_e) - \left\{6\phi(r_{1e}) + 3\phi(r_{2e}) + 12\phi(r_{3e})\right\}, \quad (2.29)$$

when the embedding function is expanded to second terms and with the utility of equations (2.6), (2.15) and (2.20) the unrelaxed vacancy formation energy is reduced to

$$E_{1V} = \frac{\rho_e^2 F''(\rho_e)}{2} - 3De^{2\alpha r_o}\left[2e^{-2\alpha r_e} + e^{-2\sqrt{2}\alpha r_e} + 4e^{-2\sqrt{3}\alpha r_e}\right] + 6De^{2\alpha r_o}\left[2e^{-2\alpha r_e} + e^{-\sqrt{2}\alpha r_e} + 4e^{-\sqrt{3}\alpha r_e}\right]. \quad (2.30)$$

2.3. Results and Discussions

In order to determine the parameters β and γ for the evaluation of the embedding function $F(\rho)$ and D, α and r_o needed for the pair potential $\phi(r)$ the required input parameters for six fcc metals Cu, Ag, Au, Ni, Pd, and Pt are presented in Table I. It is seen that there is considerable scatter in the quoted

values of elastic constants in the literature. We have used the elastic constants from Simmons and Wang [106] as quoted in Foiles *et al* [52]. The parameter γ is determined by the equation (2.17) using the cohesive energy E_c, lattice constant a and the Cauchy pressure $\frac{C_{12} - C_{44}}{2}$ determined from elastic constants and the experimental vacancy formation energy E_{1V}^F as given in Table I. The use of experimental formation energy of for unrelaxed formation energy merits some comments. We note that the dominant contribution to vacancy formation energy comes from the changes in the bond energy with lattice atoms at perfect lattice positions and the contribution due to atomic relaxation is $\approx$ -0.01eV and is rather insensitive to the fit. The experimental values of vacancy formation energy are taken from reviews by Bulluffi [107] and Siegel [108] who quoted "best values" available on the basis of various experimental techniques in literature for Cu, Ag, Au and Pt, whereas for Ni, it is taken from Siegel [108] and Wycisk and Feller-Knrepmeir [109] while in

Table I. Metal properties used to determine the potential parameters : lattice constant, cohesive energy, elastic constants and vacancy formation energy. In case of elastic constants and vacancy formation energy, values in the top rows are those calculated from the present potentials and the lower rows give the experimental values.

	Cu	Ag	Au	Ni	Pd	Pt
a	3.615	4.09	4.08	3.52	3.89	3.92[b]
E_c	3.54	2.85	3.93	4.45	3.91	5.77[b]
C11	1.70	1.23	1.86	2.38	2.86	3.25[a]
	1.70	1.24	1.86	2.465	2.341	3.47[c]
C12	1.224	0.935	1.57	1.51	1.79	2.62[a]
	1.225	0.934	1.57	1.473	1.76	2.51[c]
C44	0.75	0.46	0.42	1.28	0.73	0.87[a]
	0.75	0.461	0.42	1.247	0.712	0.765[c]
E_v^f	1.28	1.13	0.95	1.7	1.4	1.51[a]
	1.28[d]	1.13[d]	0.95[d]	1.6,1.8[e,f]	1.4[g]	1.51[d]

[a] Calculated values.

[b] Values from reference [52].

[c] Values from reference [106].

[d] Values from reference [107].

[e] Values from reference [108].

[f] Values from reference [109].

[g] Values from reference [110].

Pd it is from Kraftmakher and Strelkov [110]. The electron density parameter β is adjusted from a fit to the calculated spherically averaged atomic electron density [105]. The calculated atomic electron density using equation (2.15) is not very sensitive to variation in the values of β. However, the final values of β were chosen so as to get an overall agreement between electron density using equation (2.15) and those obtained from Hartree Fock calculations [105] . As already mentioned the parameters α, r_o and D are determined using elastic constants C_{11}, C_{12}, and C_{44} by fitting them to the shear modulus G_V and C_{44}. For a choice of α and r_o consistent with equation (2.25), equation (2.24) is used to determine D and then the set of α, r_o and D are used to calculate C_{44} and E^F_{1V}. The best fit to C_{44} and E^F_{1V} finally determines the final choice of these parameters which are then utilized to calculate C_{11} and C_{12}. The expression for the vacancy formation energy in the present model is given by equation (2.30) which is ultimately used for the calculation of E^F_{1V} as a guide to the choice of the best pair potential parameters; though in the evaluation of embedding function the vacancy tormation energy was approximated by effective

pair-potential only (Eq.(2.11)). The inclusion of calculated values of C_{11}, C_{12}, C_{44} and E^F_{1V} in Table I gives a clear idea of the quality of the fit of the present potential parameters to experimental elastic constants and vacancy formation energy.

Though in the present third-neighbour model, it is presumed that the atomic electron density function f(r) and two-body potential ϕ(r) have cut off distance somewhere between third and fourth neighbours, for a discussion of perfect crystal properties like elastic constants and the reported defect energies an exact choice of cut-off distance is not important. However, a smooth cut off procedure would be desirable for the potentials to be suitable for computer simulation studies. Such cut off procedure has been discussed among others by Mei *et al* [98], Pasianot *et al* [111] and given as

$$\begin{aligned} g(r) &= 1 && \text{for } r \leq r_{3e} \\ &= (1 - x)(1 + 3x + 6x^2) && \text{for } r_{3e} < r < r_c \\ &= 0 && \text{for } r \geq r_c \end{aligned} \qquad (2.31)$$

where $x = \frac{r - r_{3e}}{r_c - r_{3e}}$.

The values of obtained parameters for embedding function and pair potential are presented in Table II. The embedding functions for all the six metals are shown in figure 1. The embedding functions, have, in general, the right functional behaviour found from effective medium theory [99,100]. The functions exhibit a rapid initial drop and a subsequent upward curvature with the expected minimum at equilibrium electron density. The slope of the embedding function is zero at the equilibrium electron density. The effective two-body potential has been presented in figure 2 which shows the typical behaviour expected for a Morse potential representing the total interaction energy between two atoms. For the sake of comparison we plot the effective potential for copper in figure 3 along with the EAM potential obtained by Oh and Johnson [103]. As can be seen from figure 3 there is close agreement between the two curves with identical position for the potentials minima. The effective potentials are similar to

Table II. The obtained EAM potential parameters.

	Cu	Ag	Au	Ni	Pd	Pt
$\alpha(A^{o-1})$	1.89	1.795	1.91	2.13	1.94	2.145
$r_o(A^o)$	2.638	2.968	2.946	2.549	2.816	2.815
D(eV)	Ø.166	Ø.135	Ø.113	Ø.234	Ø.179	Ø.187
β	4.4	3.8	4.2	3.4	4.3	3.8
γ	Ø.847	1.353	1.445	Ø.66	1.366	1.549

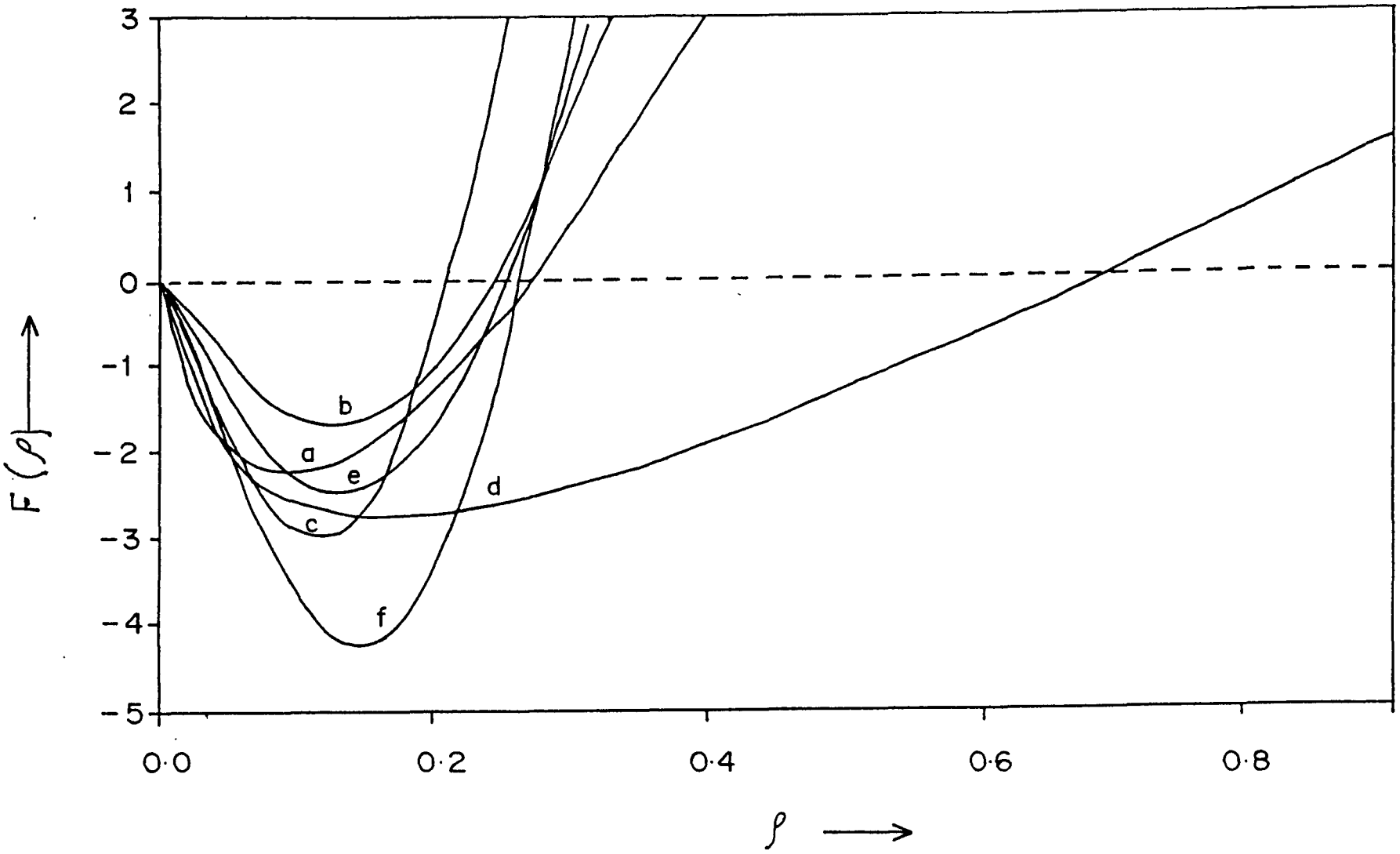

Fig. 1 : The embedding function $F(\rho)$ in eV as a function of electron density ρ in $Å^{-3}$ for Cu (a), Ag (b), Au (c), Ni (d), Pd (e), and Pt (f)

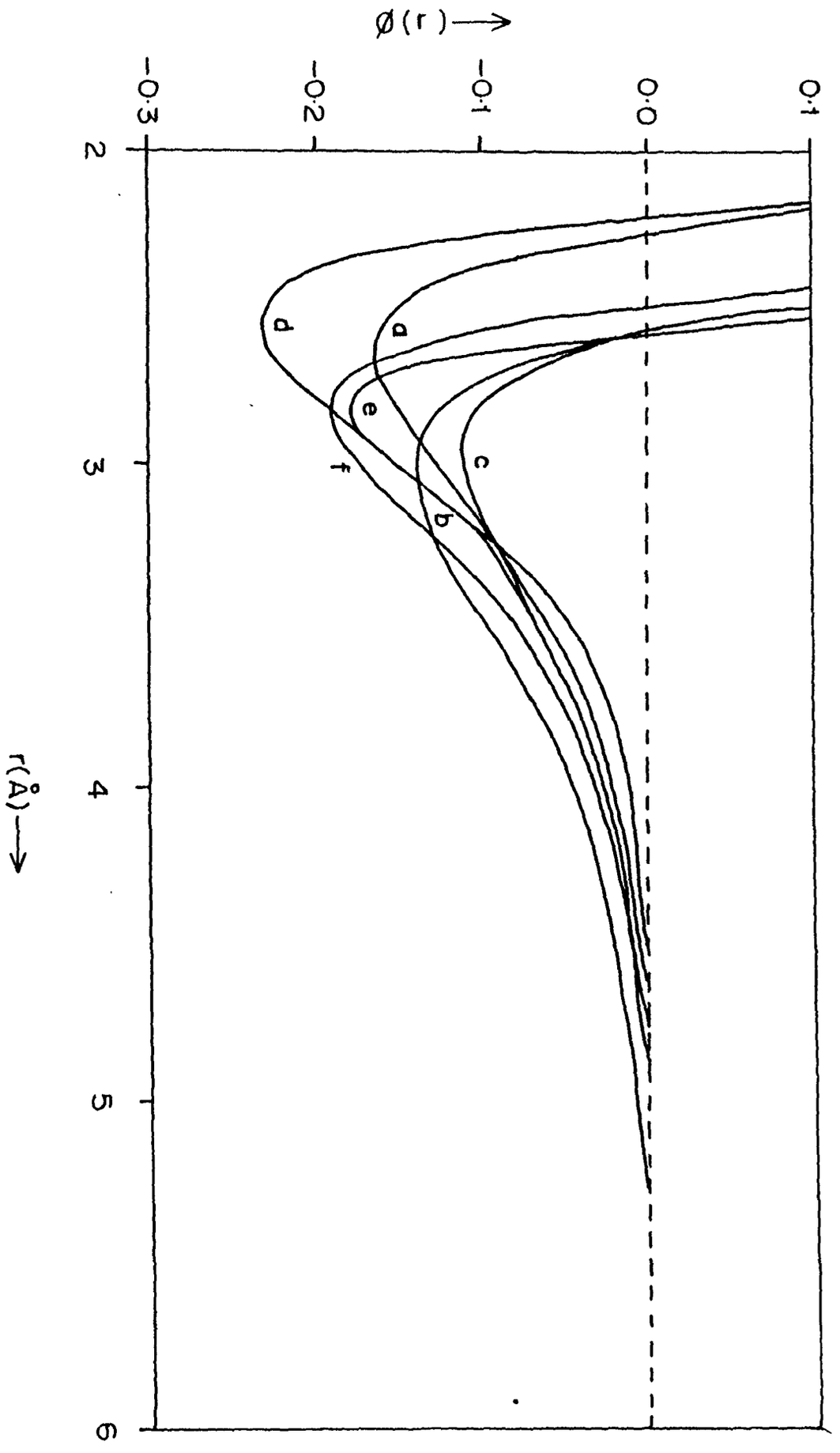

Fig. 2 : The effective two body potentials $\phi(r)$ in eV for Cu (a), Ag (b), Au (c), Ni (d), Pd (e), and Pt (f)

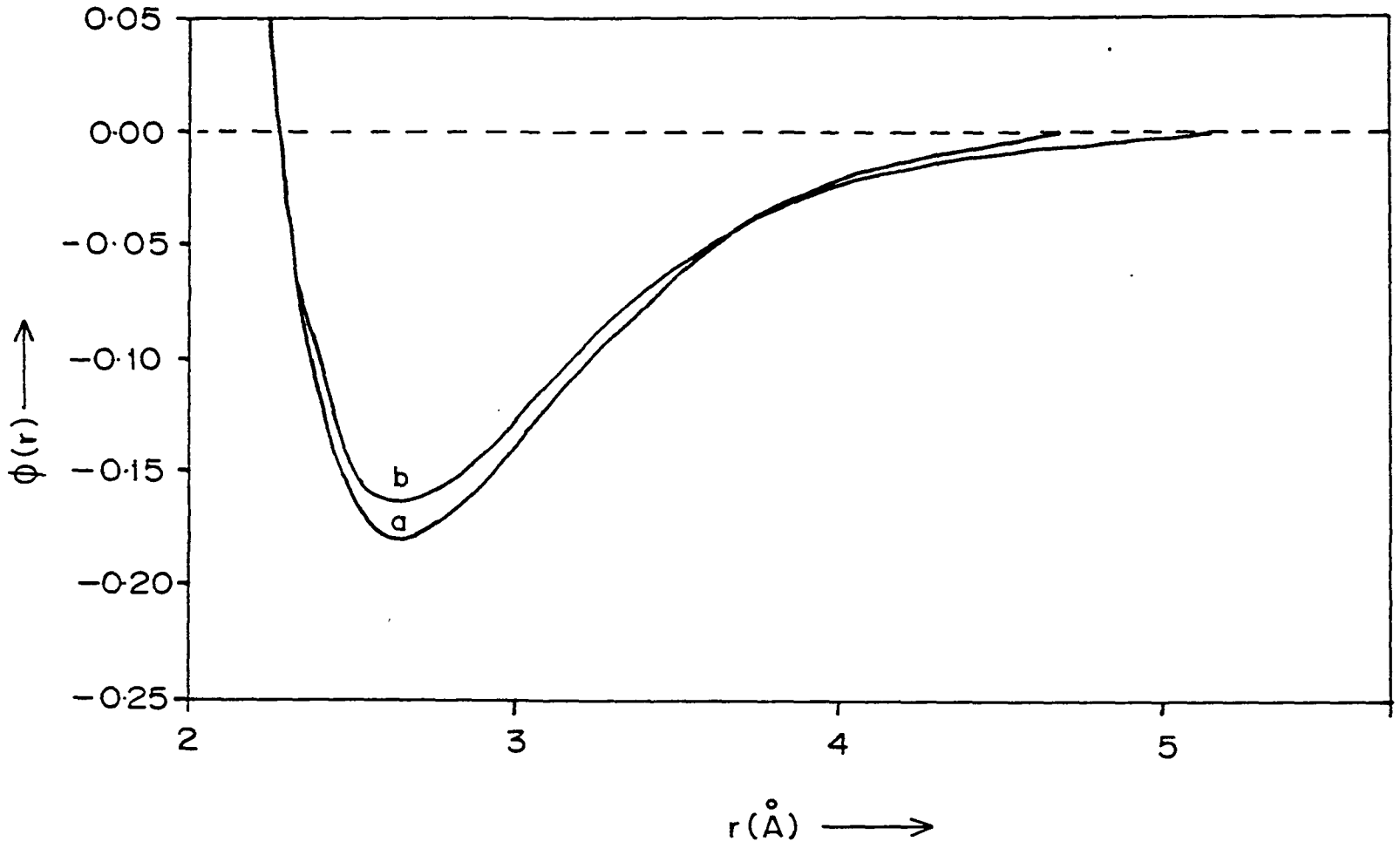

Fig. 3 : The effective two-body potential $\phi(r)$ in eV for Cu : (a) present model (b) from Oh and Johnson ref. [95].

empirical pair potentials fitted to physical properties like elastic constants, unrelaxed vacancy formation energy, reminding one why the empirical potentials have been found to be successful in explaining many properties of these metals [95,101]. As can be seen the potential curves and their slopes drop smoothly to zero between third and fourth neighbour distances.

In order to test the quality of these functions and potentials the best way is to use them for calculating those properties of the crystals which are not used in the empirical fit. We have used the potential parameters for the calculation of unrelaxed binding energy of divacancy E^B_{2V} and unrelaxed surface energies of three low-index planes for all the six metals. The unrelaxed binding energy of divacancy is defined as

$$E^B_{2V} = 2E^F_{1V} - E^F_{2V}, \qquad (2.32)$$

where E^F_{2V} is the divacancy formation energy. In the third neighbour model equation (2.32) gives

$$E_{2V}^{B} = 10F\left\{\rho_e - f(r_{1e})\right\} - 4F\left\{\rho_e - 2f(r_{1e})\right\} + 8F\left\{\rho_e - f(r_{3e})\right\} - 4F\left\{\rho_e - 2f(r_{3e})\right\} - 10F(\rho_e) - \phi(r_{1e}). \quad (2.33)$$

The surface energy is determined by dividing the total energy increase in separating bulk material on a crystallographic plane by the total new surface area created. In the third neighbour model the surface energies of the three low-index planes are

$$S_{100} = \frac{2}{a^2}\left[\Delta E_1^{100} + \Delta E_2^{110}\right], \quad (2.34)$$

$$S_{110} = \frac{\sqrt{2}}{a^2}\left[\Delta E_1^{110} + \Delta E_2^{110}\right], \quad (2.35)$$

$$S_{111} = \frac{4}{\sqrt{3}a^2}\left[\Delta E_1^{111} + \Delta E_2^{111}\right], \quad (2.36)$$

where ΔE_1 and ΔE_2 are contributions originating from changes in the embedding energy and the pair potential part, respectively, and are given by

$$\Delta E_1^{100} = F\left[\rho_e - \left\{4f(r_{1e}) + f(r_{2e}) + 12f(r_{3e})\right\}\right] + F\left[\rho_e - \left\{f(r_{2e}) + 4f(r_{3e})\right\}\right] - 2F(\rho_e) \quad (2.37a)$$

$$\Delta E_2^{100} = -2\phi(r_{1e}) - \phi(r_{2e}) - 8\phi(r_{3e}), \quad (2.37b)$$

$$\Delta E_1^{110} = F\left[\rho_e - \left\{5f(r_{1e}) + 5f(r_{2e}) + 10f(r_{3e})\right\}\right] + F\left[\rho_e - \left\{f(r_{1e}) + 2f(r_{2e}) + 4f(r_{3e})\right\}\right] + F\left[\rho_e - 4f(r_{3e})\right] - 3F(\rho_e) \quad (2.38a)$$

$$\Delta E_2^{110} = -3\phi(r_{1e}) - 2\phi(r_{2e}) - 9\phi(r_{3e}) \quad (2.38b)$$

and

$$\Delta E_1^{111} = F\left[\rho_e - \left\{3f(r_{1e}) + 3f(r_{2e}) + 9f(r_{3e})\right\}\right] + F\left[\rho_e - 3f(r_{3e})\right] - 2F(\rho_e) \quad (2.39a)$$

$$\Delta E_2^{111} = -\frac{3}{2}\phi(r_{1e}) - \frac{3}{2}\phi(r_{2e}) - 6\phi(r_{3e}). \quad (2.39b)$$

The calculated values of unrelaxed divacancy binding energy and unrelaxed surface energies are presented in Table III along with the experimental values and values obtained by other workers. The calculated E_{2V}^B values are much smaller than the

Table III. Calculated surface energies in ergs/cm^2 and binding energy of divacancy in eV.

	Cu	Ag	Au	Ni	Pd	Pt	
S_{100}	1397	1124	1268	1799	1689	2215	a
	1280	705	918	1580	1370	1650	c
	1651	1271	1084	2423	1659	2167	d
S_{110}	1482	1183	1355	1900	1796	2339	a
	1440	770	980	1730	1490	1750	c
	1642	1271	1115	2384	1670	2131	d
S_{111}	1290	1025	1104	1671	1522	1940	a
	1170	620	790	1450	1220	1440	c
	1409	1087	886	2036	1381	1656	d
S_{av}^{exp}	1770	1320	1540	2240	2000	2500	b
E_{2V}^{B}	0.1369	0.102	0.0304	0.2157	0.1280	0.066	a
E_{2V}^{B}(exp)	0.12	0.38	0.2-0.6	0.33	--	0.1-0.2	e
	0.27	0.22	0.22	0.40	0.34	0.45	c

a Present results

b Experimental values from reference [119]

c From reference [52]

d From reference [104]

e From reference [52] and references therein

experimental values. However, the present values determined as they are by counting the bonds and neglecting the elastic relaxations completely are unlikely to match the experimental values exactly. On the other hand, the quoted experimental values have been obtained through fitting the non-Arrhenius behaviour of vacancy concentration by a two-vacancy model which neglects the anharmonic temperature dependence of formation energies and as such, are to be taken with some caution. Apart from this uncertainty regarding the experimental values of divacancy formation energy the contribution due to relaxations to it is expected to be small compared to the bond energy contribution and, therefore, in view of considerable computational effort involved in relaxation calculation no attempt was made to include the relaxation effect in the binding energy calculations. In fact the calculations based on density functional theory in the local density approximation by Klemradt *et al* [112] give a value of divacancy binding energy equal to 0.07ev for Cu, Ni, Ag and Pd. The calculated unrelaxed surface energies for low-index surfaces (100), (110) and (111), S_{100}, S_{110} and S_{111}, respectively, are

within the range of the experimental values which are polycrystalline average values. We note that in order of increasing energy the sequence of surface energies is S_{111}, S_{100} and S_{110} for all the six metals as is expected for the fcc lattice.

As a further application of these potentials, we have calculated phonons in all the six metals. For the calculation of phonon dispersions, the force constants in the harmonic approximation are derived from the energy expression (1) in a straightforward manner. The force constants corresponding to the embedding part of the energy in the present model are

$$\frac{\partial^2 E}{\partial r_i^{\mu} \partial r_j^{\nu}} = - F_i'' \sum_{k \neq i} f_k'(r_{ik}) f_j'(r_{ij}) \frac{r_{ik}^{\mu} r_{ij}^{\nu}}{r_{ik} r_{ij}}$$

$$- F_j'' f_i'(r_{ji}) \sum_{k \neq j} f_k'(r_{jk}) \frac{r_{ji}^{\mu} r_{jk}^{\nu}}{r_{ji} r_{j}}$$

$$+ \sum_{k \neq i,j} F_k'' f_i'(r_{ki}) f_j'(r_{kj}) \frac{r_{ki}^{\mu} r_{kj}^{\nu}}{r_{ki} r_{kj}} \qquad (2.40)$$

where μ,ν are cartesian components. The force constant matrix

expression for the pair part is given by a well known term

$$\Phi_{\mu\nu}(l,l') = (\Phi'' - \frac{1}{r_{ij}}\Phi')\frac{r_{ij}^{\mu} r_{ij}^{\nu}}{r_{ij}^{2}} + \frac{1}{r_{ij}}\Phi'\delta_{\mu\nu} \qquad (2.41).$$

The calculated force constants consist of the embedding part and the pair part. The embedding contribution towards the force constants is quite small, especially for first neighbour and second neighbour interaction but for farther distant neighbours the embedding contribution becomes more effective. But in the dynamic calculation the dominant force constants come from the first neighbour interaction and the contribution from the other higher neighbours are not so much important. The force constants obtained are represented in table IV. The obtained force constants are then utilized for the calculation of phonons.The calculated phonon dispersions in Cu, Ag, Au, Ni, Pd and Pt are presented in figures 4-9 along with the experimental results from neutron scattering measurements in Cu [71], Ag [113], Au [114], Ni [115], Pd [116] and Pt [117]. The overall agreement with the experimental result is rather good in Cu, Ag and Ni; while in the remaining three metals : Au, Pd and Pt the

Table IV Force constants, calculated from the EAM potentials, consisting the embedding part and the pair part for six fcc metals in the unit of dynes/cm. The first column is the embedding part, the second column is the Morse part and the third column is the sum of both the contributions and gives the total force onstants.

Force constants	EAM	Morse	Total
Cu			
α_1	0.94380E+02	0.14764E+05	0.14858E+05
β_1	0.59570E+03	-0.84027E+03	-0.24457E+03
γ_1	-0.32260E+03	0.15605E+05	0.15282E+05
α_2	-0.55600E+03	-0.20669E+04	-0.26229E+04
β_2	0.31500E+03	0.37738E+03	0.69038E+03
α_3	-0.29430E+03	-0.38623E+03	-0.68053E+03
β_3	0.18790E+02	-0.38691E+02	-0.19901E+02
δ_3	-0.13290E+03	-0.11585E+03	-0.24875E+03
γ_3	-0.17910E+03	-0.23169E+03	-0.41079E+03

Ag

α_1	0.17690E+03	0.11131E+05	0.11308E+05
β_1	0.88930E+03	-0.45920E+03	0.43010E+03
γ_1	-0.47970E+03	0.11590E+05	0.11110E+05
α_2	-0.80650E+03	-0.14740E+04	-0.22805E+04
β_2	0.47520E+03	0.22867E+03	0.70387E+03
α_3	-0.43580E+03	-0.21774E+03	-0.65354E+03
β_3	0.39050E+02	-0.25611E+02	0.13439E+02
δ_3	-0.19050E+03	-0.64043E+02	-0.25454E+03
γ_3	-0.27620E+03	-0.12809E+03	-0.40429E+03

Au

α_1	0.35920E+03	0.90729E+04	0.94321E+04
β_1	0.21010E+04	-0.33318E+03	0.17678E+04
γ_1	-0.11370E+04	0.94061E+04	0.82691E+04
α_2	-0.19440E+04	-0.11642E+04	-0.31082E+04
β_2	0.11090E+04	0.17163E+03	0.12806E+04
α_3	-0.10350E+04	-0.15884E+03	-0.11938E+04
β_3	0.74010E+02	-0.19519E+02	0.54491E+02
δ_3	-0.46290E+03	-0.46441E+02	-0.50934E+03
γ_3	-0.63830E+03	-0.92881E+02	-0.73118E+03

Ni

α_1	0.64190E+02	0.25334E+05	0.25398E+05
β_1	0.27840E+03	-0.85345E+03	-0.57505E+03
γ_1	-0.14910E+03	0.26188E+05	0.26039E+05
α_2	-0.24610E+03	-0.31665E+04	-0.34126E+04
β_2	0.15090E+03	0.45049E+03	0.60139E+03
α_3	-0.13530E+03	-0.40795E+03	-0.54325E+03
γ_3	0.15200E+02	-0.51601E+02	-0.36401E+02
β_3	-0.57650E+02	-0.11878E+03	-0.17643E+03
δ_3	-0.88450E+02	-0.23756E+03	-0.32601E+03

Pd

α_1	0.27190E+03	0.15322E+05	0.15594E+05
β_1	0.16520E+04	-0.62638E+03	0.10256E+04
γ_1	-0.89430E+03	0.15948E+05	0.15054E+05
α_2	-0.15350E+04	-0.20243E+04	-0.35593E+04
β_2	0.86990E+03	0.31274E+03	0.11826E+04
α_3	-0.81490E+03	-0.29714E+03	-0.11120E+04
β_3	0.55060E+02	-0.35080E+02	0.19980E+02
γ_3	-0.36630E+03	-0.87355E+02	-0.45366E+03
δ_3	-0.49920E+03	-0.17471E+03	-0.67391E+03

Pt

α_1	0.57450E+03	0.17887E+05	0.18462E+05
β_1	0.28890E+04	-0.50251E+03	0.23865E+04
γ_1	-0.15580E+04	0.18390E+05	0.16832E+05
α_2	-0.26200E+04	-0.20983E+04	-0.47183E+04
β_2	0.15430E+04	0.27829E+03	0.18213E+04
α_3	-0.14150E+04	-0.24027E+03	-0.16553E+04
β_3	0.12680E+03	-0.32059E+02	0.94741E+02
δ_3	-0.61870E+03	-0.69404E+02	-0.68810E+03
γ_3	-0.89710E+03	-0.13881E+03	-0.10359E+04

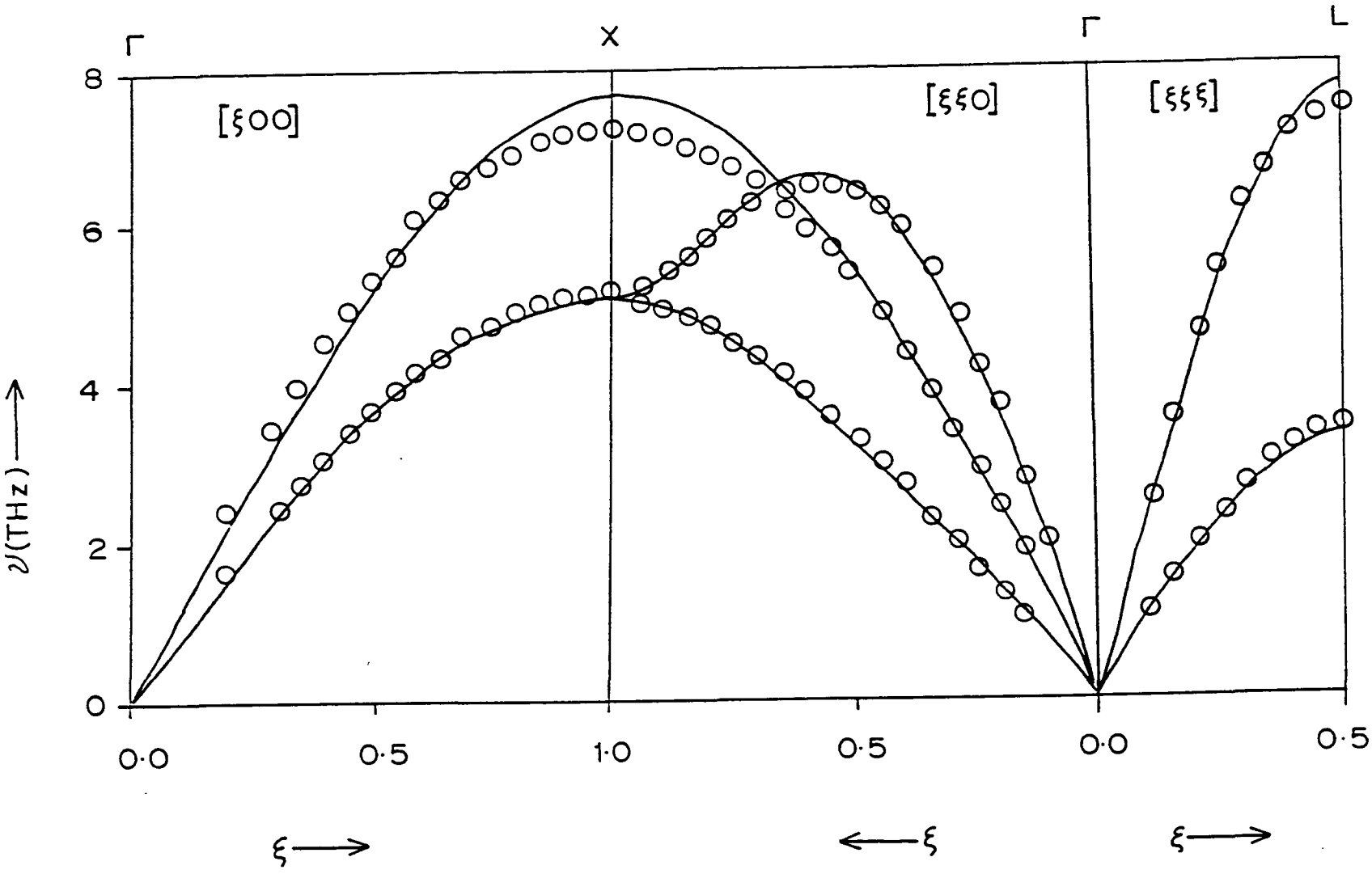

Fig. 4 : The phonon dispersion curve for Cu in high symmetry directions. Here $k = \frac{2\pi}{a}\xi$. The experimental points (o) are from Nicklow et al ref. [71].

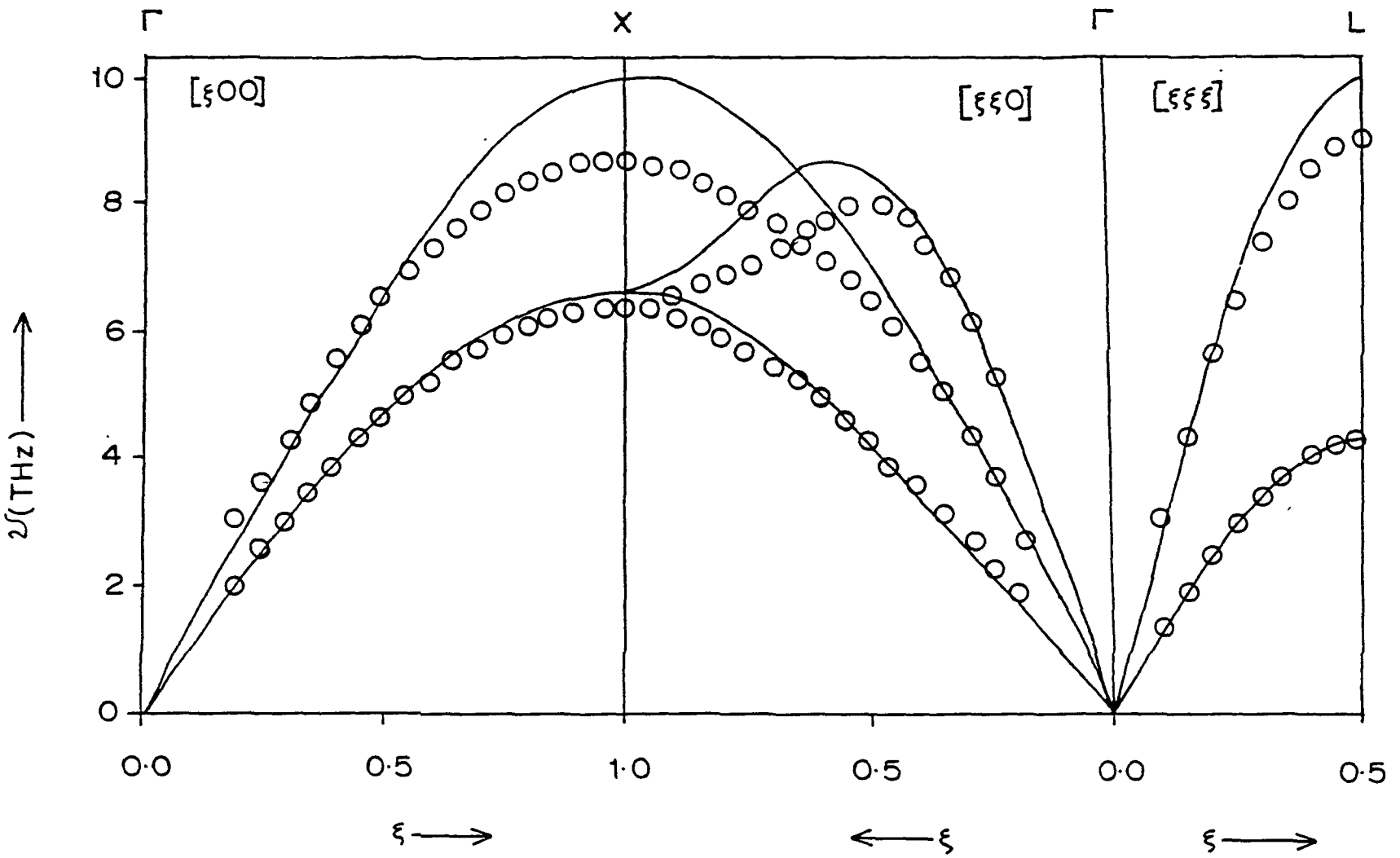

Fig. 5 : The phonon dispersion curve for Ni in high symmetry directions. Here $k = \frac{2\pi}{a}\xi$. The experimental points (o) are from Birgeneau et al ref.[115].

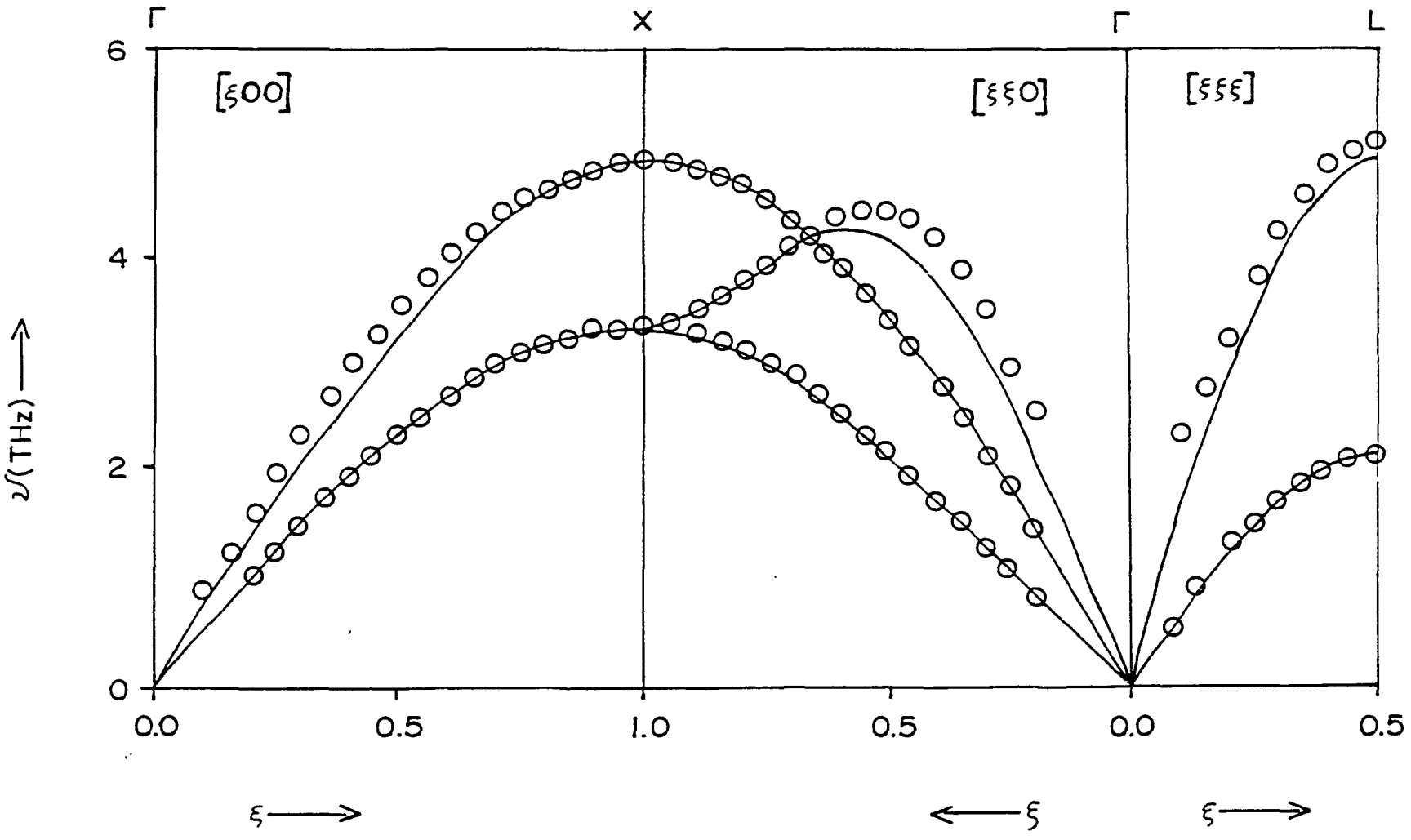

Fig. 6 : The phonon dispersion curve for Ag in high symmetry directions. Here $k = \frac{2\pi}{a}\xi$. The experimental points (o) are from Kamitakahara et al [113].

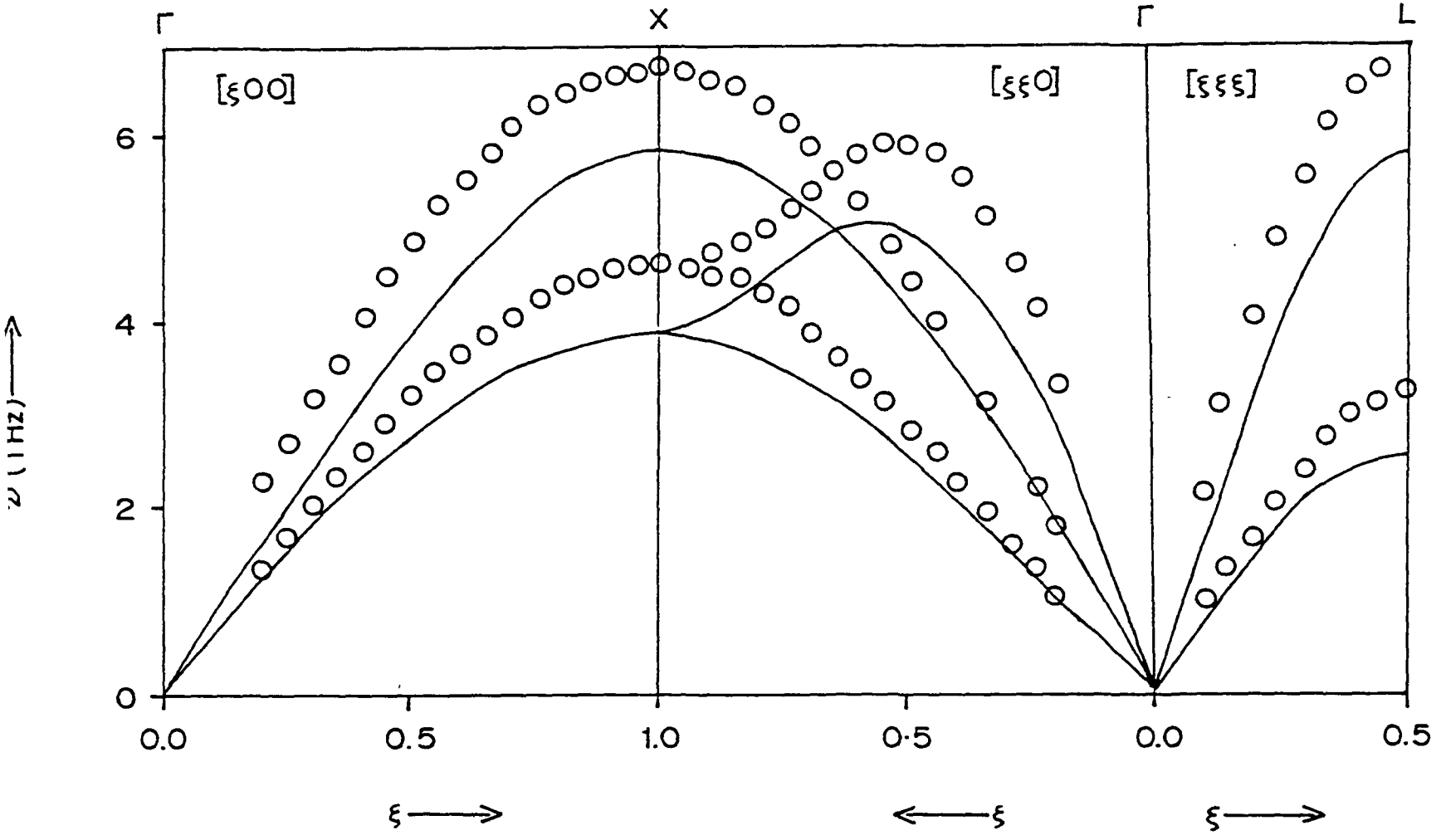

Fig. 7 : The phonon dispersion curve for Pd in high symmetry directions. Here $k = \frac{2\pi}{a}\xi$. The experimental points (o) are from Miller et al ref. [116].

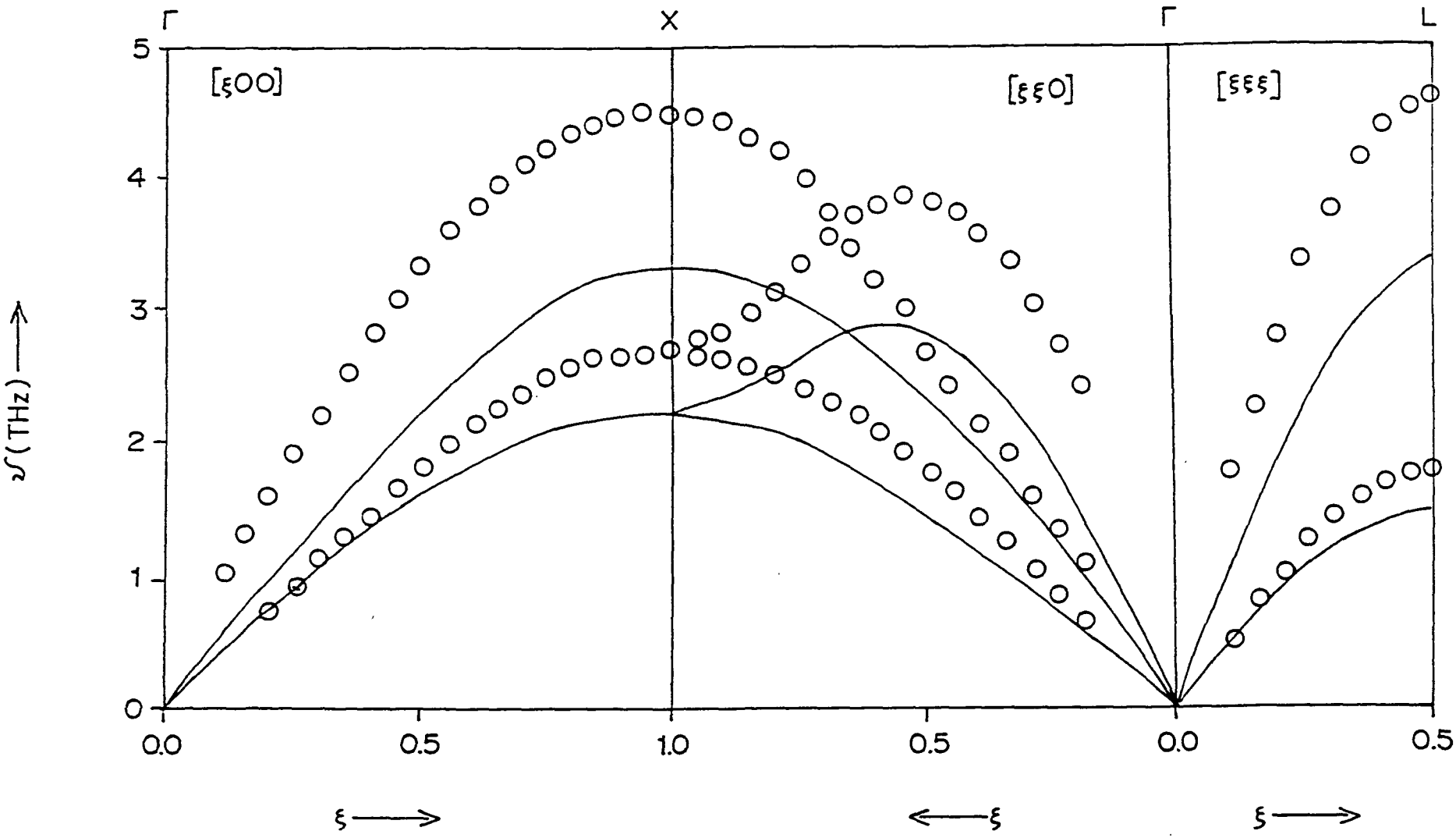

Fig. 8 : The phonon dispersion curve for Au in high symmetry directions. Here $\kappa = \frac{2\pi}{a}\xi$. The experimental points (o) are from Lynn et al ref.[114].

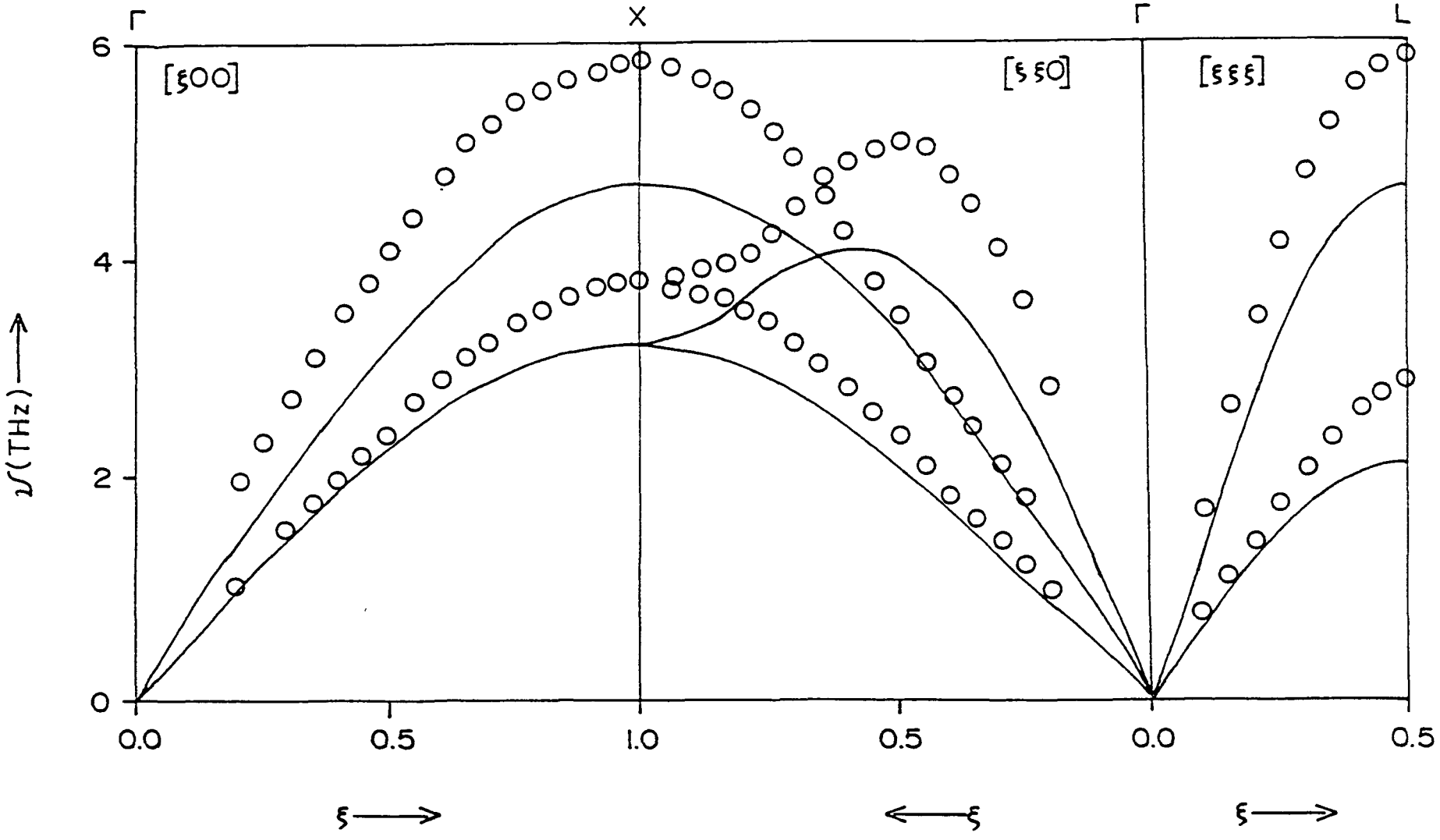

Fig. 9 : The phonon dispersion curve for Pt in high symmetry directions. Here $k = \frac{2\pi}{a}\xi$. The experimental points (o) are from Dutton et al ref.[117].

agreement is not so good, the discrepancy is maximum in the longitudinal branch in these metals; e.g., it is as large as -27% in the longitudinal [ζ00] branch of Au. The calculated phonons have been used to generate frequency spectrum of all the six metals, showing the typical behavoiur of fcc metals obtained on the basis of Born-Von Karman fits to neutron scattering results. The frequency spectrum of Cu is presented in fig. 10 as an example. The spectrum is similar to the one obtained on the basis of Born-Von Karman fits to measured phonons by Nicklow et al [71]. It is observed that the agreement with experimental phonon dispersion is better in 3d and 4d compared to 5d metals due to the effect of the core. The frequency spectrum in Cu has been used to calculate mean square displacement of an atom by using

$$\langle u^2 \rangle = \int \frac{Z(\omega)}{2M\omega} \coth \left[\frac{\hbar\omega}{2kT} \right] d\omega \qquad (2.42)$$

and has been presented in fig.11. in which experimental results from Martin and O'Connor [118] is also included. The agreement with experimental result is quite good up to a temperature 600°K. As expected, the mean square displacement varies linearly with T at high temperatures. In metals interatomic forces are long

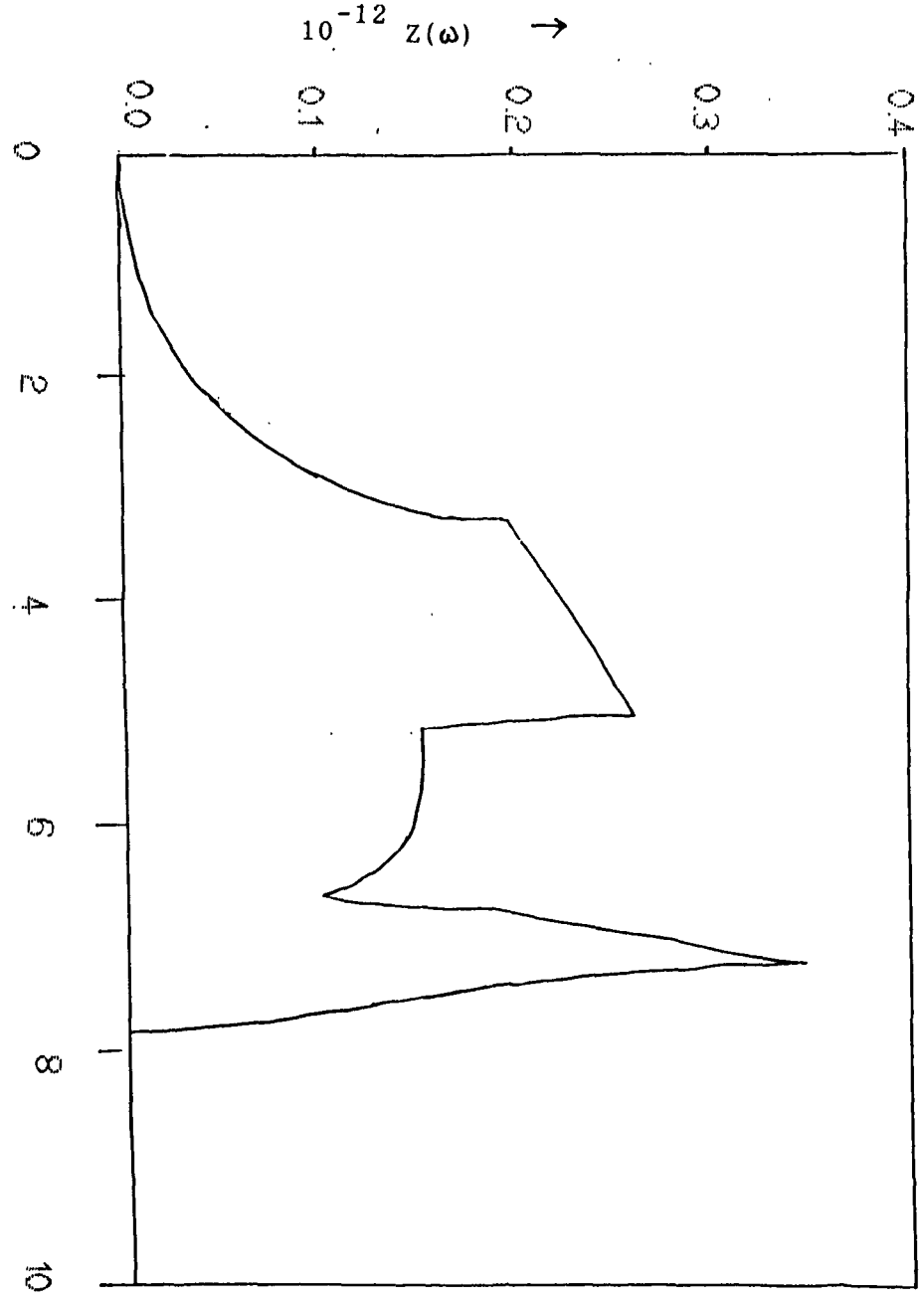

Fig. 10 : Frequency spectrum of copper

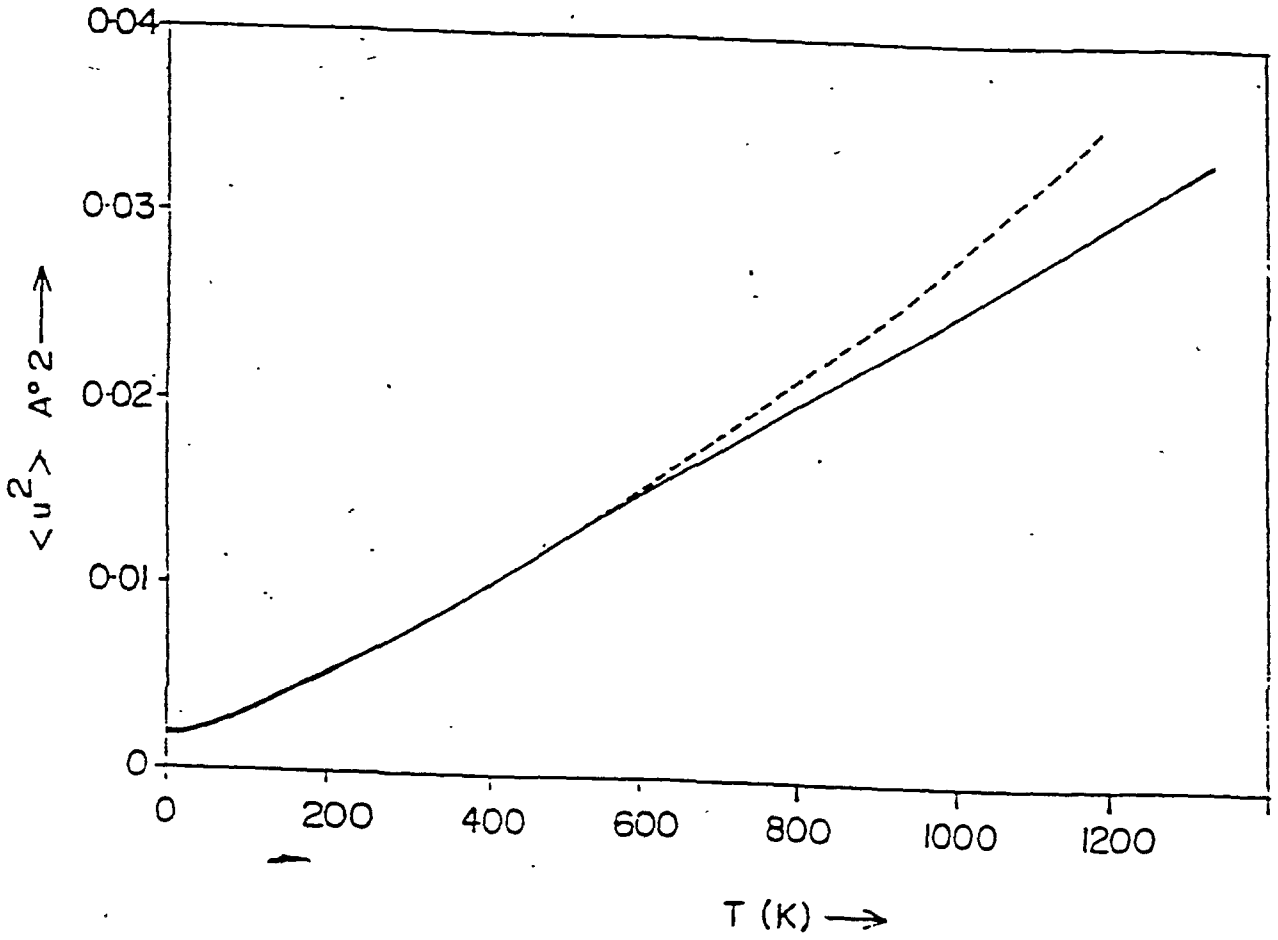

Fig. 11: Mean square displacement of an atom in copper. The experimental curve (----) is from Martin and O'Connor ref. [118].

ranged and as such the present third neighbour model may not be adequate to describe various types of deviation from perfect lattice situation, since the static properties such as defect energies involving strong distortion around the defect are well described by these potentials.

Finally we have examined the stability of the fcc structure by calculating the energies of the bcc phase. The different distances for bcc structure are expressed in terms of the fcc neighbours' distances, maintaining the volume to be constant. The distance relations are given below :

$$\left\{ r_{1e} \right\}_{bcc} = 0.972 \left\{ r_{1e} \right\}_{fcc}$$

$$\left\{ r_{2e} \right\}_{bcc} = 1.122 \left\{ r_{1e} \right\}_{fcc}$$

$$\left\{ r_{3e} \right\}_{bcc} = 1.587 \left\{ r_{1e} \right\}_{fcc}$$

$$\left\{ r_{4e} \right\}_{bcc} = 1.861 \left\{ r_{1e} \right\}_{fcc}$$

in the third neighbour model interaction for fcc metals, the interaction extends up to fourth neigbours in bcc metals at the same volume. The equilibrium electron density is given by

$$\left(\rho_e\right)_{bcc} = 8fe\left(\frac{(r_{1e})_{fcc}}{(r_{1e})_{bcc}}\right)^{n} + 6fe\left(\frac{(r_{1e})_{fcc}}{(r_{2e})_{bcc}}\right)^{n} + 12fe\left(\frac{(r_{1e})_{fcc}}{(r_{3e})_{bcc}}\right)^{n} + 24fe\left(\frac{(r_{1e})_{fcc}}{(r_{4e})_{bcc}}\right)^{n} \quad (2.43)$$

The embedding function becomes

$$F\left(\rho_e\right)_{bcc} = F\left(\rho_e\right)_{fcc}\left[1 - \gamma \ln\left(\frac{(\rho_e)_{bcc}}{(\rho_e)_{fcc}}\right)\right]\left(\frac{(\rho_e)_{bcc}}{(\rho_e)_{fcc}}\right)^{\gamma} \quad (2.44)$$

The total cohesive energy of the bcc structure is

$$E_{c}|_{bcc} = F\left(\rho_e\right)_{bcc} + \Phi_{bcc}, \quad (2.45)$$

the pair part can be written in a very straight forward manner. The fcc structure has been found to be more stable compared to bcc structure in all the cases.

CHAPTER III

3.1 THEORY OF LOCAL DENSITY OF STATES

To study the dynamical behaviour of a crystal, the important quantity is the density of states of the phonons' modes rather than the phonons themselves because the density of states applies for perfect crystals as well as for detective crystals. Phonons can be calculated only when the crystal is having a perfect crystalinity, but when the crystal is out from the perfect crystalinity, the density of states plays a very important role. The density of states is expressed as the frequency distribution of phonon spectrum $Z(\omega)$ as given by Browers and Rosenstock [120], is defined as the number of normal modes having frequency between ω and $\omega+d\omega$ and is given by

$$Z(\omega) = \frac{1}{3N} \sum_{k\sigma} \delta\ (\omega_{k\sigma}-\omega) \qquad (3.1)$$

where the summation extends over all N phonon frequencies $\omega_{k\sigma}$ within the first Brillouin zone. The vibrational spectrum reflects the nature of dependence of $Z(\omega)$ on ω. The representation of frequency spectrum in equation (3.1) in terms of delta functions is quite general in the sense that all

representations which have been used in the literature for $Z(\omega)$ can be derived from it. The frequency spectrum calculated from the general function as seen in equation (3.1) does not refer to any particular atom of the crystal and is therefore suitable for calculating the frequency spectrum of not only an ideal crystal where all atoms behave alike with the result that the vibrational excitations (phonons) are non-interacting but also in the case of highly distorted solids where the periodicity is no longer valid. The delta function can also be used to explain the frequency spectrum of crystals with defects, where apart from the modified phonon states there is also a possibility of occurence of some characteristic modes.

The important nature of the frequency spectrum is the appearence of sharp peaks and kinks associated with the critical point originating from the periodicity of the lattice and consequently from the value of $\omega_{k\sigma}$ at certain points in the Brillouin zone. These singularites can best be understood if we write the frequency spectrum as a surface integral over the constant frequency surface $\omega = \omega_{k\sigma}$ as

$$Z(\omega) = \frac{V_c}{3(2\pi)^3} \sum_{k\sigma} \int \frac{ds}{|\nabla_k \omega_{k\sigma}|} \qquad (3.2)$$

Thus we expect singularity in $Z(\omega)$ when $\nabla_k \omega_{k\sigma} = 0$.

3.2 GREEN'S FUNCTION METHOD

There are many methods with which the density of phonons' states and also the local density of states of the defective sites can be calculated : molecular dynamics [6,8], recursion method [37-39], Green function method [1-5,34-36], etc. But in the present case we are interested with the Green's function method to calculate the phonons' density of states and the local density of states of the defective site : the local density of states of the defects and also a few neighbours. The density of states can be defined through Green's function formalism which has been found to be more suitable for defective solid. As a matter of fact the whole problem of defect lattice dynamics is elegantly discussed and several reviews on the subject are available [1,2]. In general, the theory of vibrations of crystals with point defects has progressed within the framework of the

Green's function as enunciated by Lifshitz [36]. To calculate the frequency distribution of phonon spectrum, Green's functions have been used in the harmonic approximation. From the knowledge of perfect lattice Green's functions, the Green's function for the defect lattice can also be calculated. The latter are used to calculate the local density of states of the defects.

3.2.1 Perfect Lattice Green's Function

In the case of Green's function method, we can treat the problem of lattice vibration with the help of adiabatic approximation and within the harmonic approximation with the solid following the usual cyclic boundary conditions. This is equivalent to saying that the positions of all the atoms in the defect space are not so far from the perfect crystallinity and so, the expansion of the potential function can be carried up to second terms only. Now, considering a monoatomic lattice having N unit cells, the equation of motion of the lth site atom in the direction α is

$$M(l)\ddot{u}_{\alpha}(l,t) + \sum_{l'\beta} \Phi_{\alpha\beta}(l,l')u_{\beta}(l',t) = 0 \qquad (3.3)$$

where M(l) is the mass of the atom at the lth site and $u_\alpha(l,t)$ is the displacement of that atom in the direction α. The $\Phi_{\alpha\beta}(l,l')$ is the coupling parameters or force constant matrix between atoms l and l'. The force constant matrix can be expressed in terms of the dynamical matrix for convenience.

$$D_{\alpha\beta}(l,l') = [M(l)]^{-1/2}\Phi_{\alpha\beta}(l,l')[M(l')]^{-1/2} \qquad (3.4)$$

Asumming a harmonic vibration of frequency ω, the equation of motion (3.3) in terms of the dynamical matrix, is written as

$$\sum_{l'\beta} M^{1/2}(l)[D_{\alpha\beta}(l,l') - \omega^2\delta_{\alpha\beta}\delta(l,l')]M^{1/2}(l')u_\beta(l') = \emptyset \qquad (3.5)$$

in matrix form, equation (3.5) becomes

$$L(\omega^2)u = \emptyset \qquad (3.6)$$

where

$$L(\omega^2) = M^{1/2}(D - \omega^2 I)M^{1/2} \ . \qquad (3.7)$$

The Green function is defined as the inverse of the matrix $L(\omega^2)$:

$$G(\omega) = [L(\omega^2)]^{-1}, \qquad (3.8)$$

or

$$G_{\alpha\beta}(l,l';\omega) = \frac{1}{\{M(l)M(l')\}^{1/2}} \sum_{s} \frac{U^{*}_{\alpha}(l,s)U_{\beta}(l',s)}{\omega_s^2 - (\omega + i\varepsilon)^2} \qquad (3.9)$$

where $U_{\alpha}(l,s)$ is an element of a unitary matrix which diagonalizes the dynamical matrix, so that the equation (3.6) is transformed into an eigenvalue equation

$$(D - \omega_s^2)U(s) = \emptyset \qquad (3.10)$$

where U(l,s) are the eigenvectors and ω_s^2 are the eigenvalues of the dynamical matrix D. The infinitesimal positive quantity ε has been introduced to ensure causality, i.e., the so called retarded Green's functions are used. The eigen vectors U(s) satisfy the usual orthogonality relations

$$\sum_{l\alpha} U^{*}_{\alpha}(l,s)U_{\alpha}(l,s') = \delta_{ss'} \qquad (3.11a)$$

$$\sum_{s} U^{*}_{\alpha}(l,s)U_{\beta}(l',s) = \delta_{\alpha\beta}\delta(l,l') \qquad (3.11b)$$

In the case of ideal lattice, all the masses are equal and the coupling parameters $\Phi_{\alpha\beta}(l,l')$ have the translational symmetry, therefore, the eigenfunctions U(s) can be chosen to be

plane waves labelled by a wave vector k and a polarization index σ :

$$U_{\alpha}(l,k\sigma) = (1/N)^{1/2} e_{\alpha}(k\sigma)\exp(ik.R(l)) \qquad (3.12)$$

where $e_{\alpha}(k\sigma)$ is the eigenvector of the dynamical matrix belonging to the normal mode $(k\sigma)$. Thus the ideal lattice Green's function is given by

$$\overset{\circ}{G}_{\alpha\beta}(l,l';\omega) = (1/MN)\overset{\circ}{\sum_{k\sigma}} \frac{e^{*}_{\alpha}(k\sigma)e_{\beta}(k\sigma)}{\omega^{2}_{k\sigma} - (\omega + i\varepsilon)^{2}} \exp(ik.R(l)-R(l')) \qquad (3.13)$$

where $\omega_{k\sigma}$ are the eigen frequencies. In the case of ideal lattice Φ is real and symmetric, then the polarization vectors can be chosen as real, then

$$U^{*}(k) = U(-k) \text{ and } \omega_{k\sigma} = \omega_{-k\sigma}.$$

The exponential in equation (3.13) can be replaced by cos(k.R(l-l')) and therefore

$$\overset{\circ}{G}_{\alpha\beta}(l,l';\omega) = \overset{\circ}{G}_{\alpha\beta}(|l-l'|;\omega) = \overset{\circ}{G}_{\beta\alpha}(|l-l'|;\omega). \qquad (3.14)$$

Using the identity

$$1/(x - i\varepsilon) = P(1/x) + i\pi\delta(x) \qquad (3.15)$$

we can write the real and imaginary part of the Green's function as

$$\mathrm{ReG}^{\circ}_{\alpha\beta}(1,1';\omega) = (1/MN)\sum_{k\sigma} P \frac{e_{\alpha}(k\sigma)e_{\beta}(k\sigma)}{\omega^{2}_{k\sigma} - \omega^{2}} \exp(ik.R(1)-R(1'))$$

$$= \mathrm{ReG}^{\circ}_{\alpha\beta}(1,1';-\omega) \qquad (3.16)$$

$$\mathrm{ImG}^{\circ}_{\alpha\beta}(1,1';\omega) = (\pi/MN)(\mathrm{sgn}\omega)\sum_{k\sigma} e_{\alpha}(k\sigma)e_{\beta}(k\sigma)\ (\omega^{2}_{k\sigma}-\omega^{2})\ \exp(ik.R(1)-R(1$$

$$= - \mathrm{ImG}^{\circ}_{\alpha\beta}(1,1';-\omega) \qquad (3.17)$$

Obviously

$$G(\omega) = G^{*}(-\omega).$$

The real and imaginary parts of the Green's functions are not independent of each other but they are related to each other by the Kramers-Kronig relation

$$\mathrm{Re}\ G(\omega) = \frac{1}{\pi} \int d\omega' P \frac{1}{\omega'^{2} - \omega^{2}} \mathrm{Im}\ G(\omega'). \qquad (3.18)$$

The properties of Green's functions including their numerical calculation, which are quite useful for practical applications, have been discussed by Dederichs and Zeller [2] and Ram [46].

3.2.2 GREEN'S FUNCTION FOR THE DEFECT LATTICE

In the matrix form the Green's function for the defect lattice may be given by

$$(\Phi - M\omega^2)\, G(\omega) = 1 \qquad (3.19)$$

While that of the ideal lattice is given by

$$(\overset{\circ}{\Phi} - \overset{\circ}{M}\omega^2)\, \overset{\circ}{G}(\omega) = 1 \qquad (3.20)$$

where the quantities pertaining to ideal lattice are denoted by an upper index $\circ$, e.g., $\overset{\circ}{\Phi}, \overset{\circ}{M}$ etc. In general the force constant matrix Φ and the mass M of the defect lattice differ from the quantities $\overset{\circ}{\Phi}$ and $\overset{\circ}{M}$ in the ideal lattice.In the case of vacancies and interstitials the total number of atoms are also different.

For substitutional impurity, the force constants around the impurity atom are changed in addition to the mass change at the impurity site. In general, the change in force constants far away from the impurity is negligibly small and only changes in the

force constants between the defect and its immediate neighbours are considered. Then the Green's function for the defect lattice is evaluated in terms of the ideal lattice Green's function and the "perturbation" which is strongly localized in space.

Assuming only one impurity atom, we write equation (3.19) as

$$(\overset{\circ}{\Phi} - \overset{\circ}{M}\omega^2 + V(\omega))G(\omega) = 1 \qquad (3.21)$$

where

$$V(\omega) = \Phi - \overset{\circ}{\Phi} - (M - \overset{\circ}{M})\omega^2$$
$$= \Delta\Phi - \Delta M\omega^2 \qquad (3.22)$$

is the perturbation matrix. From equation (3.21) the Green's function for the defect crystal is obtained to be

$$G(\omega) = \overset{\circ}{G}(\omega) - \overset{\circ}{G}(\omega)V(\omega)G(\omega). \qquad (3.23)$$

This can be directly solved for Green's function $G(\omega)$ as

$$G(\omega) = (1 + \overset{\circ}{G}V)^{-1}\overset{\circ}{G} = \overset{\circ}{G}(1 + V\overset{\circ}{G})^{-1} \qquad (3.24)$$

An equivalent expression for $G(\omega)$ can be obtained by inserting expression (3.24) into the right-hand side of expression (3.23)

$$G(\omega) = \overset{o}{G} - \overset{o}{G}\overset{o}{V}\left(1 + \overset{o}{G}\overset{o}{V} \right)^{-1}\overset{o}{G} = \overset{o}{G} - \overset{o}{G}\overset{o}{t}(\omega)\overset{o}{G}. \qquad (3.25)$$

where we have introduced the so called t-matrix

$$t = V \left(1 + \overset{o}{G}V \right)^{-1}. \qquad (3.26)$$

In this way the Green's function for the defect lattice can be expressed in terms of the ideal lattice Green's function and the t-matrix which is localized to the defect space spanned by the impurity and its immediate neighbours where there is a force constant change. In order to calculate $t(\omega)$ we have to invert the finite matrix $\left(1 + \overset{o}{G}V \right)$ with dimension 3n, if n is the number of atoms affected by the perturbation. The use of Group theory by exploiting the point symmetry of the impurity can further reduce the problem.

To appreciate the two equivalent expressions for the defect lattice Green's function we write the equation of motion of the perturbed crystal once again

$$(\overset{\circ}{\Phi} - \overset{\circ}{M}\omega^2 + V(\omega))u = \emptyset. \qquad (3.27)$$

The effect of perturbation on the vibrations of the lattice may be interpreted in at least two distinct ways. First the equation (3.27) may be viewed as a scattering problem.In this case one can calculate the scattering matrix and look for the resonances. In this case the expression (3.25) for the defect Green's function in terms of the t-matrix is relevant. Alternatively, equation (3.27) may be viewed as an eigenvalue problem similar to the perfect lattice but with changed values of some of the elements of the dynamical matrix. In this case the solutions are new set of frequencies and eigenvectors and the defect Green's function can be evaluated exactly like perfect lattice Green's functions. The two descriptions can be made to correspond to each other if we note that the resonant scattering in the first case corresponds to the second description to normal modes at the same frequencies having large amplitudes of vibration in the vicinity of the defect than at other locations in the lattice. The choice of a particular description largely depends upon the convenience and suitability to a particular problem. However, in the actual

applications the Green's function for the defect lattice can always be computed in terms of the perfect lattice Green's function and perturbation.

The theory outlined above for substitutional impurities is not directly applicable to the case of interstitials where additional degrees of freedom are introduced into the lattice. However, viewed as an eigenvalue problem the additional degrees of freedom hardly creates any complication, it is only while aplying the t-matrix theory that care has to be taken in evaluating the perturbation matrix $v(\omega)$. In the present thesis, equation (3.27) is treated as an eigenvalue problem, where we follow an alternative formulation of the defect problem as has been proposed by Litzmann and Rosza [121], Krumhansl and Mathews [46] and others [122]. Dederichs and Zeller [2,123] have used this method to discuss the resonance and localized defect vibrations and have derived some important relations about the local vibrational behaviour of point defects. The method is particularly suitable for interstitials where additional degrees of freedom introduced by the defect are treated in a natural way on equal footing like any other coordinate in the problem. We get

a direct description of the local vibrational properties of the defect in the sense that the description has a simple Einstein oscillator like structure.

The whole space of all atoms has been divided into a central subspace C containing the defect and its immediate neighbours (in most cases the defect alone) and the subspace R containing the other remaining atoms. The force constant matrix has been partitioned as

$$\Phi = \begin{pmatrix} \Phi_{CC} & \Phi_{CR} \\ \Phi_{RC} & \Phi_{RR} \end{pmatrix} = \begin{pmatrix} \Phi_{CC} & \Phi_{CN} & 0 \\ \Phi_{NC} & \Phi_{NN} & \Phi_{NU} \\ 0 & \Phi_{UN} & \Phi_{UU} \end{pmatrix} \qquad (3.28)$$

where Φ_{CC} is the Einstein coupling of the central region when the rest lattice is in the frozen state, Φ_{RR} is the coupling of the atoms in the rest lattice while the defect is fixed and Φ_{CR} describes the coupling of the defect with the neighbours in the rest lattice. The right hand side of equation (3.28) shows that the subspace R can be further split up into a neighbour region N, consisting of all atoms which are either directly coupled to the central region or for which force constants are changed, and into

an unperturbed subspace U of host atoms such that in this the coupling constants are unchanged, i.e., $\Phi_{NU} = \overset{\circ}{\Phi}_{NU}$ and $\Phi_{UU} = \overset{\circ}{\Phi}_{UU}$. Similar to the coupling matrix Φ we write the Green's function and mass matrices in the partitioned form :

$$G = \begin{pmatrix} G_{CC} & G_{CR} \\ G_{RC} & G_{RR} \end{pmatrix} M = \begin{pmatrix} M_{CC} & \emptyset \\ \emptyset & M_{RR} \end{pmatrix} \tag{3.29}$$

By inserting the partitioned form of the quantities in equation (3.19) we get

$$(\Phi_{CC} - M_{CC}\omega^2)\, G_{CC} + \Phi_{CR} G_{RC} = 1 \tag{3.30}$$

$$\Phi_{RC} G_{CC} + (\Phi_{RR} - M_{RR}\omega^2) G_{RC} = \emptyset \tag{3.31}$$

$$\Phi_{RC} G_{CR} + (\Phi_{RR} - M_{RR}\omega^2) G_{RR} = 1 \tag{3.32}$$

$$(\Phi_{CC} - M_{CC}\omega^2) G_{CR} + \Phi_{CR} G_{RR} = \emptyset \tag{3.33}$$

Equations (3.30) and (3.31) couples the Green's function $G_{CC}(\omega)$ of the defect, i.e., the displacement of the defect, with Green's function $G_{RC}(\omega)$ i.e., the atomic displacements in the rest

lattice due to unit force on the defect. Similarly equations (3.32) and (3.33) describes the coupling of the Green's function for the rest of the lattice $G_{RR}(\omega)$ with the Green's function $G_{CR}(\omega)$. From equations (3.30) to (3.33), the Green's functions G_{CC}, G_{RR}, G_{CR} and G_{RC} are easily determined :

$$G_{CC} = (\Phi_{CC} - \Phi_{CR}\hat{G}_{RR}\Phi_{RC} - M_{CC}\omega^2)^{-1} \tag{3.34}$$

$$G_{RR} = (\Phi_{RR} - \Phi_{RC}\hat{G}_{CC}\Phi_{CR} - M_{RR}\omega^2)^{-1} \tag{3.35}$$

$$G_{RC} = - \hat{G}_{RR}\Phi_{RC}G_{CC} \tag{3.36}$$

$$G_{CR} = - G_{CC}\Phi_{CR}\hat{G}_{RR} = \tilde{G}_{RC} \tag{3.37}$$

where $\tilde{G}_{RC}$ is the transpose of G_{RC}. Here $\hat{G}_{RR} = (\Phi_{RR} - M_{RR}\omega^2)^{-1}$ describes the vibration of the atoms in the rest lattice when the interstitial is fixed and $\hat{G}_{CC} = (\Phi_{CC} - M_{CC}\omega^2)^{-1}$ describes the Einstein vibrations of the interstitial. The Green's function $G_{CC}(\omega)$ determines the local vibrational properties of the interstitial which is more easily elucidated if we put in terms of the effective force constant [2]

$$G_{CC} = (\Phi^{eff}_{CC}(\omega) - M_{CC}\omega^2)^{-1}, \tag{3.38}$$

where

$$\Phi^{eff}_{CC}(\omega) = \Phi_{CC} - \Phi_{CR}\hat{G}_{RR}(\omega)\Phi_{RC} \tag{3.39}$$

is the effective coupling of the defect when it is embedded in the lattice. Clearly equation (3.38) has the form of Einstein approximation for the interstitial region where the correction $-\Phi_{CR}\hat{G}_{RR}(\omega)\Phi_{RC}$ to the Einstein term Φ_{CC} describes the effect of the dynamic relaxations of the atoms in the rest lattice. The poles or quasipoles of $G_{CC}(\omega)$ are the perturbed frequencies of the interstitial subspace. For determining $G_{CC}(\omega)$, first $\hat{G}_{RR}(\omega)$ has to be determined. For the case of interstitial the subspace R contains all the atoms of the ideal lattice and $\hat{G}_{RR}$ can easily be calculated in terms of the ideal lattice Green's function $\overset{\circ}{G}$ in exactly the same way one [illegible] for the case of substitutional impurities (Equation (3.25)):

$$\hat{G} = \overset{\circ}{G} - \overset{\circ}{G}t\overset{\circ}{G} \tag{3.40}$$

where t-matrix is given by

$$\hat{t} = V_{RR}\left(1 + \overset{\circ}{G} V_{RR}\right)^{-1}, \qquad (3.41)$$

with

$$V_{RR} = \Phi_{RR} - \overset{\circ}{\Phi} - \left(M_R - \overset{\circ}{M} \right)\omega^2, \qquad (3.42)$$

i.e., only force constant changes in the space of the rest lattice are involved. In the calculation of the t-matrix, one has to invert a complex matrix of dimension 3 times the number of perturbed atoms in the subspace R.

The Green's function $G_{RR}(\omega)$ is especially useful for the interstitial problem since it gives the vibrations of the host material in the presence of interstitial by eliminating the additional degrees of freedom due to its presence. The elimination of interstitial coordinates leads to an effective coupling between the lattice atoms. Again the expression for G_{RR} (equation (3.35)) has the simple Einstein oscillator like structure. The term $-\Phi_{RC}\hat{G}_{CC}\Phi_{CR}$ represents the interstitial reaction to the lattice system. Thus $G_{RR}(\omega)$ describes the collective motion of the lattice giving the perturbed phonons of the defect lattice. Again G_{RR} can

be calculated by standard Green's function method

$$G_{RR} = (\overset{\circ}{\Phi} - \overset{\circ}{M}\omega^2 + \tilde{V}_{RR})^{-1} = \overset{\circ}{G} - \overset{\circ}{G}\tilde{V}_{RR}G_{RR}, \tag{3.43}$$

if we add to the perturbation V_{RR} the interstitial induced reaction between the host atoms

$$\tilde{V}_{RR} = V_{RR} - \Phi_{RC}\hat{G}_{CC}\Phi_{CR}. \tag{3.44}$$

In terms of the t-matrix G_{RR} is given by

$$G_{RR} = \overset{\circ}{G}t\overset{\circ}{G} \tag{3.45}$$

with

$$\tilde{t} = \tilde{V}_{RR}(1 + \overset{\circ}{G}\tilde{V}_{RR})^{-1}. \tag{3.46}$$

Compared with the standard Green's function method, the advantage of the presence method lies in the fact that the Green's function $G_{CC}(\omega)$ of the defect is described by an Einstein-type force constant $\Phi_{CC}^{eff}(\omega)$ which gives the local vibrational properties of the defect. However the numerical effort is same in both the cases.

3.2.3 CONNECTION BETWEEN THE DENSITY OF STATES AND GREEN'S FUNCTIONS

The local density of states is one of the most affected physical quantities due to the presence of the defect and the calculation of this function helps to calculate the other properties of the defects, especially the thermodynamical properties. The density of states can be expressed in terms of the imaginary part of the Green's functions. Here we present the same site ideal lattice Green's function at the site l as

$$G_{\alpha\alpha}(l,l,\omega) = \frac{1}{MN} \sum_{k\sigma} \frac{e_{\alpha}(k\sigma)\ e_{\beta}(k\sigma)}{\omega_{k\sigma}^{2} - (\omega + i\varepsilon)^{2}} \qquad (3.47)$$

Making use the orthonormality of the polarization vectors, we can write

$$\mathrm{Im} \sum_{\alpha} \overset{\circ}{G}_{\alpha\alpha}(l,l;\omega) = \frac{\pi}{MN} \mathrm{Sgn}\omega \sum_{k\sigma} \delta(\omega_{k\sigma}^{2} - \omega^{2})$$

$$= \frac{\pi}{MN} \frac{1}{2\omega} \sum_{k\sigma} \delta(\omega_{k\sigma} - \omega), \qquad \omega > 0. \qquad (3.48)$$

Summing all the lattice sites we have

$$\mathrm{Im}\sum_{l\alpha}{}^{\circ}G_{\alpha\alpha}(l,l;\omega) = \frac{\pi}{2M\omega}\sum_{k\sigma}\delta(\omega_{k\sigma}^{2} - \omega^{2}) = \frac{\pi}{2M\omega}\,{}^{\circ}Z(\omega), \qquad (3.49)$$

where ${}^{\circ}Z(\omega) = \sum_{k\sigma}\delta(\omega_{k\sigma} - \omega)$ is the total density of states of the ideal lattice , i.e., the number of frequencies in the interval $(\omega, \omega+d\omega)$. Equation (3.49) shows that the total density of states can be expresses as the sum of the imaginary parts of the same site Green's functions over all the sites. Alternatively, it can be interpreted that the total density of states is expressed as the sum of the densities of all the atoms in the lattice, though in the perfect lattice all such densities of all the atoms are identical.

3.2.4 Local Density of States

The local density of states of a defect provides an important quantity to discuss the various physical properties in the defect lattice. This suggests the way to define in a non-ideal lattice, the so called local density of states of the atom l in the αth direction. The local density of states may be expressed in as the immaginary parts of the Green's functions as

$$Z_{\alpha}(l,\omega) = \frac{2\omega M(l)}{\pi} \text{ Im } G_{\alpha\alpha}(l,l';\omega) \qquad (3.50)$$

We can write the imaginary part of the same site Green's functions in terms of the eigenvectors U(l,s) of the dynamical matrix and then

$$Z_{\alpha}(l,\omega) = \sum_{s} |U_{\alpha}(l,s|^{2}\delta(\omega_{s}-\omega), \qquad \omega > 0.$$

We note that

$$\int_{0}^{\alpha} d\omega \; Z_{\alpha}(l,\omega) = \sum_{s} |U_{\alpha}(l,s)|^{2} = 1, \qquad (3.51)$$

i.e., the spectrum $Z_{\alpha}(l,\omega)$ is normalized with respect to ω. $Z_{\alpha}(l,\omega)$ gives the number of frequencies in the interval $(\omega, \omega+d\omega)$ multiplied by the square of the amplitude of the atom l in the α-direction. Thus we see that the local density of states is the quantitative measure of the number of modes contributing to the vibrational behaviour of an atom. In the case of defect lattice the quantity $Z_{\alpha}(l,\omega)$, generally is different for different lattice sites and direction.

3.2.5 Frequency Spectrum of a perturbed Crystal :

The vibrational behaviour of a perturbed crystal is strongly influenced by the defect and few of its close neighbours. The presence of the defect in the crystal changes the frequencies of the normal modes of the crystal and hence results to the excitations of certain characteristic modes, resonance and localized modes. These defect modes appear in the local frequency spectrum of the defect and some of the close neighbours. The resonance modes are not the exact eigenstate of the perturbed crystal and their frequencies always lie within the in-band spectrum of the host; consequently, even in the harmonic approximation resonance modes have a finite width due to the interaction with the normal modes of the host spectrum. On the other hand the localized modes are exact eigenstates of the perturbed crystal and are non-propagating in nature and have a delta function type of peaks in the frequency spectrum.

In order to evaluate the defect-induced changes of some additive functions of normal mode frequencies e.g., thermodynamic functions one needs to calculate the change in frequency spectrum

due to defects. For low concentration c of defects, the change in total spectrum is linear in c.

$$\Delta Z(\omega) = N_d \Delta z(\omega) \tag{3.52}$$

where $N_d = cN$ is the total number of defects present in the crystal.

The calculation of $\Delta Z(\omega)$ has been discussed, among others, by Dederichs and Zeller [2] and P.N. Ram [46]. In terms of local density of states it is given by

$$\Delta Z(\omega) = \sum_{l\alpha} \left[Z_\alpha(l,\omega) - \overset{\circ}{Z}_\alpha(l,\omega) \right] \tag{3.53}$$

since the perturbation is confined to atoms within the defect space, the sum over α, l is replaced by

$$\Delta Z(\omega) = 3N_d \sum_{d} \left[Z(d,\omega) - \overset{\circ}{Z}(d,\omega) \right] \tag{3.54}$$

where d refers to atoms in the defect space and the local density of states of atom 'd' is the average over cartesian components.

$$Z(d,\omega) = \frac{1}{3}\sum_{\alpha} Z_{\alpha}(d,\omega). \qquad (3.55)$$

Obviously, the features in $\Delta Z(\omega)$ are dominated by the local density of states of the defect atoms and few of its closest neighbours.

3.3 Application of the Local Density of States to Thermodynamic Properties

The local density of states of the defect and its neighbours play very important role in the defect studies since most of the defect properties are reflected through them especially that of the defect. So, from the obtained local density of states, many important physical properties can be calculated.The occurrence of resonance modes is signalled by the increase in the density of states near the resonant frequencies, while localized modes are identified as additional peaks in the spectrum. Very often the characteristic modes are dominated by the vibrations of the defect and a few of its neighbours, and,

therefore the local density of states of the defect and its neighbours are important in the calculation of many thermodynamic properties of the defect crystals.

3.3.1 Calculation of the thermal displacements and thermal velocities

As pointed out earlier, the presence of the resonance modes increases the thermal displacements of the atoms in the defect space. The mean-square thermal displacements for the defects can be expressed in terms of the local density of states as

$$\langle u_\alpha \rangle = \int \frac{Z_\alpha(d,\omega)}{M\omega^2} \varepsilon(\omega,T)\, d\omega, \qquad (3.56)$$

where $\varepsilon(\omega,T) = \frac{\hbar\omega}{2}\coth\left(\frac{\hbar\omega}{2kT}\right)$ (3.57)

As it is, the thermal displacements squared is the integral of the local density of states weighted by $1/\omega^2$. The occurrence of the low-frequency resonance modes is expected to increase the thermal displacement of the SIAs by a large amount. In case of the vacancies the thermal displacements of the first neighbours

are expected to be changed most but the effect is much less compared to the SIAs. The energy expression $\varepsilon(\omega,T)$ can be expressed in the limiting cases of low and high temperatures. At very low temperatures

$$\varepsilon(\omega,T) \longrightarrow \hbar\omega/2 \qquad \text{for } kT \ll \hbar\omega$$

and at very high temperatures $\varepsilon(\omega,T) \longrightarrow kT$ for $kT \gg \hbar\omega$ and, therefore we have

$$\langle u_\alpha^2 \rangle = \begin{cases} (\hbar/2M)\langle 1/\omega \rangle & \text{for } kT \ll \hbar\omega \\ (kT/M)\langle 1/\omega^2 \rangle = kTG_{\alpha\alpha}(d,d;\emptyset) & \text{for } kT \gg \hbar\omega \end{cases} \qquad (3.58)$$

We see that even at very low temperatures the thermal displacement is large due to the presence of low frequency resonance mode. At high temperatures $\langle u_\alpha^2 \rangle$ is especially large and increases linearly with temperatures due to increasing thermal population of resonance modes. Evidently in the classical limit of high temperatures displacement correlations are independent of masses.

The mean square thermal velocities of the defects can also be expressed in terms of the local density of states. It can be

written as

$$\langle v^2 \rangle = \int \frac{Z_\alpha(d,\omega)}{M_d} \varepsilon(\omega,T)\,d\omega \qquad (3.59)$$

Again in the limiting case of low and high temperature, we get

$$\langle v^2 \rangle = \begin{cases} (\hbar/2M_d) \int \omega Z_\alpha(d,\omega)\,d\omega = (\hbar/2M_d)\langle\omega\rangle & \text{for } kT \ll \hbar\omega \\ (kT/M_d) \int Z_\alpha(d,\omega)\,d\omega = kT/M_d & \text{for } kT \gg \hbar\omega \end{cases} \qquad (3.60)$$

Contrary to the case of $\langle u^2 \rangle$ the square of the thermal velocities are dominated by high frequencies at low temperatures.

3.3.2 Change in thermodynamic properties : Formation entropy

In the harmonic approximation the thermodynamic quantities are represented by additive functions of the normal mode frequencies and as a result they can be expressed as average over the frequency spectrum.

Taking advantage of the local representation of the total frequency spectrum we can express the thermodynamical quantities in terms of the local frequency spectra of all the atoms in the

lattice. Thus the thermodynamic function X(T) is expressed as

$$X(T) = \sum_{\alpha l} \int x(\omega,T) Z_{\alpha}(l,\omega) d\omega \qquad (3.61)$$

and the change in the property is

$$\Delta X(T) = \sum_{\alpha l} \int x(\omega,T) \left\{ Z_{\alpha}(l,\omega) - \overset{\circ}{Z}_{\alpha}(l,\omega) \right\} d\omega \qquad (3.62)$$

In the limit of the low concentration of the defects the change in $\Delta X(T)$ is given by

$$\Delta X(T) = 3N_d \int x(\omega,T) \left\{ \sum_{d} \left[Z(d,\omega) - \overset{\circ}{Z}(d,\omega) \right] \right\} d\omega \qquad (3.63)$$

This expression helps to calculate the defect-induced changes in thermodynamic properties utilizing the local frequency spectra of the defect and its immediate neighbours.

Leaving apart a negligible small electronic contribution , the vibrational contribution to the entropy is given by

$$S = k \sum_{s} \sigma(\omega_s, T), \qquad (3.64)$$

with

$$\sigma(\omega,T) = \frac{\hbar\omega/kT}{\exp(\hbar\omega/kT) - 1} - \ln\left[1 - \exp(-\hbar\omega/kT)\right]. \quad (3.65a)$$

In the classical limit of high temparatures , the expression for $\sigma(\omega,T)$ reduces to

$$\sigma(\omega,T) = 1 - \ln(\hbar\omega/kT). \quad (3.65b)$$

With the use of total frequency spectrum, the entropy is expressed as

$$S = k \int_0^\infty \sigma(\omega,T)\ Z(\omega)\ d\omega \quad , \quad (3.66)$$

whereas the formation entropy is given by

$$S_{1V}^{F} = 3k \sum_{d} \int_0^\infty \sigma(\omega,T) \left[Z(d,\omega) - \overset{\circ}{Z}(d,\omega) \right] d\omega, \quad (3.67)$$

Other thermodynamical properties of the crystal can also be calculated with the use of the density of states.

CHAPTER IV

LOCAL DENSITY OF STATES OF <100>-DUMBBELL IN FCC METALS USING EAM POTENTIALS

4.1 INTRODUCTION

The study of point defects in crystals plays an important role in understanding the problems of radiation damage in metals. In the case of self-interstitial atoms (SIAs), extensive studies have been made in the case of fcc metals regarding structures, energies and dynamics, where the <100>-dumbbell or split interstitial configurations has been found to be the most stable.

The study of the dynamics of SIAs in fcc metals has been carried out extensively by a large number of workers and many authors have reviewed the subject [44,46,54]. In the earlier

studies on the vibrational properties of the SIAs, empirical pair potentials have been used and the most striking feature about it is the presence of some characteristic modes: the low-frequency resonance modes occuring within the in-band region and the high-frequency localized modes occuring above the maximum frequency of the solid. The first experimental evidence for the existence of the resonance modes has been provided by measurements of the change in elastic constants after neutron irradiation by Rehn *et al* [17] in Cu and after electron irradiation by Robrock and Schilling [18] in Al. Strong resonant effects are expected in the phonon dispersion as has been pointed out by Wood *et al* [57] and Schober *et al* [56].

As has been pointed out in Chapter II the empirical pair potentials are not expected to model the metal properties in a realistic way and there is a need for potentials including electronic contribution to total energy of the metal. The EAM has been sucessfully applied to discuss various properties of metals including defect structure, energies etc. However, to our

knowledge no attempt has been made to apply the EAM to discuss the dynamical properties of defects in metals.

In the present Chapter, therefore, we apply the EAM potentials presented in Chapter II to discuss the dynamics of <100>-dumbbell in a typical fcc metal : copper. The EAM potential for copper is used to calculate the ideal lattice Green's function as well as for evaluating the force constant changes in the vicinity of the dumbbell. Especially we have calculated the local density of states of <100>-dumbbell in Cu. Like earlier results with empirical pair potentials we get a number of resonance and localized modes as reflected by peaks in the local frequency spectrum. However, the number of such modes as well as their frequencies are changed in the present calculation. Of special interest are the low-frequency resonance modes. The lowest frequency resonance is E_g mode, a result also found from computer simulation using pair potentials, which is instrumental in explaining many properties of irradiated metals Cu including

large negative shear modulus change and long range migration of interstitials. However, in the present calculation the other resonance mode A_{2u} appears near the maximum crystal frequency when the EAM potential is used consistently but spills to become localized mode when experimental phonons are used in the calculation of ideal lattice Green's functions, though this mode has been consistently found as a low-frequency resonance mode in calculations using pair potentials.

4.2 <100>-DUMBBELL IN FCC LATTICE.

The <100>-dumbbell configuration in fcc lattice is shown in Figure 12. The centre of the dumbbell is at a perfect lattice site which is left vacant and can be taken as the origin. Two interstitial atoms at ($\pm$x,0,0)a/2 are surrounded by 12 nearest

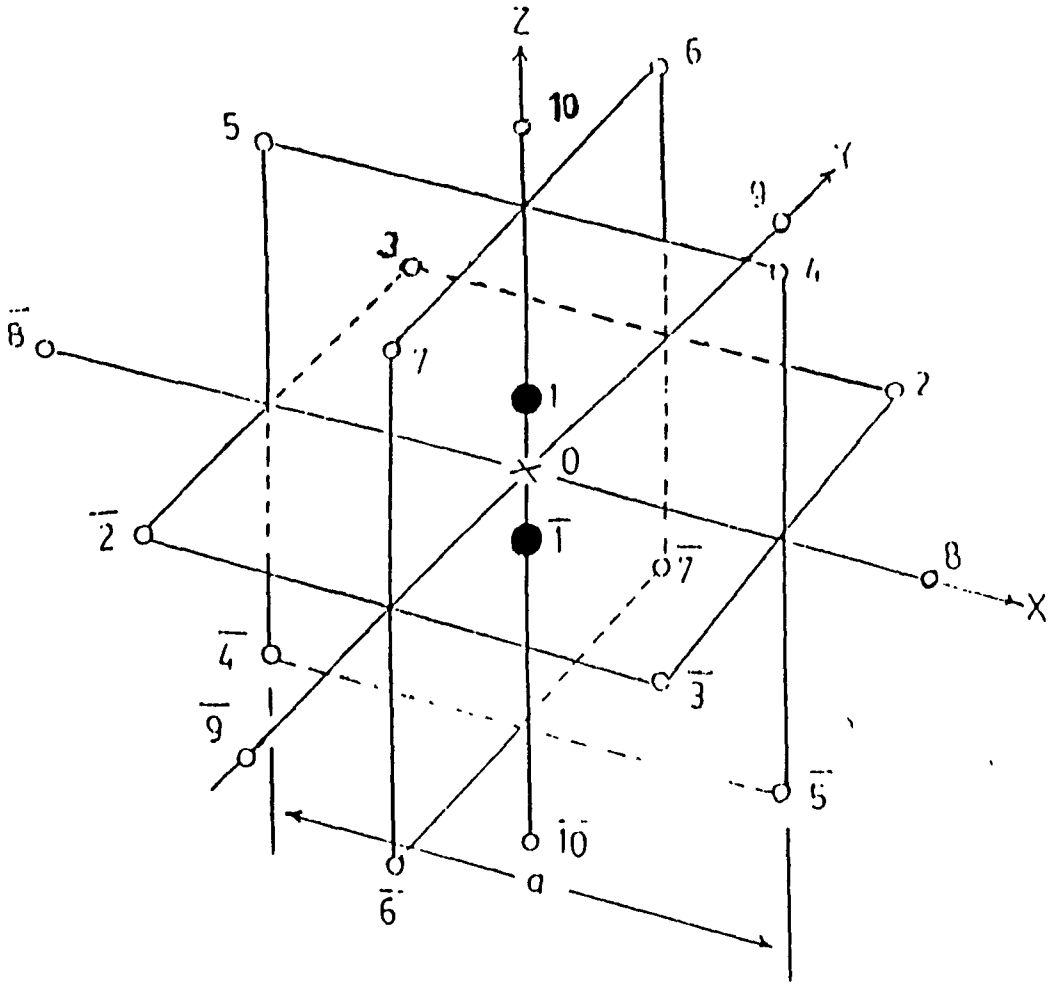

Fig. 12. Defect space of <001>-dumbbell in fcc

neighbours and 6 second nearest neighbours; altogether there are 21 lattice sites when we consider the defect to extend only up to second neighbours. Therefore one has to deal with 63x63 complex matrices. Assuming that all the neighbouring atoms are at their own lattice sites, there are seven different new distances in the defect space:

$$
\begin{aligned}
R1 &= 2xa/2 \\
R2 &= \{(1-x)2 + 1\}1/2\ a/2 \\
R3 &= \{(1+x)2 + 1\}1/2\ a/2 \\
R4 &= (2+x2)1/2\ a/2 \\
R5 &= (2-x)\ a/2 \\
R6 &= (4 + x2)1/2\ a/2 \\
R7 &= (2 + x)\ a/2\ ,
\end{aligned}
\qquad (4.1)
$$

where a is the lattice constant. The vacancy is described by zero coupling to its neighbours. Due to the presence of interstitials, the different atoms in defect space undergo relaxation and the

distances between them also change, but in this calculation such relaxations have been ignored.

The different force constants in the defect space are expressed in terms of longitudinal force constants A_l and transverse force constants, B_l (l=1,2.....7). For the pair part

$$A_l^1 = \left.\frac{d^2\phi}{dr^2}\right|_{r=r_l}$$

$$B_l^1 = \left.\frac{1}{r}\frac{d\phi}{dr}\right|_{r=r_l}. \qquad (4.2)$$

The force constants corresponding to the embedding energy are expressed as the first and second derivatives of the embedding energy as given by equation (2.6); and the electron density by equation (2.2). The force constants are :

$$A^2 = F''(\rho_e)\left\{\sum_k f'\left(r_{jk}\right)\delta_{jk}^{lJ}\right\}^2 + F'(\rho_e)\left\{\sum_k f''\left(r_{jk}\right)\delta_{jk}^{lJ}\right\}^2 \qquad (4.3a)$$

and $$B^2 = \frac{1}{r} F'(\rho_e) \sum_k f'(r_{jk}) \delta^{1j}_{jk} \qquad (4.3b)$$

where the Kronecker delta refers to the distance between the atom i and atom j (ij); and between the atom j and atom k (jk).

The first and second derivatives of the embedding energy at equilibrium in the interstitial space are expressed in terms of the ratio of equilibrium electron density in the interstitial space to that in perfect space as :

$$F'(\rho_{eI}) = -F(\rho_e) \frac{2}{\rho_e} \ln\left(\frac{\rho_{eI}}{\rho_e}\right)\left(\frac{\rho_{eI}}{\rho_e}\right)^{\gamma-1} \qquad (4.4)$$

$$F''(\rho_{eI}) = -F(\rho_e) \frac{2}{\rho_e^2}\left(\frac{\rho_{eI}}{\rho_e}\right)^{\gamma-1}\left\{1+(\gamma-1)\ln\left(\frac{\rho_{eI}}{\rho_e}\right)^{\gamma-1}\right\} \qquad (4.5)$$

The electron density in the defect site ρ_{eI} is expressed as a sum of electronic charge density of all the neighbours in the defect space.

$$\rho_{el} = f(R1) + 4f(R2) + 4f(R3) + 4f(R4) + f(R5) + 4f(R6) + f(R7). \quad (4.6)$$

Similarly charge densities at other atoms in the defect space are found.

The total force constants in the defect space is the sum of the pair part coming from the Morse form and those from the embedding function, that is the total force constants $A = A^1 + A^2$ and $B = B^1 + B^2$.

The force constants of the ideal lattice are represented by A_i^o, B_i^o, with $i = 1,2$ referring to the first and second neighbour distances. Using the force constants and the force constant changes in the defect space the force constant matrices for the host and the defect lattice, $\overset{\circ}{\Phi}$ and Φ, respectively are obtained which are then used to calculate the perturbation matrices V_{RR} or $\tilde{V}_{RR}$. The elements of the Green's function matrix G^o follow the

symmetry of ideal lattice (O_h in this case) which restricts the number of non-zero distinct elements. The number of non-zero distinct elements of $G^{o}(\omega)$ in the present model is 19.

Apart from destroying the translational symmetry of the lattice complex, defects like dumbbell interstitials cause a reduction in the site symmetry from the the cubic to some group of lower order. In the case of <100>-dumbbell the point-group symmetry is tetragonal (D_{4h}). The cartesian components of the amplitude of the displacements of the atoms from their equilibrium positions in the defect space provide basis functions for the reducible representation of the point group D_{4h}. The total defect space is decomposed into its different irreducible subspaces according to irreducible representations of the point group D_{4h} [57]:

$$\overline{D}_{4h} = 6A_{1g} + 3A_{2g} + 4B_{1g} + 3B_{2g} + 7E_g + A_{1u}$$
$$+7A_{2u} + 2B_{1u} + 3B_{2u} + 10E_u \qquad (4.7)$$

The symmetry coordinates used in the decomposition of the defect space are taken from the review by Ram [46]. The different irreducible representations together with the symmetry coordinates are useful to identify the different characteristic defect modes (resonance modes and localized modes) in the frequency spectrum of the dumbbell.

4.3 Local Density of States

The vibrational frequency spectrum of the defect can be expressed from the imaginary part of the defect Green function $G_{\alpha\alpha}(d,d;\omega)$, which is the dynamical response of the defect d in the presence of perturbation in the α-direction due to a unit

force with frequency ω on the defect d is given by equation (3.50). The defect Green's function can be projected in different subspaces of the defect space as :

$$G_{\alpha\alpha}(d,d;\omega) = \langle d\alpha|G(\omega)|d\alpha\rangle$$

$$= \sum_{\Gamma} \sum_{\mu} \sum_{jj'}^{d_\Gamma c_\Gamma} \langle d\alpha|\Gamma\mu j\rangle\langle\Gamma\mu j|G(\omega)|\Gamma\mu j'\rangle\langle\Gamma\mu j'|d\alpha\rangle \qquad (4.8)$$

where c_Γ gives the number of times that the Γ-th irreducible representation with dimension d_Γ occurs in the total representation Γ_{D4h}. The coefficient $\langle d\alpha|\Gamma\mu j\rangle$ can be calculated from the symmetry coordinates [46] which facilitate the calculation of the defect Green's function:

$$G_{XX}(d,d;\omega) = G_{YY}(d,d;\omega) = (G_{CC}^{Eg} + G_{CC}^{Eu})/2 \qquad (4.9a)$$

$$G_{ZZ}(d,d;\omega) = (G_{CC}^{A1g} + G_{CC}^{A2u}). \qquad (4.9b)$$

From the above equations, the dumbbell motions occurs in A_{1g}, E_g, A_{2u} and E_u modes. The local density of states of the dumbbell given by equation (3.50) takes the form :

$$Z(d,d;\omega) = \frac{\omega M_d}{3\pi} \operatorname{Im} \left[2G_{CC}^{Eg} + 2G_{CC}^{Eu} + G_{CC}^{A1g} + G_{CC}^{A2u} \right] \qquad (4.10)$$

From the different elements of the defect Green's function, $G_{XX}(d,d;\omega)$, $G_{YY}(d,d;\omega)$ and $G_{ZZ}(d,d;\omega)$, one can already see the displacement pattern of atoms in the defect space of various irreducible representations. This can also be inferred from the symmetry coordinates. The vibrational motion of the dumbbell and its nearest neighbours for all the four irreducible representations where interstitial motion is involved is shown in Fig.13. As can be inferred from Fig.13, except for the breathing mode A_{1g}, where a more dominant longitudinal force constant between the dumbbell atoms is involved, in all other irreducible representations the nature of the vibrational modes is controlled by transverse force constants and consequently the nature of the

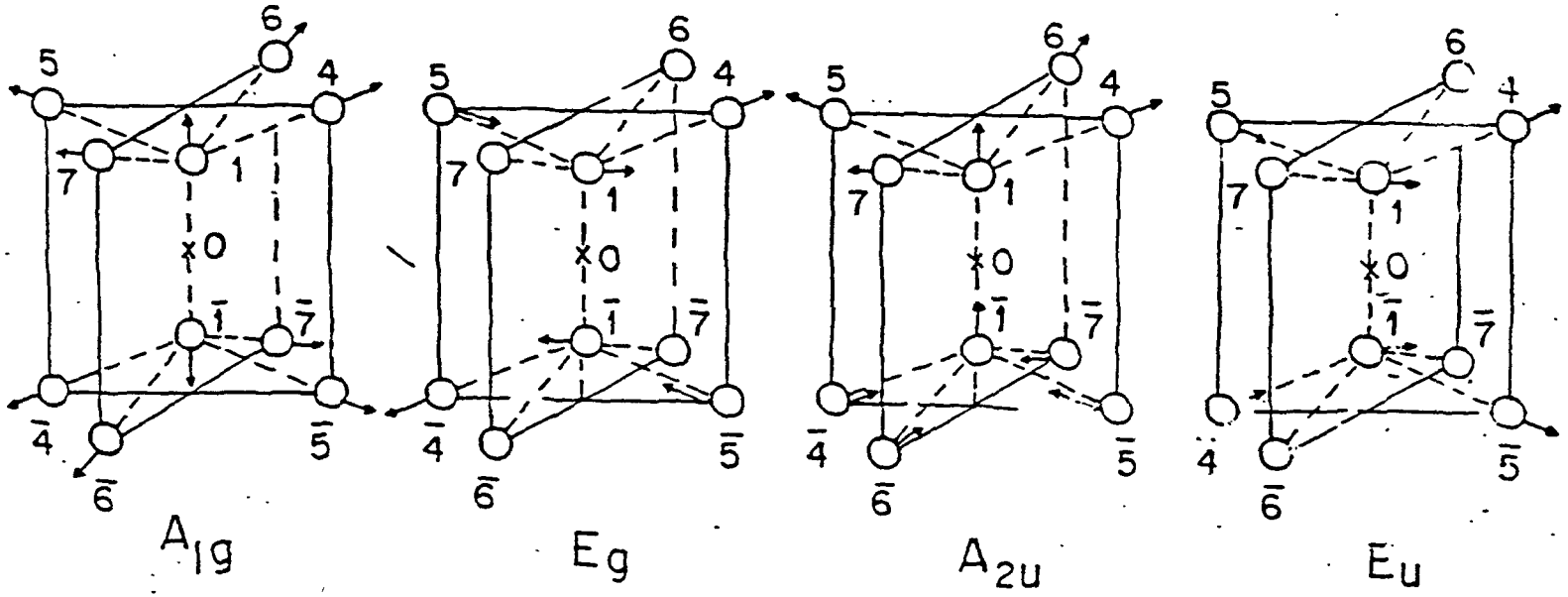

Fig.13. Vibrational modes of <001>-dumbbell in fcc metals

characteristic mode is determined by the phase shift between the motions of the dumbbell atom and its neighbours. They are in phase in resonance modes and out of phase in localized modes. Not surprisingly, the local density of states of the dumbbell shows only localized mode, in the case of A_{1g} whereas in the other irreducible representations both resonance as well as localized modes may occur.

4.4 Results and discussions.

We have calculated the local density of states of <100>-dumbbell in Cu, a typical example of fcc metals. To do this we have generated the ideal lattice Green's functions $G^{o}(\omega)$, in addition to evaluating the force constant changes in the vicinity of the defect. To compute $G^{o}(\omega)$, we have chosen two sets of force constants: (1) the force constants given by Nicklow *et al* [71] on the basis of the Born von-Karman force model from the measured

phonons in neutron scattering experiment and (ii) the force constants calculated from the EAM potentials as discussed in Chapter II. The modified Gilat-Raubenheimer method [126] is used to compute the Green's functions family. Case (ii) has been done to extend the use of the EAM potentials in defect calculations, especially the local density of states of the <100>-dumbbell in Cu, where the obtained ideal-lattice phonons are in good agreement with the experimental phonons. To calculate the defect Green's function $G(\omega)$, the force constant changes in the defect space has been calculated from the EAM potentials with the interaction extending up to second neighbours only. The position of the dumbbell atoms are taken from Oda *et al* [37] (± 0.5666, 0, 0)a/2.

Knowing the position of the dumbbell atom and the other atoms in the defect space which are assumed to be in their ideal respective positions, we have calculated seven sets of force constants (A_l,B_l, l=1,7) corresponding to different distances in

the defect space. Two parts of force constants have been calculate: (1) the force constants corresponding to the EAM part and (2) the force constants corresponding to the Morse part of the energy. To calculate the force constants corresponding to the EAM part of the energy, the electron density in the interstitial space is calculated by using equation (4.6), the first and the second derivatives of the embedding energy are expressed in terms of the electron density ratio in the defect space, using equations (4.4) and (4.5) with other EAM potential parameters already calculated in Chater II. The electron density in the defect space is higher compare to that in the perfect lattice space due to the presence of an additional interstitial atom and this is crucial for the embedding energy and its derivatives in the defect space. Then the force constants are calculated from equations (4.3a) and (4.3b). The force constants corresponding to the Morse part are calculated in a straight forward manner, using equations (4.2). The force constant changes in the defect space are the sum of the force constants from these two parts. The

calculated force constants are presented in Table V. The obtained force constant changes are utilised to calculate the defect Green's function for both the cases.

Table V : Force constants and force constant changes in the units of 10^4 dynes/cm, for ideal lattice and for <100>-dumbbell in Cu, using EAM potentials.

Force Constant	Embedding Part	Morse Part	Total
Ao1	-0.04069	3.03682	2.99613
Bo1	0.05957	-0.08402	-0.02445
Ao2	-0.05560	-0.20669	-0.26229
Bo2	0.03130	0.03773	0.06903
A1	3.8455	27.62917	31.47467
A2	5.5418	41.58510	46.82690
A3	0.1319	-0.23746	-0.10616
A4	5.5418	0.90803	6.44983
A5	0.7757	2.57096	3.34666
A6	0.1311	-0.17336	-0.04226
A7	0.0163	-0.04071	-0.02441
B1	-0.2978	-2.82077	-3.11857
B2	-0.4058	-4.64450	-5.0503
B3	-0.0130	0.05638	0.04338
B4	-0.4058	0.05855	-0.34725
B5	-0.0709	-0.04739	-0.11829
B6	-0.0104	0.02825	0.01785
B7	-0.0028	0.00474	0.00194

The local density of states of <100>-dumbbell are then calculated and presented in Fig. 14 when $G_o(\omega)$ is calculated from the force constants based on the experimental phonons and Fig.15 when the EAM potentials are used consistently. In the first case the force constant changes are scaled according to the experimental force model to ensure the consistency of force constants used. In each of these figures the host density spectrum is also included for comparison. The dummbell spectrum shows the occurence of characteristic modes. The resonance modes, within the in-band spectrum and the localized modes beyond the crystal frequency.

When the EAM potentials are used consistently, two resonance modes, E_g and E_u occur in the low frequency region of the spectrum whereas the A_{2u} resonance mode occurs near the maximum frequency of the crystal; as expected the breathing A_{1g} mode does not show any resonant characteristic but instead it shows up as a localized mode only. When the experimental phonons are used, only

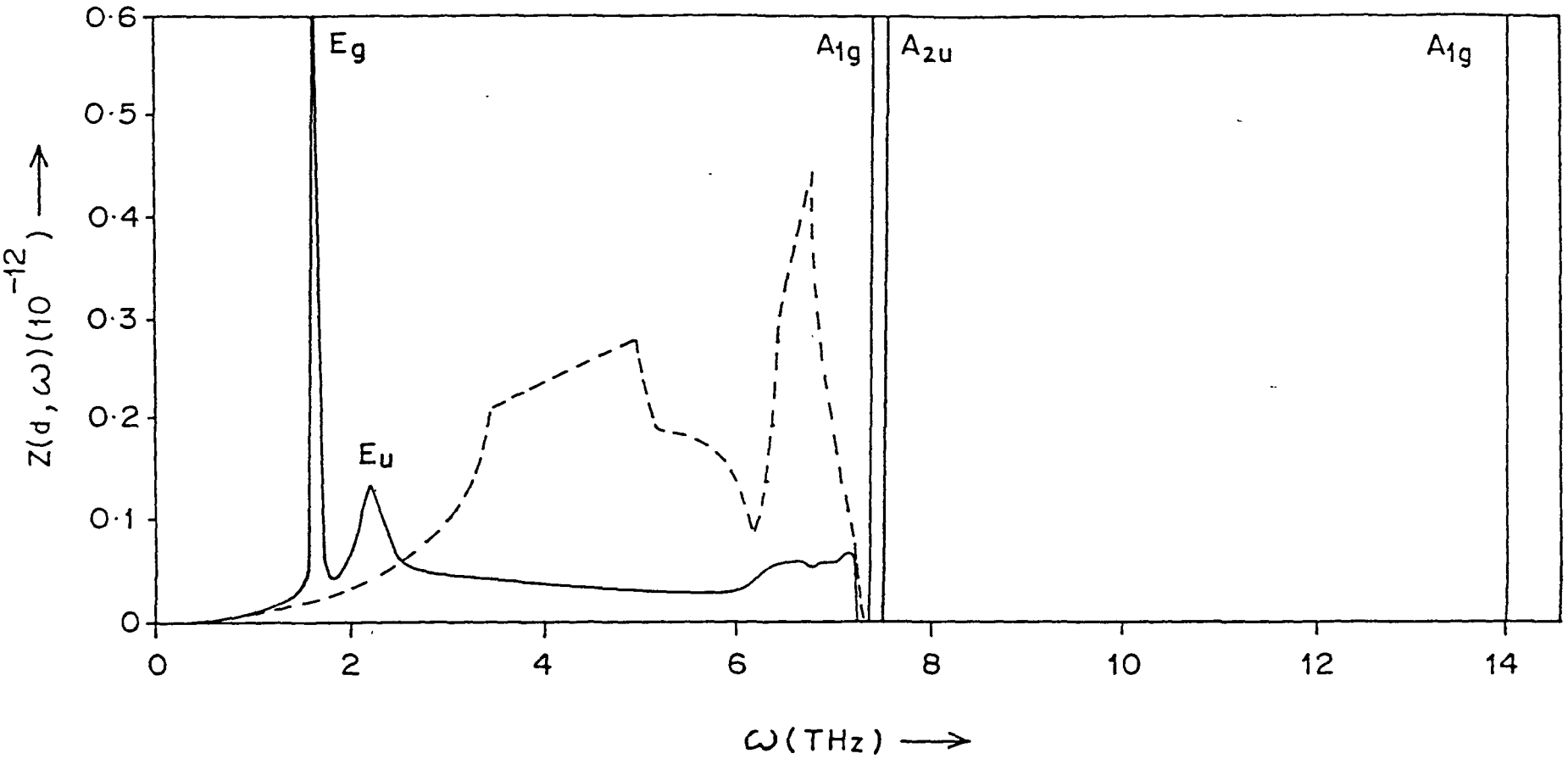

Fig. 14. Local frequency spectrum <100>-dumbbell in Cu (———) along with the host spectrum (- - - -), when the the experimental phonons are used.

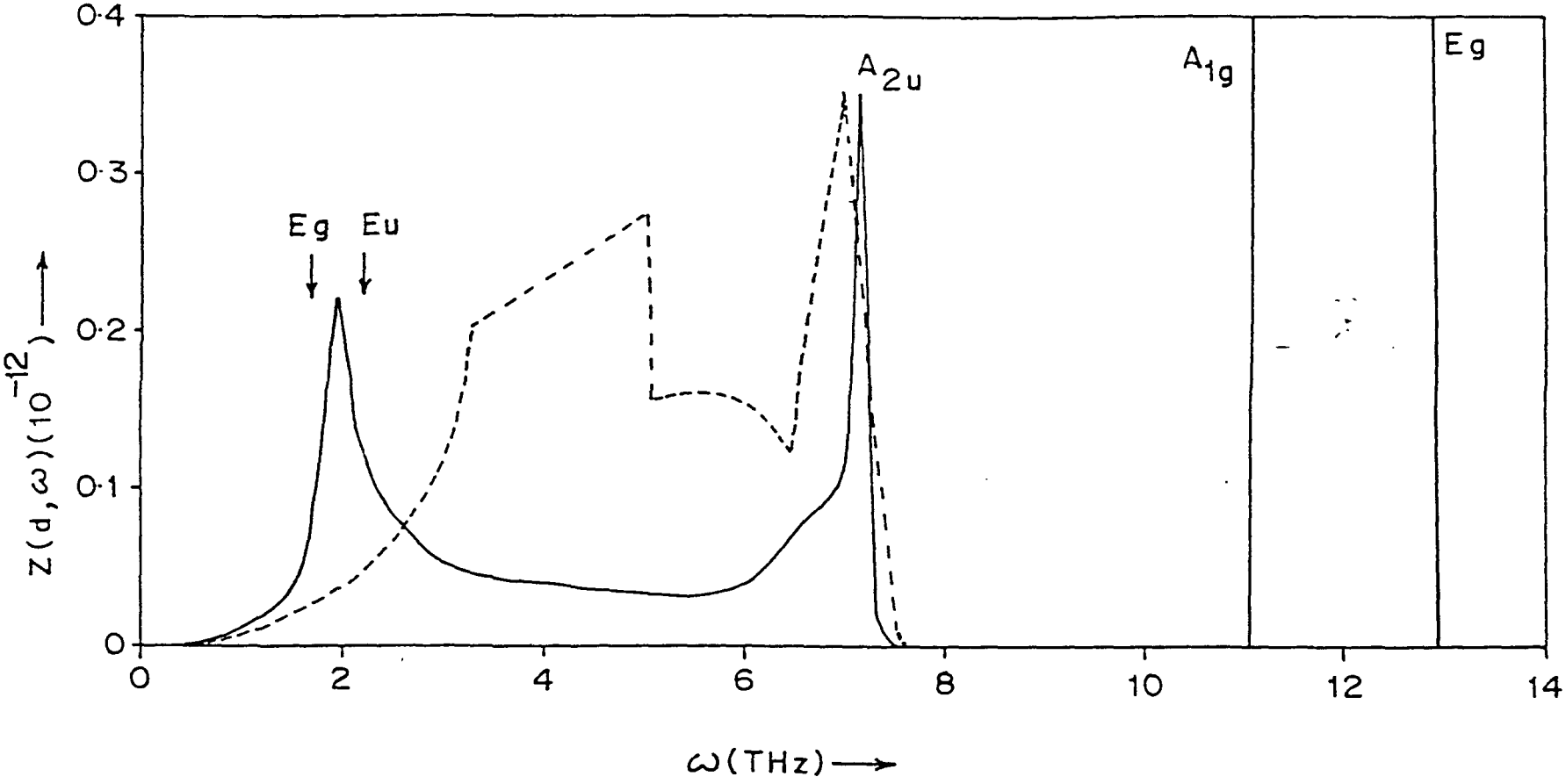

Fig.15. Local frequency spectrum <100>-dumbbell in Cu (———) along with the host spectrum (- - - -), when the the EAM potentials are used consistently.

the E_g and E_u resonance modes occur, whereas the A_{2u} mode spills out to become localized mode. The frequencies of resonance and localized modes in both the cases are presented in Table VI. One can see that when the EAM potentials are used in the defect space to calculate the force constant changes, the defect modes shift towards the higher frequencies, especially in the case of A_{2u} resonance modes which even spills out to become localized modes. It may be noted that the number of localized modes are also reduced compared to ealier results by Dederichs [44] and Ram [46] using first neighbour defect model. The decrease in the number of defect modes may be because of the complete neglect of relaxations around the interstitial which is quite drastic in the case of <100>-dumbbell in fcc metals.

Table VI: Frequencies (in Thz) of resonance and localized modes in Cu, when the EAM potentials are used consistently (a) and when experimental based phonons are used (b).

Irreducible representations	Resonance modes	Localized modes	Remark
A_{1g}	—	11.08	a
E_{g}	1.98	12.94	a
A_{2u}	5.56	—	a
E_{u}	2.12	13.16	a
A_{1g}	—	7.30,14.06	b
E_{g}	1.62	—	b
A_{2u}	—	7.36	b
E_{u}	2.20	—	b

To conclude we note that the most important feature of the dumbbell spectrum, i.e., the presence of low-frequency resonance modes and high-frequency localized modes with little participation from the normal modes of the host lattice, is reproduced by the EAM potentials. This is presumably the first application of EAM potentials to the study of defect lattice dynamics. We hope that in a detailed application including the static distortion around the defect more accurate results would be obtained so as to facilitate a comparison with possible experimental findings.

CHAPTER V

LOCAL DENSITY OF STATES OF <110>-DUMBBELL IN BCC METALS

5.1 INTRODUCTION

The study of dynamics of point defects, self-interstitials and vacancies plays an important role in understanding the properties of radiation damage in metals. Compared to fcc metals less attention has been paid to the study of SIAs in bcc metals, though the symmetry and structure have been invetigated by computer simulations and experiments. For normal bcc metals the <110>-dumbbell configuration seems to be the most stable one. The stability of <110>-dumbbell configuration has been found out in computer simulation studies in α-Fe by Erginsoy *et al* [29] and by Johnson [30]. The same structure has been found in Mo [31] and in W [32]. The result is well supported by experimental measurements : diffuse X-ray scattering in Mo [12] and α-Fe, elastic after-effect in α-Fe [22] and W [23], internal friction in α-Fe [24], Mo [25] and W [26]; magnetic after-effect in α-Fe [27] and change in elastic constants in Mo [19,28].

As regards the dynamics of the SIAs in bcc metals, it is not yet fully investigated as compared to that of fcc metals. Recently, Ram [47] has reported a calculation of the local density of states of the <110>-dumbbell in Mo. This study was extended by Blah *et al* [48] to calculate the local density of states of the neighbours of the dumbbell which were expected to affect the properties of the irradiated metal significantly :of special interest was the local density of states of the closest neighbours of the dumbbell in the $(1\bar{1}0)$ plane which is supposed to be substituted by the Mössbauer impurity ^{57}Co in irradiated Mo^{57}Co and was expected to have significant bearing on the observed reduction in the Debye-Waller factor [47]. As expected many of the characteristics of the dynamical behaviour of SIAs in fcc metals are also exhibited by SIAs in bcc metals : the local spectrum of <110>-dumbbell consists of low-frequency resonance modes and high-frequency localized modes with little contribution from the eigenfrequencies of the perfect lattice, and the resonance modes lead to a large thermal displacements of the defect, can explain the large reduction in shear moduli and provide a consistent picture of long-range migration of SIAs in Mo. However, contrary to earlier expectations, the vibrational

modes of the closest neighbour of the dumbbell in $(1\bar{1}0)$ plane, which is substituted by the Mössbauer impurity, do not explain the observed reduction in the Debye-Waller factor and the question of its interpretation is considered to be open [48]. Obviously the need for the further investigation in the dynamics of SIAs in bcc metals can not be overemphasized. In the calculation of local density of states of <110>-dumbbell and its neighbours in Mo, the ideal lattice Green's functions were calculated using phonons based on force constant model obtained from Born-von Karman fits to the measured phonons in neutron scattering experiments [126]. On the other hand for calculating the equilibrium positions of various atoms in the defect space and thereby for evaluating the various force constants in the vicinity of defect, we have used the potential constructed by Johnson and Wilson (JW) [41] from elastic constants and unrelaxed vacancy formation energy. To achieve some measure of consistency the force constants obtained on the basis of the JW potential are scaled with the most dominant nearest neighbour longitudinal force constants appearing in the lattice-dynamical force model derived on the basis of experimental phonons and thus the JW potential is used only to estimate the relative magnitudes of

different force constants in the defect space. Though with the procedure outlined the perfect phonons are correctly described, normally, in any such point defect calculation the potential used for calculating force constants near the defect should be consistent with the force constant model used to generate the ideal lattice Green's functions. Since the potential function corresponding to the force constant model used for the perfect lattice description is not known, an alternate and more consistent procedure is to use the same pair potential to calculate the Green's functions as well as the force constants in the vicinity of the defect. Therefore in the present chapter we used the JW potential consistently for both the calculation of the perfect lattice Green's functions as well as for calculating the force constants between various atoms in the defect space in all the three metals : α-Fe, Mo and W. In fact, the chapter also includes the study of the vibrational behaviours of the above metals by using the phonon-based force constants to calculate the ideal lattice Green's functions as done earlier [47,48].

As the JW potential is simple in nature, it can be easily applied to any defect calculations. It has been used in

calculations of irradiation-produced point defects in bcc metals and gives the correct trend for the properties of point defects in various bcc metals. More importantly, the JW potential clearly represents the difference in elastic property between two group of bcc metals; i.e., between so called normal metals α-Fe, Mo and W and superconductors, V, Nb and Ta, a property quite vital for the configuration and migration characteristics of SIAs in these metals. However,apart from the use of the constant unrelexed vacancy formation energy of 1.8 eV for all the bcc metals considered, the JW potential has a shortcoming in that it leads to a very high value of activation energy of interstitial migration. This indicates that the electronic effects might be quite important in bcc metals as many pair potentials also fail to give low activation energies found in experiments [55] . Incidentally, the improved N-body potentials based on the embedded atom method [50] gives lower values of migration energy, though still much larger than experimental values, but they fail to give the correct configuration of SIAs in Mo and W. Under these circumstances, the JW potentials are considered to be the only available set at present which represents the crystal properties well though some pair potentials have been constructed

by a similar method. Nevertheless we feel that the JW potentials can be used consistently to calculate the dynamics of normal bcc metals.

In order to study the effect of the pair potential used to describe the host metal we have calculated the local density of states of <110>-dumbbell in α-Fe, Mo and W by two methods : (i) by using the JW potential consistently and (ii) by following the procedure used in the earlier work [47,48] where perfect lattice is described by phonons measured in neutron scattering experiments. The broad feature of the local frequency spectrum of <110>-dumbbell in all the three metals remains the same irrespective of the description of the host metals either by JW potential or by measured phonons: the spectrum consists of a number of low frequency resonance modes and high frequency localized modes, with little contribution from the host frequencies. However, important differeces are observed in some of the resonance and localized modes, e.g., the libration mode B_{1g} gives a prominent peak in the case of α-Fe, while it is absent in W irrespective of the pair potential used for the perfect lattice description. On the other hand the behaviour of

Mo is quite different : while two B_{1g} resonance modes - one at low frequency and the other just below the top of the band are obtained when force model consistent with measured phonons are used, it is absent when JW potential is used consistently.

5.2 <110>-DUMBBELL IN BCC LATTICE

The <110>-dumbbell configuration in bcc metals is shown in the Fig.16. The centre of the dumbbell is taken as the origin of coordinate systems. The positions of the two interstitial atoms then are ($\pm$ x,$\pm$ x, 0) in the unit of half lattice constant. Due to the presence of the defect there is a change in force constants and we consider a second-neighbour model with force constant changes extending up to second neighbours of the dumbbell site. In this model the dumbbell is surrounded by 8 nearest neighbours and 6 second nearest neighbours. Altogether there are 17 lattice sites and one has to deal with a 51X51 complex matrices. To simplify the computational problem, group theory exploiting the site symmetry of the defect can be used.

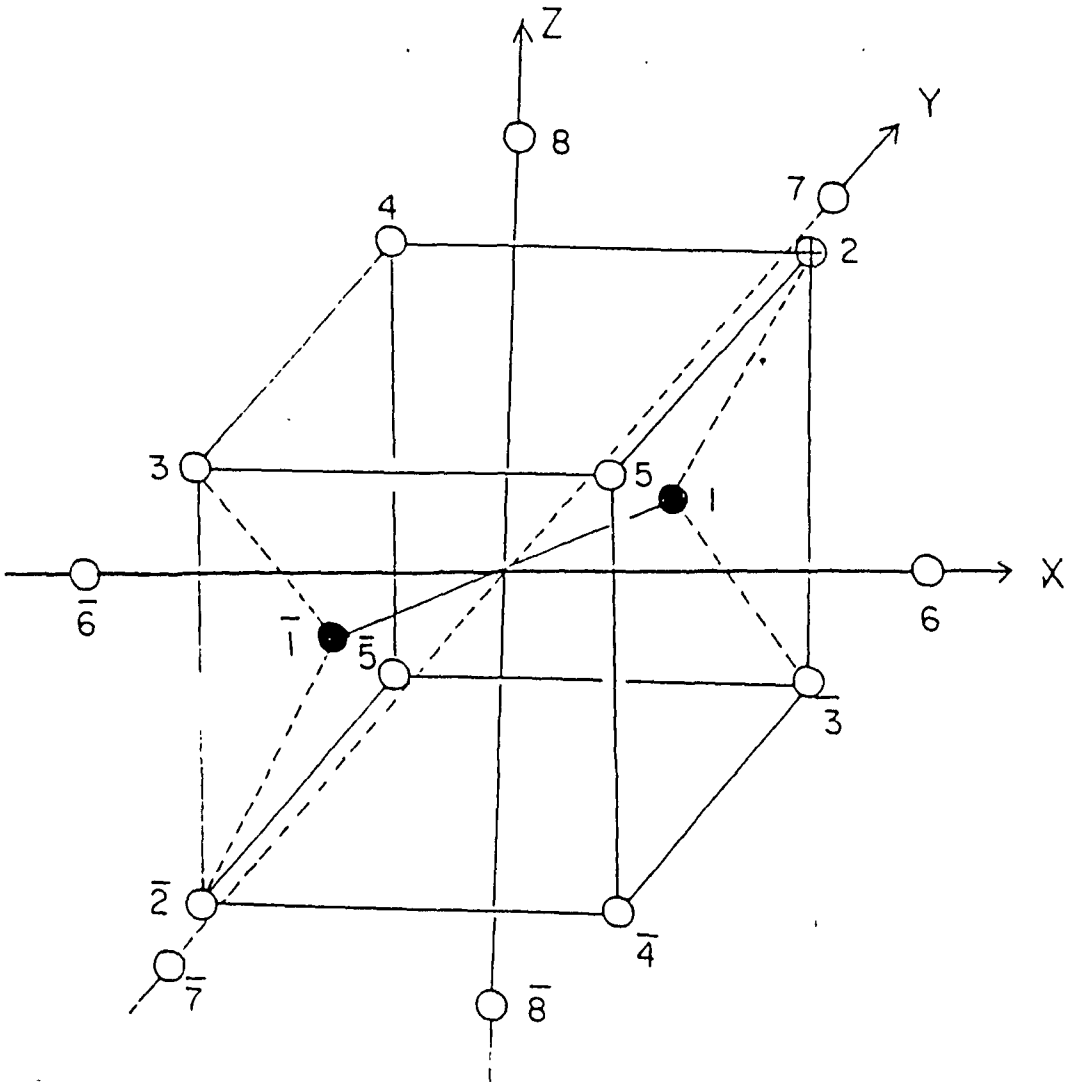

Fig. 16. Defect space for <110> dumbbell in bcc lattice

In order to construct the defect matrix, one has to consider the force constants between one of the dumbbell atoms with the other atoms : the force constants between $(1,\bar{1})$, between one of the dumbbell atoms and its nearest neighbours in $(1\bar{1}0)$ plane e.g., (1,2) between the dumbbell with one of its four nearest neighbours in (110) plane, e.g., (1,4), between the dumbbell atoms with one of its second neighbours in (001) plane, e.g., (1,6) and between the dumbbell atom with one of the second neighbours in Z-axis, e.g., (1,8). Within the defect space there are five sets of new distances which give rise to five sets of new force constants. The new distances are :

$$
\begin{aligned}
R1 &= \sqrt{2}xa \\
R2 &= [\, 1 + 2(1-x)^2 \,]^{1/2} a/2 \\
R3 &= [\, 1 + (1 - x)^2 \,]^{1/2} a/2 \\
R4 &= [\, x^2 + 2 - x)^2 \,]^{1/2} a/2 \\
R5 &= [\, 4 + 2x^2 \,]^{1/2} a/2.
\end{aligned}
\qquad (5.1)
$$

Corresponding to these distances the force constants are denoted by A_i, B_i (i=1,5), with

$$A_1 = \frac{d^2\phi}{dR^2}\Big|_{R=R_1} \quad \text{and} \quad B_1 = \frac{1}{R_1}\frac{d\phi}{dR}\Big|_{R=R_1} \tag{5.2}$$

The vacancy is described by zero coupling to the neighbours. The force constants of the ideal lattice are represented by A_1^o B_1^o, i=1,2 referring to the first and second neighbour distances. Using these force constants, the force-constant matrix for the defect lattice and the host lattce Φ and $\overset{o}{\Phi}$ respectively are obtained. The elements of the ideal lattice Green's function $\overset{o}{G}$ needed in the present defect model are 16 in number. These elements are determined by O_h symmetry of the host lattice.

In the present case of <110>-split interstitials the site symmetry is reduced from cubic (O_h) to orthorhombic (D_{2h}). The total defect space is decomposed into its different irreducible subspaces according to irreducible representations of the point group D_{2h},

$$\Gamma_{D_{2h}} = 8A_g + 5B_{1g} + 6B_{2g} + 5B_{3g} + 3A_u + 8B_{1u} + 8B_{2u} + 8B_{3u} \tag{5.3}$$

The required symmetry coordinates for different irreducible representations are taken from Ram [46,47] which also helps to

identify the different modes of vibration of the dumbbell. Such identification is quite helpful in discussing the local density of states of the dumbbell and the possible resonance and localized modes of the dumbbell atoms and their neighbours.

5.3 Local density of states of the dumbbell

The local density of states of the defect atom is expressed in terms of the defect Green's function $G(d,d,\omega)$ (Eq.(4.7)). For the dumbbell atom the defect Green's function is [46,47]

$$G_{xx}(d,d;\omega) = G_{yy}(d,d;\omega)$$
$$= 1/4 \left(G_{CC}^{Ag} + G_{CC}^{B1g} + G_{CC}^{B2u} + G_{CC}^{B3u} \right) \qquad (5.4)$$

$$G_{zz}(d,d;\omega) = 1/2 \left(G_{CC}^{B2g} + G_{CC}^{B1u} \right) \qquad (5.5)$$

The local density of states of the defects is then given by

$$Z(d,\omega) = (\omega M/3\pi)\ \mathrm{Im}\ [G_{CC}^{Ag} + G_{CC}^{B1g} + G_{CC}^{B2u} + G_{CC}^{B3u} + G_{CC}^{B2g} + G_{CC}^{B1u}]. \qquad (5.6)$$

where $G_{CC}(\omega) = (\Phi_{CC} - \Phi_{CR}\dot{G}_{RR}(\omega)\Phi_{RC} - M_{CC}\omega^2)^{-1}$ describes the local vibrational properties of the interstitial whose poles (quasipoles) determine the frequencies of the localized (resonant) modes. From the elements of the defect Green's function $G(d,d;\omega)$ and the symmetry coordinates [58], it can be concluded that the dumbbell atoms move parallel to its axis in A_g and B_{3u} modes and perpendicular to it in all other four modes. In B_{1g} and B_{2u} modes dumbbell atoms move along $[1\bar{1}0]$ while in B_{2g} and B_{1u} modes the dumbbell atoms motion is in the Z- direction. The motion of dumbbell atoms and its four nearest neighbours in $(1\bar{1}0)$ plane in different modes is depicted in Fig. 17. From the figure, it is evident that the force constants between the dumbbell atoms are involved only in the case of even modes (A_g, B_{1g}, and B_{2g}). While in the case of A_g mode the dominant longitudinal force constant between dumbbell atoms is involved and the relatively weak transverse force constant is not important, in the other two modes the longitudinal force constants are not involved and, therefore, the transverse force constants are quite effective. Consequently, in the A_g mode, one expects a localized mode, while in the other modes, both the resonance and localized modes may be expected depending upon the

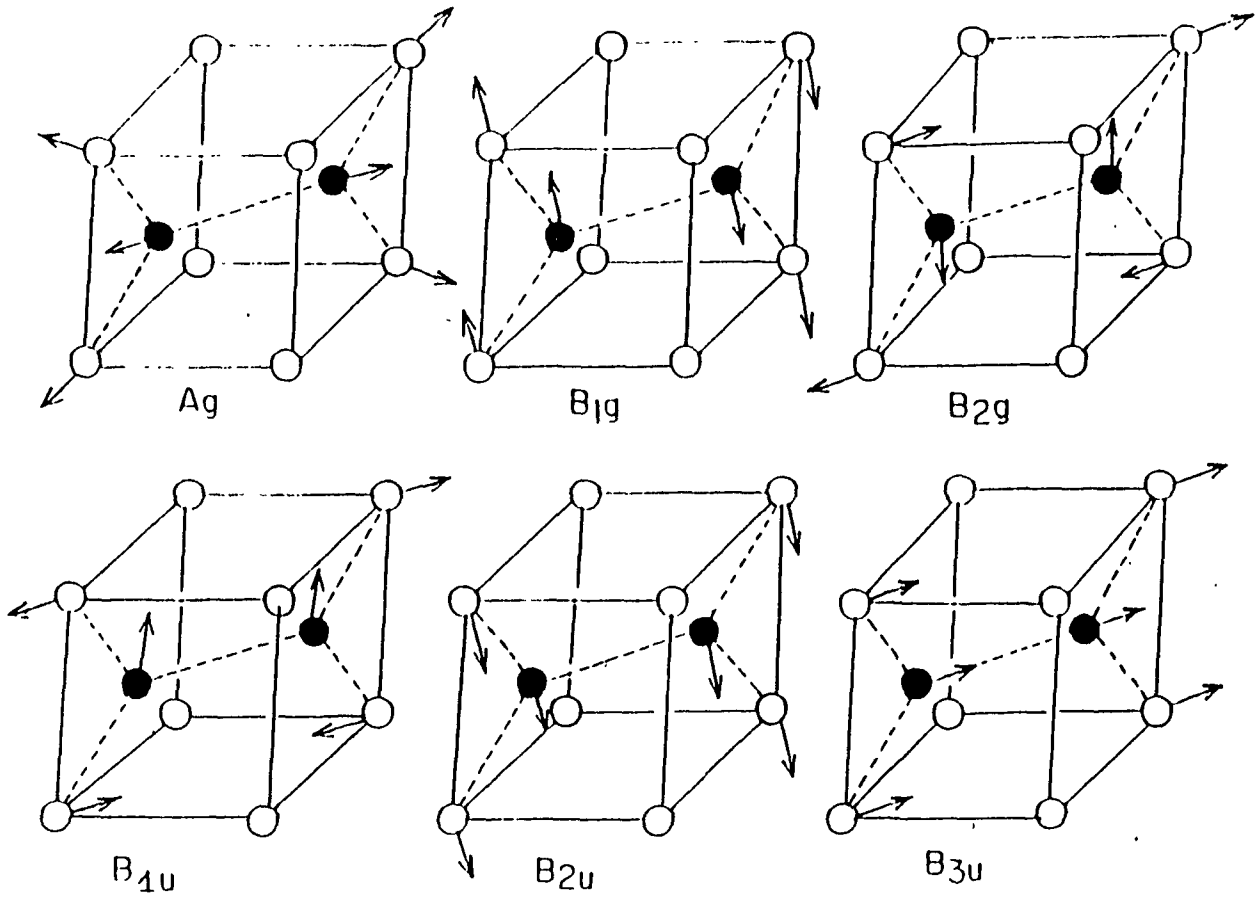

Fig 17. Vibrational modes of ⟨110⟩-dumbbell in bcc metals

motion of the neighbouring atoms of the dumbbell. If the neighbours move in phase or out of phase with the dumbbell atom we get resonance mode or localized mode accordingly. For odd-symmetry translation modes B_{1u}, B_{2u}, and B_{3u} also the nature of the characteristic mode is decided by phase shift between motions of the dumbbell and its neighbours, i.e., they are in phase for the resonance modes and out of phase for localized modes.

5.4 Results and discussions

In order to calculate the local density of states one has to evaluate the force constants in the vicinity of the defect in addition to generating the ideal lattice lattice Green's functions. In order to calculate the force constants in the defect space using JW potential the relaxed positions of atoms have to be determined. The equilibrium positions of various atoms in the defect space have been determined by the Green's function method of lattice statics [45]. However, the equilibrium positions of the dumbbell in α-Fe (± 0.5330, ± 0.5330, 0), Mo (± 0.5283, ± 0.5283, 0) and W (± 0.5434, ± 0.5434, 0) are

taken from Tajı *et al* [33] who have used the same JW potentials ın their molecular-dynamics sımulation. The strongest dıstortıon ıs sufferred by four nearest neıghbours of the dumbbell ın the $(1\bar{1}0)$ plane with the obtaıned magnıtude 0.225a/2 for all the three metals. On the other hand Ergınsoy *et al* [29] reported a value 0.29a/2 for the displacement of the same atoms on the basıs of computer sımulatıon of α-Fe. The Green's functıon method of lattıce statıcs, whıch ıs based on harmonıc approxımatıon, underestımates the dıstortıon nearest to the dumbbell and, therefore, ın the calculatıons reported here the magnıtude of dıstorıon for these atoms was taken to be 0.29a/2 ın all the three metals. Thıs ıs consıdered to be reasonable ın vıew of the fact that ın unıts of a/2, the separatıon between the dumbbell atoms ıs almost the same for all the three metals: α-Fe, Mo and W as also the lattıce statıcs value (= 0.225a/2) of the dıstortıon of these nearest neıghbours. Wıth the equılıbrıum posıtıon of the atoms ın the defect space thus taken ınto account, the sets of forces constants A_1, B_1 (ı = 1, 5) are calculated usıng JW potentıal. The result ıs presented ın Table-VII. The Table Vll contaıns the ıdeal-lattıce nearest neıghbour and second neıghbour force constants (A_1^o, B_1^o, ı= 1,2) as well.

Table VII: Force constants in the units of 10^4 dynes/cm in the ideal lattice as well as in the defect space of <110>-dumbbell in α-Fe, Mo and W. The force constants are derived from the JW potentials.

Force Constants	α-Fe	Mo	W
Ao1	5.23743	6.45776	8.18506
Bo1	-0.34882	-0.55420	-0.53278
Ao2	1.76953	5.27710	5.96631
Bo2	0.16626	0.17877	0.13684
A1	44.97021	49.55249	67.24194
A2	58.64685	62.14331	90.52246
A3	4.44385	3.60510	2.73730
A4	14.50427	14.83508	25.62451
A5	0.89282	3.42505	3.23877
B1	-3.49475	-4.42053	-5.33844
B2	-5.13007	-6.11572	-8.33142
B3	-0.10712	-0.29208	-0.25525
B4	-0.85602	-1.05573	-1.48389
B5	0.19904	0.31140	0.29517

The perfect lattice Green's function of α-Fe, Mo and W was calculated by a modified Gilat-Raubenheimer method [126]. Two sets of phonon data have been utilized for each metal: (i) phonons calculated on the basis of the JW potential and (ii) phonons calculated with the force models derived from Born-von Karman fits to the measured phonons; these include a fifth-neighbour general force model derived by Minkiewicz, Shirane, and Nathans [73] for α-Fe, a third neighbours axially symmetric model by Woods and Chen [72] for Mo and a third neighbour general force model by Chen and Brockhouse [74] for W. Thus two sets of local density of states curves are obtained (i) one using JW potential consistently and (ii) the other using Green's function based on force models derived on the basis of measured phonons and force constants in the defect space using JW potential. However, in this case the force constants obtained with JW potentials are scaled by a factor equal to A_1^o(phonons)/A_1^o(JW) where A_1^o(phonons) is the nearest neighbour longtudinal force constant occurring in force model derived from measured phonons and A_1^o (JW) is the same force constant based on JW potential. This type of procedure is essential for ensuring consistency between used phonons in the calculation of the Green's functions

and the used force constant changes in the defect space.

The calculated local frequency spectra of the <110>-dumbbell in α-Fe, Mo and W, using JW potential consistently are plotted in Figs. 18-20. The dumbbell spectra based on experimental phonons are presented in Figs. 21-23. In these figures the host-lattice spectrum is also included for comparison. The result for local spectrum of <110>-dumbbell in Mo using measured phonons has been reported earlier [47,48]. The broad features of the defect spectra in all the three metals are similar. The spectra consist of a number of low-frequency resonance modes and high frequency localized modes with little contribution from the normal modes of the host lattice. This conclusion is independent of the type of phonons used for the perfect lattice description. This result of <110>-dumbbell is identical with that of <100>-dumbbell in fcc metals. This pattern of defect spectra should be common to all split-configuration of interstitials in metals which stem from following discussions: in the highly compressed region near the interstitial, the force constants are very large and even the transverse force constants become comparable to nearest neighbour longitudinal force constant A_1^o in the ideal lattice. However, due

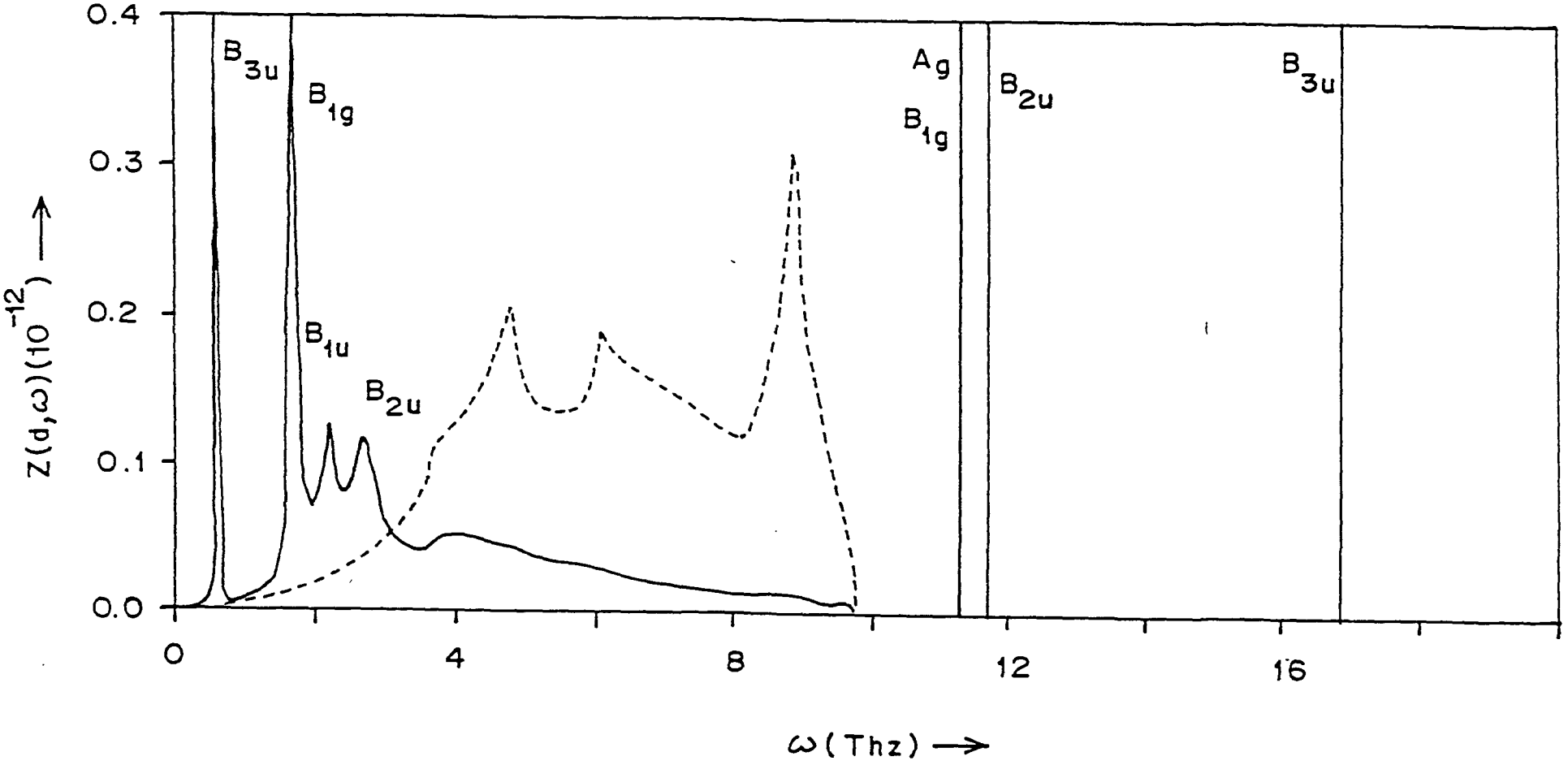

Fig. 18 Local density of states of the <110>-dumbbell in α-Fe (————) along with the host spectrum (- - - -), when the ideal phonons are calculated from the JW potential.

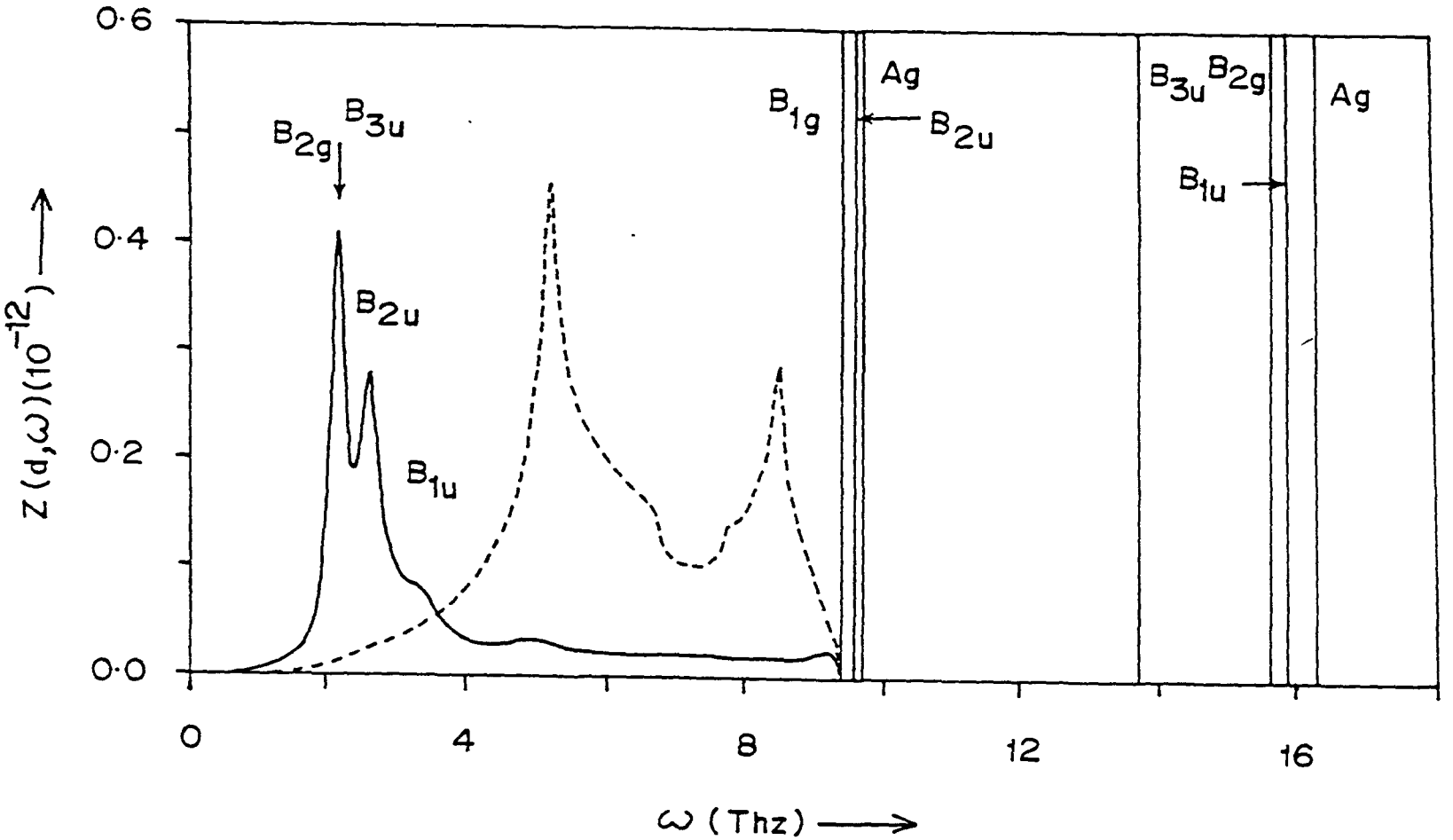

Fig. 19 Local density of states of the <110>-dumbbell in Mo (————) along with the host spectrum (- - - -), when the ideal phonons are calculated from the JW potential.

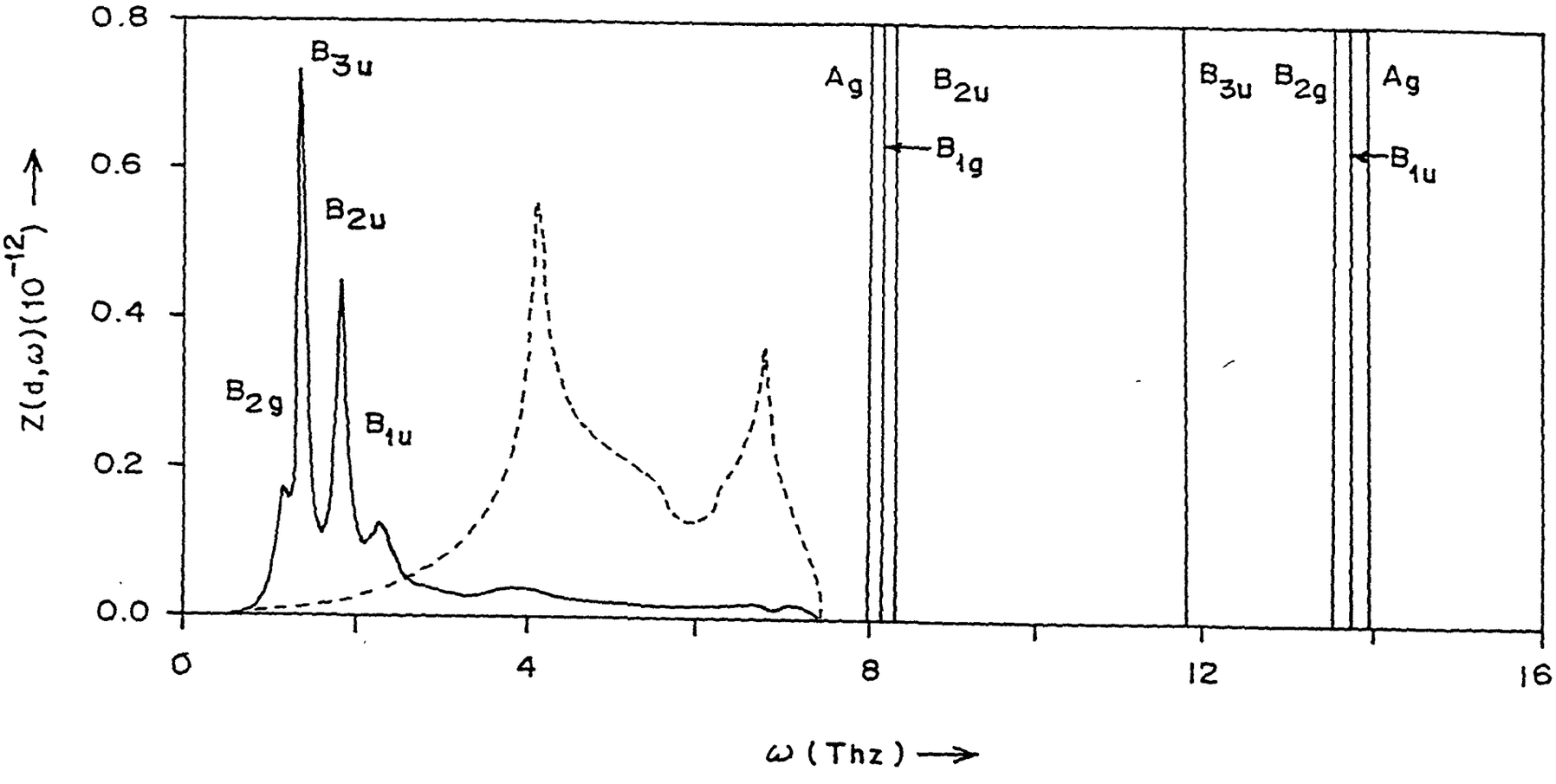

Fig. 20 Local density of states of the <110>-dumbbell in W (————) along with the host spectrum (- - - -), when the ideal phonons are calculated from the JW potential.

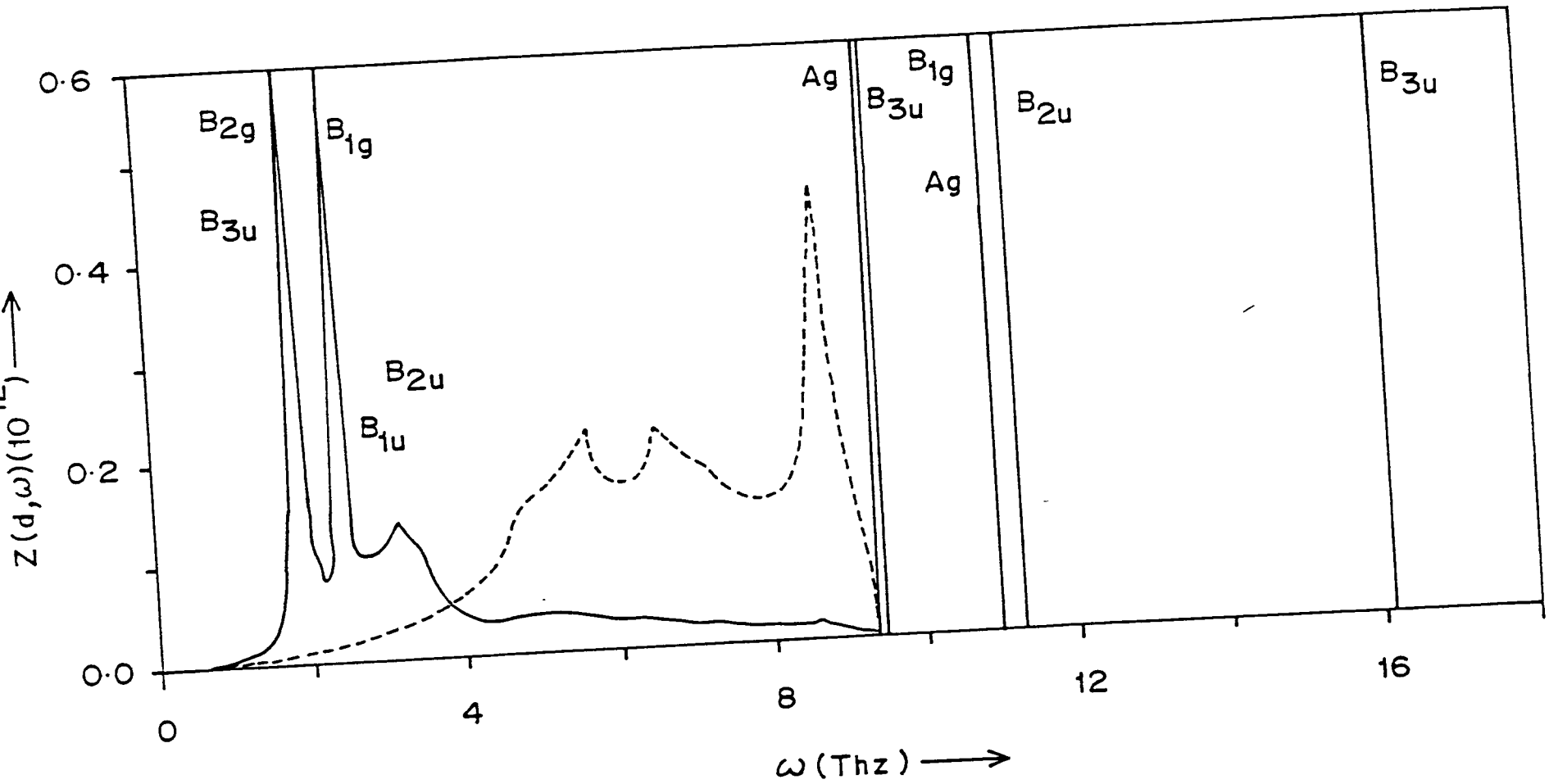

Fig. 21 Local density of states of the <110>-dumbbell in α-Fe (————) along with the host spectrum (- - - -), when the ideal phonons are taken from ref. [73].

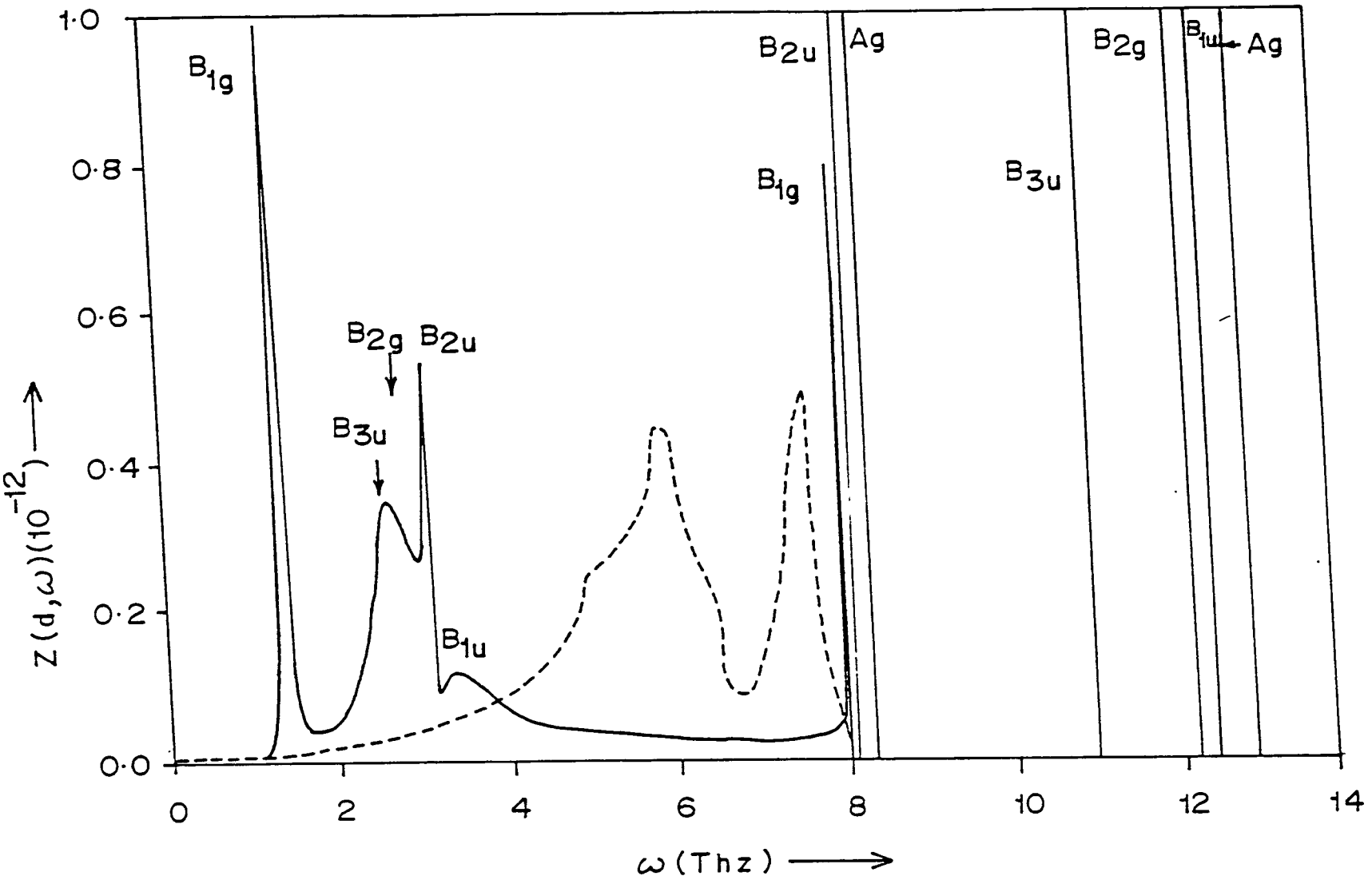

Fig. 22 Local density of states of the <110>-dumbbell in Mo (————) along with the host spectrum (- - - -), when the ideal phonons are taken from ref. [72].

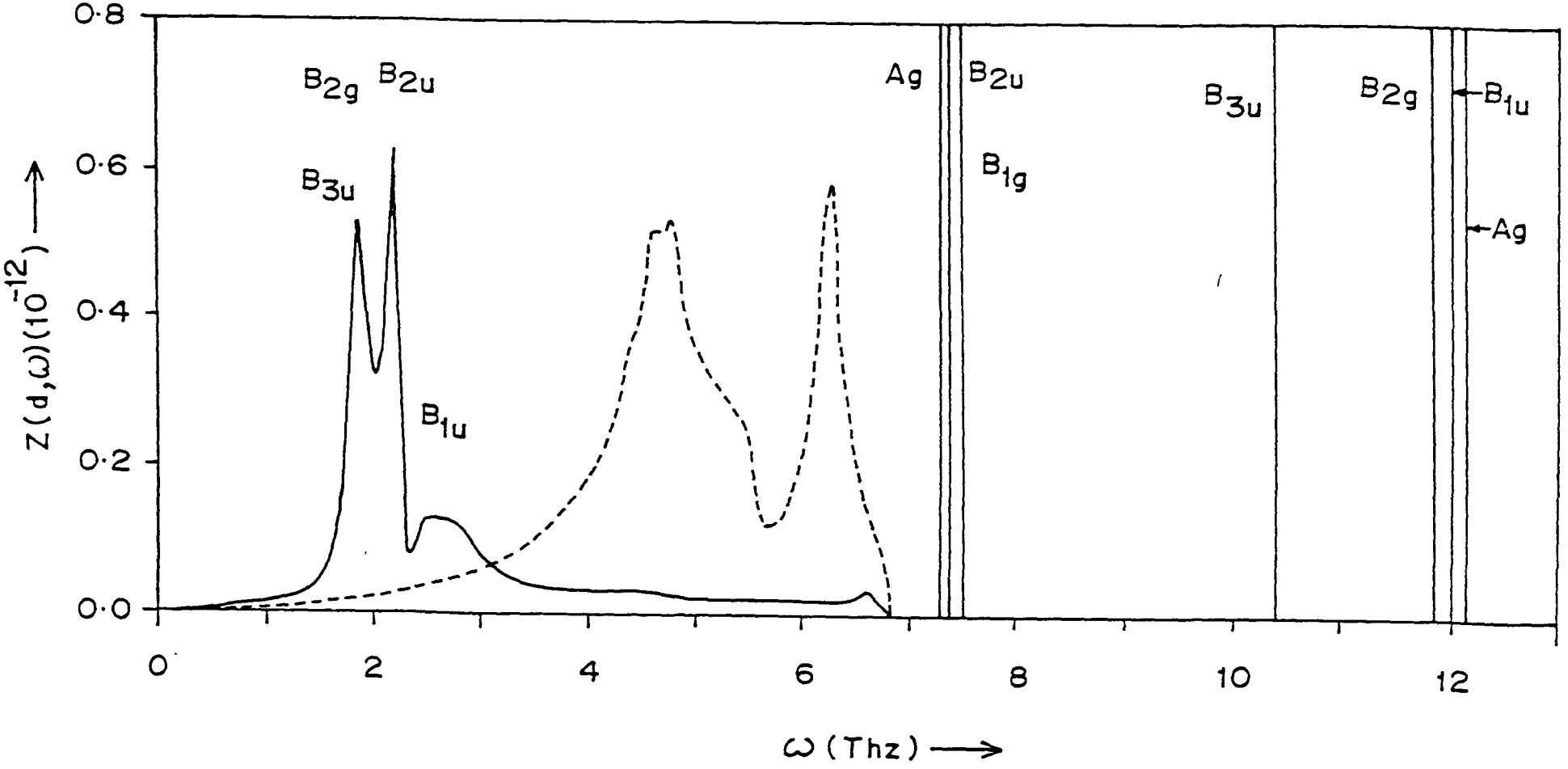

Fig. 23 Local density of states of the <110>-dumbbell in W (————) along with the host spectrum (- - - -), when the ideal phonons are taken from ref. [74].

to repulsion of the atoms the transverse force constants are always negative. Thus whenever the large longitudinal force constants between dumbbell atoms or the dumbbell and some of its neighbours are involved one gets high frequency localized modes *in which the dumbbell motion is out of phase with that of the* neighbours, on the other hand when the neighbouring atoms move in phase with dumbbell atoms so that connecting strong longitudinal forces are not effective and consequently the negative transverse force constants cause the mode frequency to be lowered, one gets low-frequency resonance modes.

The obtained resonance- and localized mode frequencies when (JW) potentials are used consistently are given in Table-VIII while Table IX contains the defect mode frequencies when measured phonons are used. Irrespective of the potential used to describe the perfect crystal in all the three metals, the breathing mode A_g shows localized modes whereas in all other modes where dumbbell motion is involved generally both resonance and localized modes are found. Another common features of dumbbell spectrum in different metals is the occurrence of resonance modes pertaining the irreducible respesentation B_{1u}, B_{2u} and B_{3u}

Table VIII: Frequencies (in Thz) of resonance and Localized modes for α-Fe, Mo and W in different irreducible representations when the JW potentials are used consistently.

Metals	Irreducible Representations	Frequency of resonance modes	Frequency of localized modes
α-Fe	A_g	-	11.32
	B_{1g}	1.68	11.32
	B_{2g}	-	-
	B_{1u}	2.18	-
	B_{2u}	2.70	11.70
	B_{3u}	0.59	16.88
Mo	A_g	-	9.70,16.28
	B_{1g}	-	9.38,15.62
	B_{2g}	2.16	-
	B_{1u}	3.28	15.86
	B_{2u}	2.64	9.58
	B_{3u}	2.16	13.72

A_g	-	8.04,13.92
B_{1g}	-	8.14
B_{2g}	1.14	13.54
B_{1u}	2.28	13.72
B_{2u}	1.82	8.30
B_{3u}	1.38	11.76

Table IX : Frequencies (in Thz) of resonance and Localized modes for α-Fe, Mo and W in different irreducible representations when experimental phonons are used.

Metals	Irreducible Representations	Frequency of resonance modes	Frequency of localized modes
α-Fe	A_g	-	9.37,10.99
	B_{1g}	2.42	10.94
	B_{2g}	1.86	-
	B_{1u}	3.08	-
	B_{2u}	3.26	11.24
	B_{3u}	1.88	9.46,16.10
Mo	A_g	-	8.26,12.77
	B_{1g}	1.39,7.995	-
	B_{2g}	2.73	12.17
	B_{1u}	3.55	12.38
	B_{2u}	3.11	8.07
	B_{3u}	2.59	10.965

A_g	-	7.30,12.12
B_{1g}	-	7.34
B_{2g}	1.98	11.84
B_{1u}	2.78	12.00
B_{2u}	2.18	7.46
B_{3u}	1.86	10.40

whether the perfect lattice is represented by phonons based on JW potential or by measured phonons. The behaviour of B_{2g} mode is typical in α-Fe, both resonance and localized modes are absent when the JW potential is used consistently but when the experimental phonons are used, it appears as a resonance mode only. In the other two metals the B_{2g} resonance mode appears irrespective of the phonons used,but the localized mode is absent in the case of Mo when the JW potential is used consistently. The behaviour of B_{1g} mode is unique in the sense that in the three metals studied the mode has different character. In α-Fe one gets resonance as well as localized modes and in W only localized modes are obtained and this results is independent of the type of phonons used in the calculations. In Mo one gets only localized mode when JW potential is used consistently while only resonance modes are obtained when measured phonons are used. As regards, differences based on use of different potentials for the perfect lattice description, from Tables -VIII and -IX, we observe that, we get less number of characteristic modes when JW potential based phonons are used as compared to when measured phonons are used in α-Fe, while in Mo and W same set of defect modes are

obtained except for reshuffling of resonance and localized modes in some irreducible representations. This indicate that some of the important structures in the frequency spectra of the host metals must be shifted in frequencies when the JW potentials are used to calculate the phonons.

The calculated frequency spectra have been used to calculate the mean-square thermal displacements of dumbbell atoms as well as the host atoms. For the calculation of the mean-square thermal displacements, equation (3.56) is used. The calculated mean-square displacements for the dumbbell and the host in all the three metals are presented in Figs. (24-26) when the JW potentials are used consistently and Figs. (27-29) when the experimental phonons are used. We see that $\langle u^2 \rangle$ of the dumbbell is large and increases essentially linearly with T for temperatures greater than 40 K. The results in all the three metals are similar to what was reported previously for Cu and Mo [45].

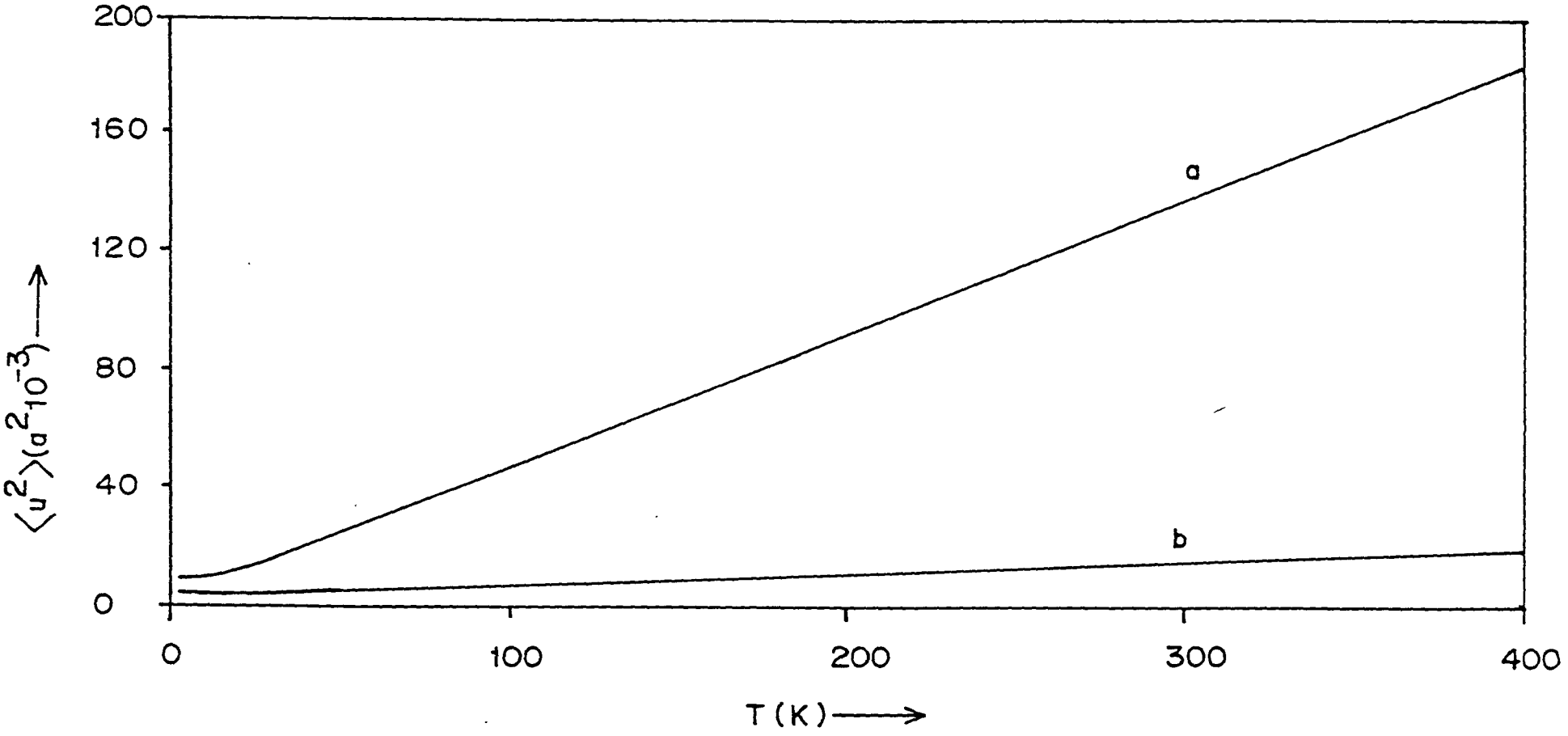

Fig. 24 Mean square displacement of <110>-dumbbell (a), and the host (b) in α-Fe when the JW potential is used consistently.

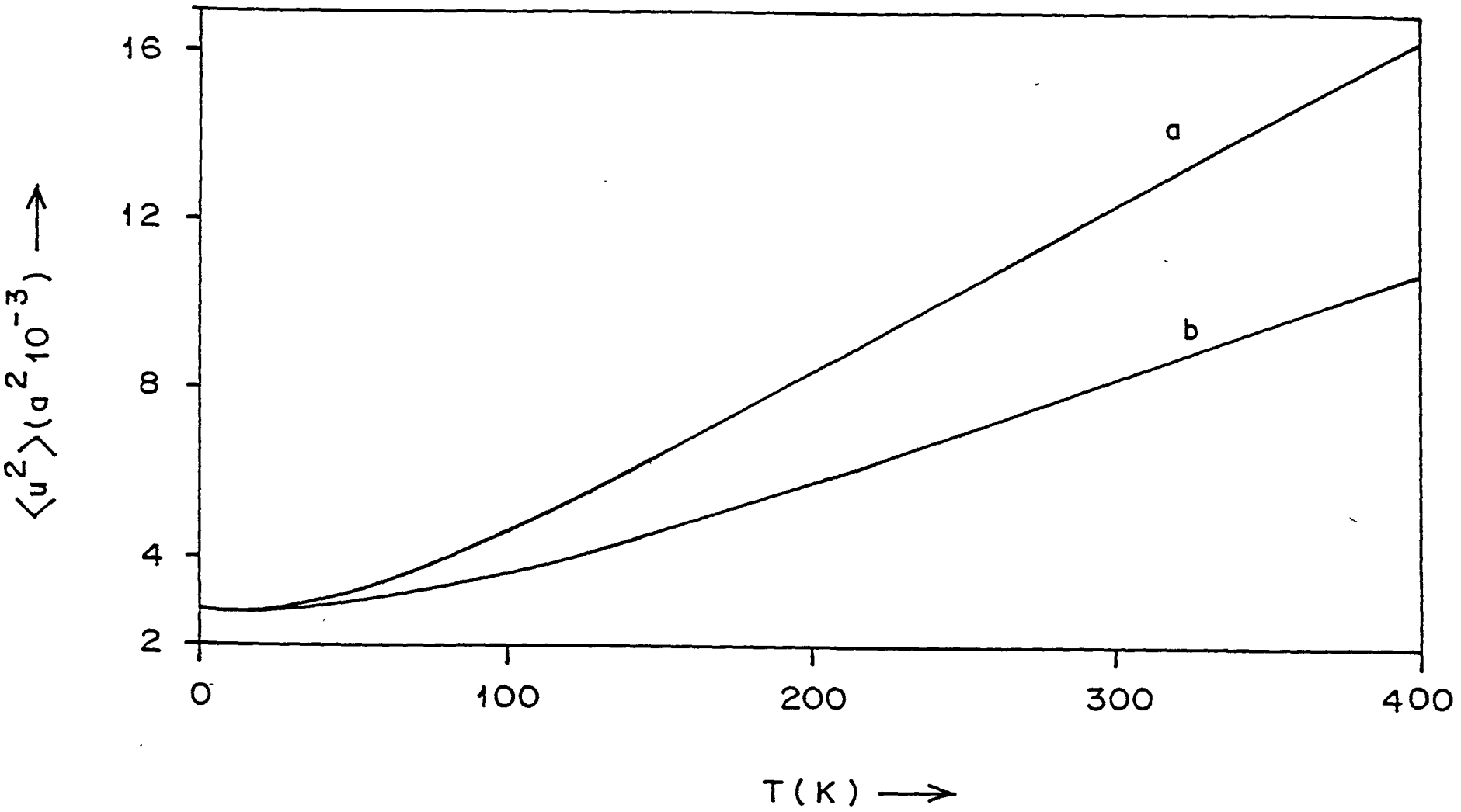

Fig. 25 Mean square displacement of <110>-dumbbell (a), and the host (b) in Mo when the JW potential is used consistently.

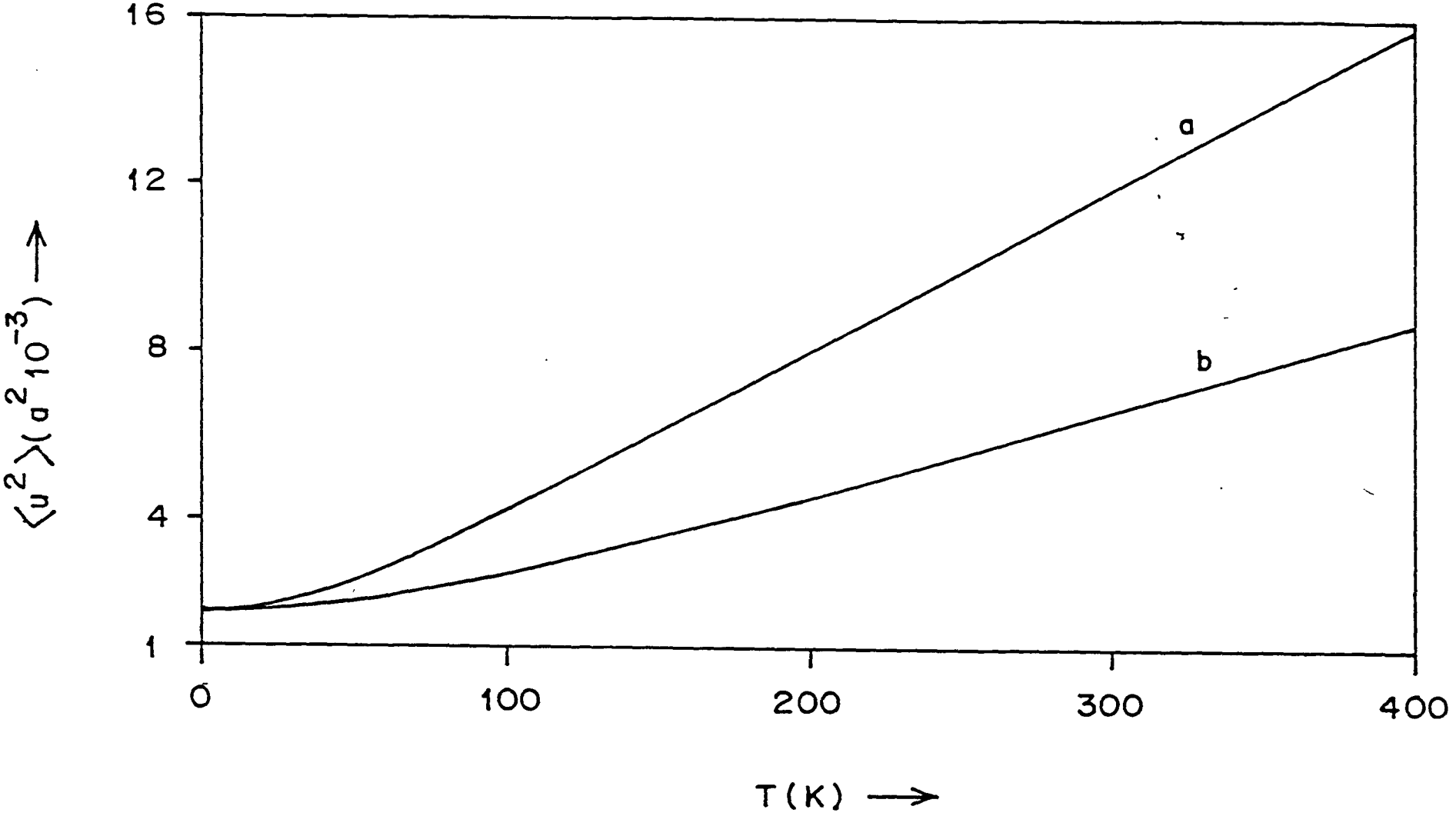

Fig. 26 Mean square displacement of <110>-dumbbell (a), and the host (b) in W when the JW potential is used consistently.

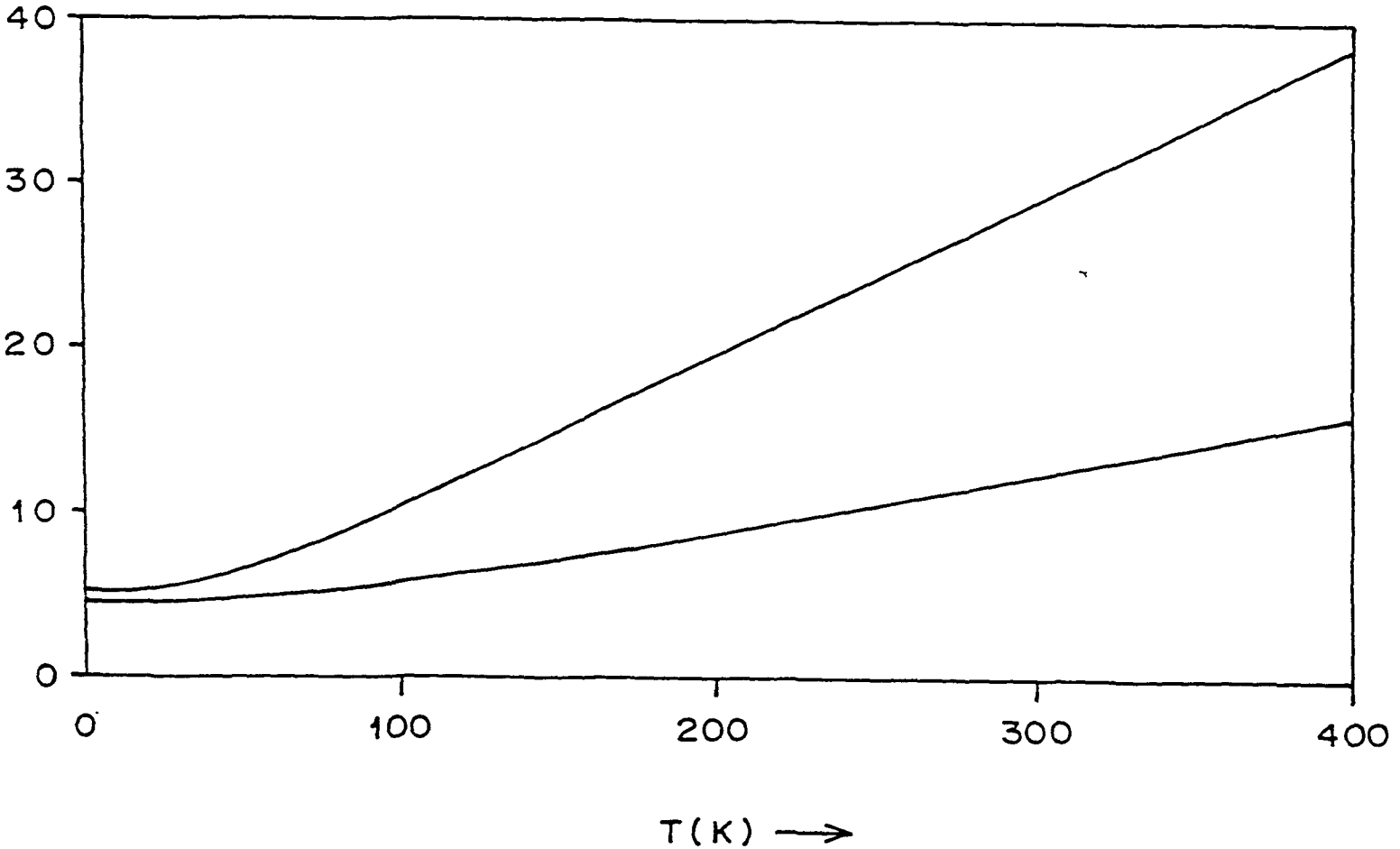

Fig.27. Mean square displacement of ⟨110⟩-dumbbell (a), and the host (b) in α-Fe when the experimental based phonons are used.

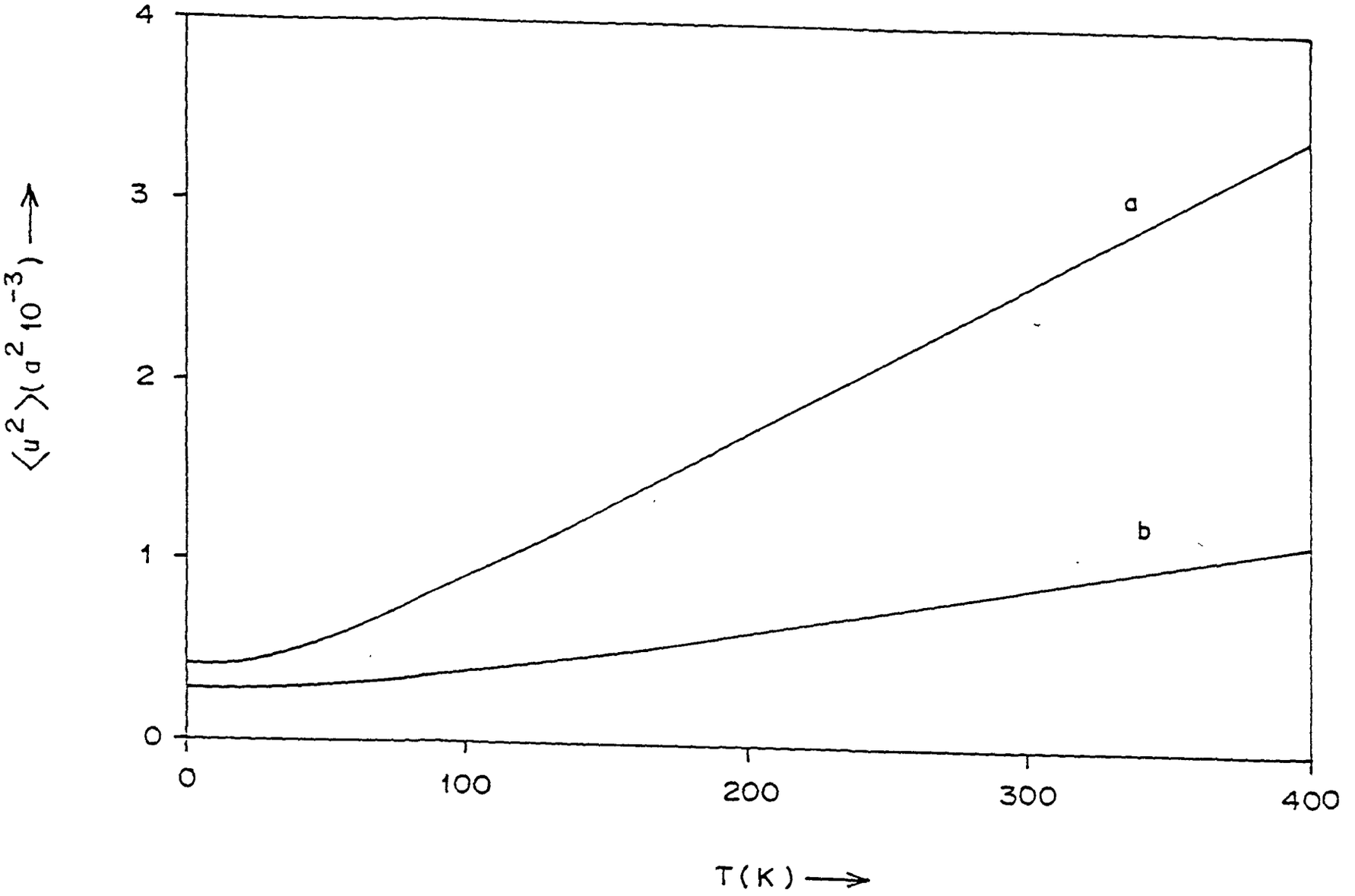

Fig.28. Mean square displacement of <110>-dumbbell (a), and the host (b) in Mo when the experimental based phonons are used.

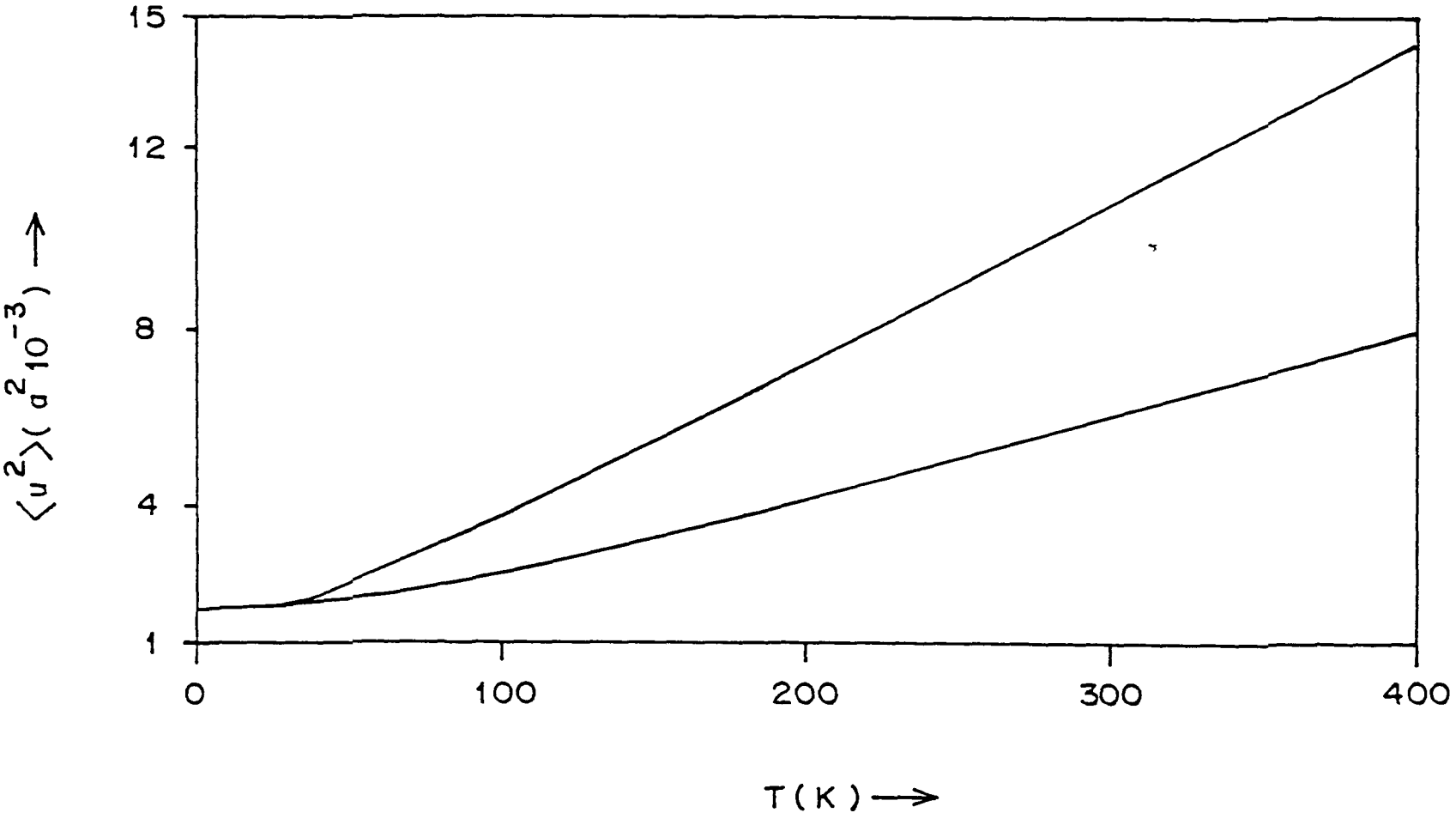

Fig.29. Mean square displacement of <110>-dumbbell (a), and the host (b) in W when the experimental based phonons are used.

As a result of low frequency resonance mode the SIAs show large diaelastic polarizability. The most important contribution to change of elastic moduli is given by [46,63].

$$\Delta C^{D} = \frac{C}{V} < \epsilon^{c} R | t(0) | \epsilon^{c} R > \qquad (5.7)$$

Where ϵ^{c} are eigenstrains, R are the position vectors of atoms, t(o) is the t matrix in the static limit, V_c is the unit cell volume and c is the concentration of defects. The changes in different elastic moduli $\Delta(C_{11} + 2C_{12})$, $\Delta(C_{11} - C_{12})$ and $\Delta(2C_{44})$ are determined by t^{A_g}, $(t^{A_g}, t^{B_{1g}})$ and $(t^{A_g}, t^{B_{2g}}, t^{B_{3g}})$ respectively [58]. In the presence of sharp resonance modes it is clear that $\Delta(C_{11} - C_{12})$ and $\Delta(2C_{44})$ are determined by librational modes B_{1g} and B_{2g}, respectively. For resonance modes the t-matrix is approximated by [2]

$$t(0) = V - V \frac{|r><r|}{M\omega_r^2} V \approx - V \frac{|r><r|}{M\omega_r^2} V \qquad (5.8)$$

where $V = \Phi - \Phi^{c}$ is the force-constant change matrix pertaining to the entire defect space and $|r>$ is the normalized resonance state. For resonance modes change in shear moduli is always

negative. The reduction in shear moduli is inversely proportional to the resonant frequency. We see from Table IX that for Mo $\omega_r^{B_{1g}} < \omega_r^{B_{2g}}$, we conclude that $-\Delta C' > -\Delta C_{44}$ which is in agreement with the experimental measurement of Okuda and Mitzubayashi [135]. However, in α-Fe $\omega_r^{B_{1g}} > \omega_r^{B_{2g}}$ the reverse result $-\Delta C_{44} > -\Delta C'$ is obtained. In W the librational modes B_{1g} is absent and, therefore no such conclusion regarding relative magnitudes of $\Delta C'$ and ΔC_{44} can be drawn.

In fact the absence of librational resonance mode B_{1g} in W is an important features of the present results since this mode has important effect on elastic constants. Obviously, only a measurement of elastic constants of irradiated W and α-Fe and further work using improved potentials for the description of perfect lattice as well as the defect will clarify the situation.

As discussed previously by Ram [47] the long range migration of SIA's should occur through a combination of the translational modes B_{3u} and the librational mode B_{2g}. However,

there would be two possibble mechanism (i) a three demensional migration with reorientation of the dumbbell axis by 60°, a process found in computer simulation, [44,30] and (ii) a two dimemsional migration with out reorientation in which the dumbbell jumps to neighbouring sites while its axis remains in the $(1\bar{1}0)$ plane. The three dimensional migration process has been identified in magnetic after effect measurements in Fe [127,128] as discussed fully by Ehrhart *et al* [129]. On the other hand Jacques and Robrock [130] proposed a planar migration of the SIAs in order to explain their elastic after effect measurements in electron irradiated Mo where a reorientation of the dumbbell axis was not observed upto 500K. The crucial question which of the two mechanisms is dominant in a particular metal for a particular environment e.g., temperature irradiation condition etc. As pointed out by Jacques and Robrock [135], according to Flynn and Stoneham [131] the transtion probabilty from the initial to the final state depends explicitly on the displacement amplitudes in both the states, the probability being large if there is a large overlap between the displacements in both the states. Since, both the resonance modes B_{3u} and B_{2g} the strong displacement are confined to $(1\bar{1}0)$ plane naturally the overlap is maximum when the

axis of the dumbbell remains in the plane. In any case, a plannar migration of SIAs in Mo not only explains the elastic after effect measurement, it also accounts for the peculiar behaviour of resistivity recovery observed in bcc metals, e.g., the occurrence of a close pair recovery stage beyond the temperature of uncorrelated recovery [132]. We conclude, that, a plannar jump provides a consistent picture of long range migration of the SIAs in Mo. Even in α-Fe a more complex migration process has been suggested [133] where long range migration is thought to be due to a plannar jump of interstitial without rotation, but in the same temperature range, (1_E) another mechanisms is activated which cause the interstitial to rotate at its place without jump or migration. The existence of both the process in the same temperature range is made possible by proximity of the activation energies for reorientational migration and rotation at the dumbbell site [44]. A plannar migration model seems to be appropriate for W also which is compatible with resistivity recovery and with the observation of relaxation peaks associated with rotational motion without migration at low temperatures compared to interstitial migration temperature [23] a result similar to mixed dumbbell in Fe-Si alloy [134] which provided

basis for the suggestion of plannar migration of SiAs in Fe. In Mo also there is experimental evidence for the existence of purely rotational jump with the observation of elastic relaxation peak at about 25K which has <110> symmetry and which anneals at about 45K [135]. Thus, a two-dimensional migration mediated by resonance modes of <110> dumbbell seems to be applicable to all normal bcc metals.

CHAPTER VI

LOCAL DENSITY OF STATES OF FIRST AND SECOND NEIGHBOURS OF VACANCIES IN BCC METALS

6.1. INTRODUCTION

The study of dynamics of irradiation-produced point defects,vacancies and self-interstitials, is of fundamental importance in an understanding of physical properties of irradiated metals. The study of dynamics not only provides direct interpretation to some of the physical properties but also illucidates aspects of the general problem of radiation damage in these metals. In this context most of the recent studies on the dynamics of point defects in metals, the focus of attention has been on self-interstitials while relatively less attention has been paid to the dynamics of vacancies in metals though they are expected to play an equally important role in the interpretation of various properties of the irradiated metals and also the structures of vacancies are simpler than those of the interstitials.

The earlier studies [79,44] of vacancies in metals were mostly concerned with their static properties like, energies and relaxations around the vacant site and only few of them have discussed the dynamical aspects of vacancies. The works on static relaxation around the vacancy have, in general, shown that there is an inward relaxation of first neighbours and outward relaxation of second neighbours of the vacancy [79,33]. The production of vacancy together with the relaxation of different atoms in the vicinity of the vacant site alters the elements of the interaction matrix between various pairs of atoms besides the missing force constants between the vacant site and its neighbours. All these result in a modification of the local vibrational spectra of the different neighbours of the vacancy, especially the spectra of the first and second neighbours. The appearances of some characteristic defect modes, resonant and localized modes in the frequency spectra are also possible. As for dynamics, Land and Goodman [80] carried out an investigation of the vibrational effects of vacancies in cubic metals with short- ranged forces using a molecular approximation. Their result for copper showed appearance of a mode slightly above the

maximum frequency of the crystal which they regarded as a local mode. On the other hand, Hatcher *et al* [81] have used Green's function method to discuss the vibrational behaviour of vacancy in Cu and α-Fe and have found that no local mode appears. Therefore, from the above inconclusive results on the dynamical aspects of the vacancies, it has been felt that more work is needed to get a further insight and understand the vibrational behaviour of vacancies in metals. Quite recently Biah and Ram [136] have discussed the vibrational behaviour of vacancy in Mo.

Another aspect which plays an important role in the study of vacancies is the choice of an appropriate potential suitable in the distorted region round the vacant site. Hatcher *et al* [81] have calculated the local density of states of the first neighbours by using the Born-Mayer potential and the Morse potential and then pointed out that Morse potential seems to work well for most of fcc metals, while for a typical bcc metal, α-Fe, a spline fit type potential due to Chang and Graham [82,83] works well. From our experience with vibrational properties of self-interstitials in α-Fe, Mo and W and their neighbours in Mo

[47,48], using Green's function method, it has been felt that the potential constructed by Johnson and Wilson (JW) [40] provides a resonable description of dynamical properties of point defects in these metals. The JW potential is fitted to elastic constants and unrelaxed vacancy formation energy and being a short range potential, it is expected to give a good account of the force constants in the region surrounding the vacancy [41], especially when we model the vacancy with interactions up to the second neighbours only. The most important merit of the JW potentials lies in the fact that they clearly represent the difference in elastic properties between two groups of bcc metals, i.e., between the so called normal metals α-Fe, Mo and W and superconductors V, Nb and Ta and correctly gives the structure -<110>-dumbbell of the self-interstitials in normal bcc metals as found experimentally. Further, except at some high symmetry points in the first Brillouin zone, the phonon dispersion in bcc metals is correctly described by the JW potential [40]. Therefore, in this chapter the JW potential is used to study the vibrational behaviour of the vacancy in three normal bcc metals :

α-Fe, Mo and W and calculate the local density of states of the atoms surrounding the vacancy. The local density of states is used to calculate dynamical properties such as formation entropy and mean square displacements of concerned atoms. The calculation of formation entropy for vacancies is important in more than one way : a knowledge of formation entropy enables one to determine the concentration of vacancies and to calculate the self-diffusion constant in metals; and in view of the non-availability of any reliable experimental value of formation entropy for vacancies, a theoretical calculation of its value is worthwhile. As a matter of fact, most of the earlier work on the vibrational properties of vacancies in metals concerned with the calculation of formation entropy. Earlier calculations of formation entropy of vacancy in bcc metals include those by Burton [137] who obtained values ranging from 2.2k to 2.6k for bcc metals. Apart from the formation entropy, only the frequency spectrum of the first neighbours of the vacancy has been discussed using Green's function method. Besides the absence of local modes, the frequency spectrum of the first neighbours in the relaxed lattice has been found to be somewhat shifted to

lower frequencies. This is explained by the absence of coupling to the vacancy in the (111) direction.

We have calculated the local density of states of the first and second neighbours of vacancies in α-Fe, Mo and W by two methods : (i) by using the JW potential consistently , i.e., for the calculation of perfect lattice Green's functions and the changes in force constants in the vacant site and (ii) by following the procedure used in the earlier work regarding self-interstitials [47,48] where perfect lattice is described by phonons measured in neutron scattering experiments [72-74] while the force constants near the vacancy are found from JW potentials and they are scaled by nearest neighbour force constant in the lattice dynamic model. From the local frequency spectra of the first and second neighbours of the vacancy, the vacancy formation entropy can be calculated at ease since the change in frequency spectrum of the lattice is closely related to the local frequency spectra of the neighbours. The vacancy formation entropy are calculated both for the case of relaxed lattice as well as for the case of unrelaxed lattice. It is expected that the formation entropy for the unrelaxed lattice will be smaller than that of

the relaxed case.

6. 2.1 Local density of states

As in the case of SIAs, we use the Green's function method to obtain the local density of states of neighbours of a vacancy. The vacancy is taken at the origin and its interaction with the first and second neighbours is modelled by missing springs to these atoms which are then relaxed to new positions. This results in modifications of force constants between neighbouring atoms. The remaining atoms of the host crystal beyond second neighbours are assumed to be unperturbed. The change in force constant due to the defect is

$$\Delta\Phi = \Phi - \Phi^{o}, \qquad (6.1)$$

where Φ is the force constant in a relaxed lattice and Φ^{o} that in the ideal lattice . With interactions extending up to second neighbours , Φ and Φ^{o} are both (45 x 45) matrices.

By defining two subspaces C and R with C containing the defect and R the other host atoms the force constant matrix for the host lattice is

$$\overset{o}{\mathcal{J}} = \begin{bmatrix} \overset{o}{\Phi}_{CC} & \overset{o}{\Phi}_{CR} \\ 0 & \overset{o}{\Phi}_{RR} \end{bmatrix}, \qquad (6.2)$$

while for a defect lattice

$$\mathcal{P} = \begin{bmatrix} \emptyset & \emptyset \\ \emptyset & \Phi_{RR} \end{bmatrix}, \qquad (6.3)$$

since the subspace C does not contain any atom in the present case. Then the force constant change is given by

$$\Delta\Phi = \begin{bmatrix} \overset{o}{-\Phi}_{CC} & \overset{o}{-\Phi}_{CR} \\ 0 & \Phi_{RR} - \overset{o}{\Phi}_{RR} \end{bmatrix}. \qquad (6.4)$$

The Green's functions for the defect lattice are given from equations (3.19) to (3.23). The same site Green's function is related to the local density of states according to Equation (3.50).

6.2.2 Formation entropy

The production of a vacancy in a crystal increases the entropy of the latter and this increase in entropy is known as the vacancy formation entropy. The vacancy formation entropy is closely related to the local density of states of the neighbours of the vacancy, especially to those of the first and second neighbours. The formation entropy of the vacancy may be calculated in terms of the change in the frequency spectrum in the presence of the vacancy. The theory of vacancy formation entropy has been given in Chapter III and the expression for vacancy formation entropy, using the change in the density of states is given by equation (3.67).

Apart from the vibrational contribution to the formation entropy , the contribution due to image forces is also taken into consideration for a relaxed lattice. The displacements due to image forces for vacancies lead to a homogeneous contraction of the lattice and hence to the strengthening of the force constant ,i.e., a negative contribution to formation entropy. The volume change caused by image forces is [46]

$$\Delta V^{Im} = \frac{2}{3}\,\frac{1 - 2p}{1 - p}\,\Delta V \ , \qquad (6.6)$$

where ΔV is the total volume change and p is the Poisson's ratio.

The change in formation entropy due to volume relaxation is obtained from the thermodynamic relation

$$\left[\frac{\partial S}{\partial V}\right]_T = \left[\frac{\partial P}{\partial T}\right]_V = - V \left[\frac{\partial P}{\partial V}\right]_T \frac{1}{V}\left[\frac{\partial V}{\partial T}\right]_P = K\beta, \qquad (6.7)$$

where K is the isothermal bulk modulus and β the volume expansion coefficient. The change in formation entropy due to image forces is

$$\Delta S^{F}_{IV}(\text{Image}) = K\beta\ \Delta V^{Im}. \qquad (6.8)$$

6.3. Calculated Results and Discussions

We have calculated the local density of states of the neighbours of the vacancies in three normal bcc metals : α-Fe, Mo and W with Green's function method. To calculate the local density of states of atoms near a vacancy we have evaluated the

force constants in the vicinity of the vacant site as also the ideal lattice Green's function $G^{o}(\omega)$. The vacancy is described by zero coupling to its neighbours. For calculation of $G^{o}(\omega)$, two sets of force constants have been used : (i) calculated force constants based on the JW potentials and (ii) force constants obtained from the experimental-based phonons fit to the Born von-Karman force models. Therefore, in this case two sets of Green's functions $G^{o}(\omega)$ are obtained with the help of modified Gilat Raubenheimer method [126]. For calculation of matrix elements of $\tilde{F}$ in a relaxed lattice , the static displacements of first and second neighbours of the vacancy are taken from molecular dynamics calculations of Taji *et al* [33] which give inward displacements of first neighbours and outward displacements of second neighbours away from the vacant site along the coordinate axes. The atoms falling in the cluster of first and second neighbours of the vacant site take up new equilibrium positions, while other atoms beyond the second neighbours are considered to be in their perfect lattice positions. With new equilibrium positions of atoms in the defect space we have eight new distances between these atoms. These

distances are :

$$R_1 = \left[(1 + x + y)^2 + 2 (1 - x)^2 \right]^{1/2}$$

$$R_2 = \left[(1 - x)^2 + 2(1 + x)^2 \right]^{1/2}$$

$$R_3 = \left[3(1 + x)^2 \right]^{1/2}$$

$$R_4 = \left[(2 + x)^2 + 2x^2 \right]^{1/2}$$

$$R_5 = \left[4(1 - x)^2 \right]^{1/2}$$

$$R_6 = \left[2 + (1 - y)^2 \right]^{1/2}$$

$$R_7 = \left[y^2 + 4 \right]^{1/2}$$

$$R_8 = \left[(2 - y)^2 \right]^{1/2} , \qquad (6.9)$$

where the distance are given in the unit of half lattice constant, x is the displacement of first neighbour in each

cartesian direction and y is the displacement of the second neighbour along the coordinate axes. Using JW potential, the force constant changes A_i, B_i (i=1,8) are calculated at the new equilibrium interatomic distances and they are presented in Table X along with the perfect lattice force constants A_o^i, B_o^i (i=1,2) when the perfect lattice Green's functions $G_o(\omega)$ are calculated by using force constants obtained from Born-von-Karman fits to measured phonons in neutron scattering experiment, the force constants determined on the basis of JW potential are scaled by A_1^o which is the nearest neighbour force constant in the ideal lattice occuring in the phonon model. This means that the force constants calculated on the basis of JW potential are scaled according to the measured phonon force model. This type of procedure is essential for ensuring consistency between used phonons in the calculation of Green's functions and the used force constant changes in the defect space.

The local density of states of the first and second neighbours of the vacancy in all the three metals are calculated both for unrelaxed lattice as well as for the relaxed lattice by

Table X. Different force constants near the vacant site and also the ideal lattice force constants from the JW potentials in 10^4 dynes/cm.

Parameters	α-Fe	Mo	W
Aol	5.23743	6.45776	8.18506
Bol	-0.34882	-0.55420	-0.53278
AO2	1.76953	5.27710	5.96631
BO2	0.16626	0.17877	0.13684
A1	4.5394	6.1974	7.7944
A2	4.1270	5.2512	6.5295
A3	3.4196	3.8193	4.1719
A4	1.1753	4.4939	5.2007
A5	3.6152	5.9236	6.5610
A6	7.5718	8.0568	10.3370
A7	1.7568	5.2708	5.9618
A8	3.0032	5.8049	6.4761
B1	-0.3105	-0.5399	-0.5168
B2	-0.2855	-0.4869	-0.4664
B3	-0.1953	-0.3906	-0.3755
B4	0.1901	0.2515	0.2041
B5	0.0730	0.0030	-0.0216
B6	-0.4677	-0.6425	-0.6254
B7	0.1669	0.1795	0.1373
B8	0.1065	0.0859	0.0486

using the JW potential phonons and also by using the experimental phonons. However, in the unrelaxed case, no significant change in the local density of states of the first and second neighbours of vacancy as compared to that of the host lattice atom is expected, while in the relaxed case, significant changes are expected. The obtained local density of states of first and second neighbours of the vacancy in a relaxed lattice, when the phonons are calculated from the JW potential are shown in Figs. 30-32, for α-Fe, Mo and W; when the experimental phonons are used, the local density of states are shown in Figs. 33-35. In the figures the host spectra are also presented in all the six figures for comparison. The frequency spectrum of the first neighbour is considerably shifted to lower frequency side of the spectrum in all the cases with some kind of weak peaks which may be treated as incipient resonances. In all the cases, irrespective of the phonons used, no local modes have been found. This behaviour is explained by the loss of coupling between the vacancy and the neighbouring atom in the (111) direction. This is also in accordance with the reduced value of Einstein frequency

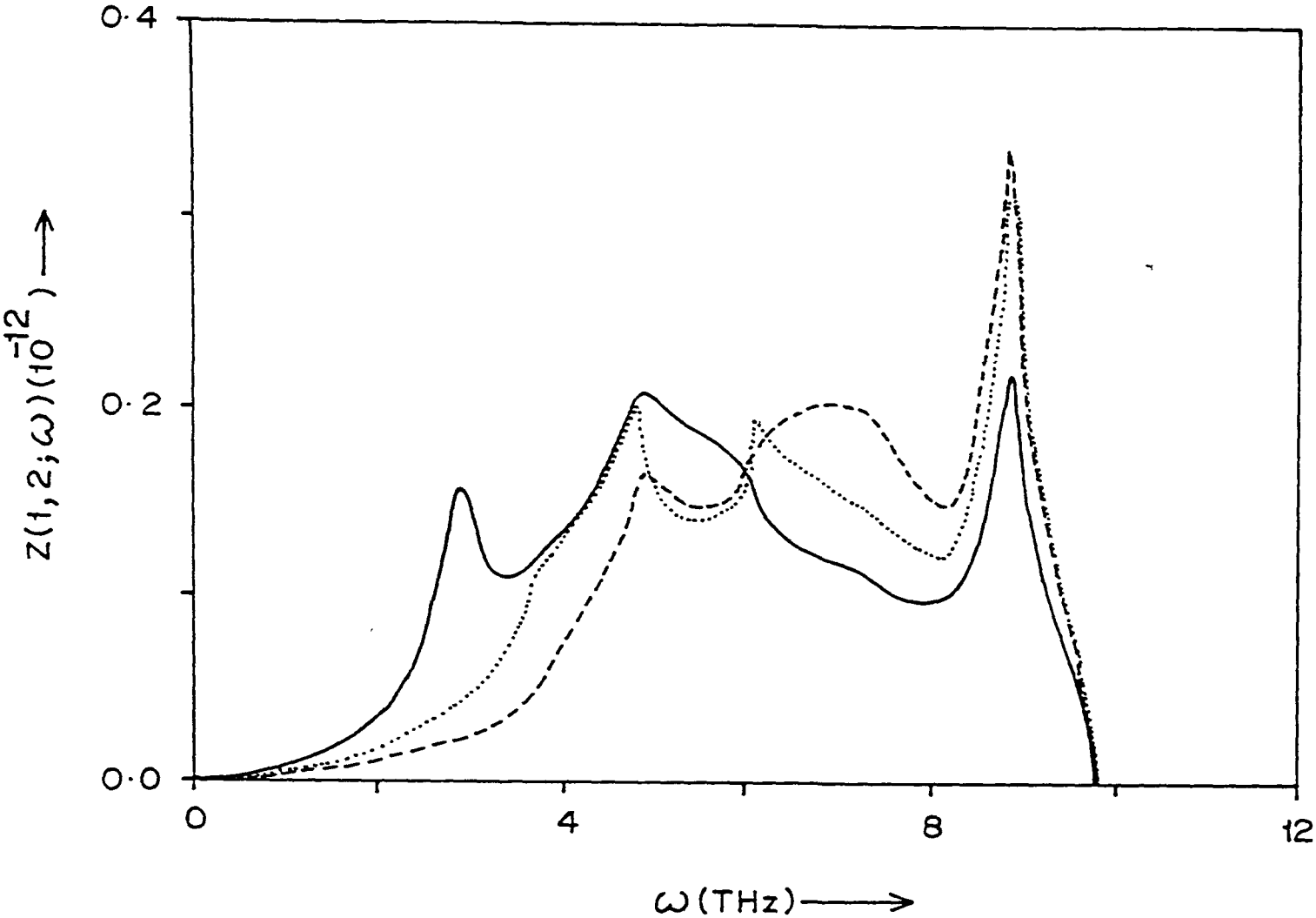

Fig.30 Local density of states of first neighbour (——), second neighbour (- - -) of a vacancy and a host atom (....) in α-Fe in the case of a relaxed lattice, with ideal phonons calculated from the JW potential.

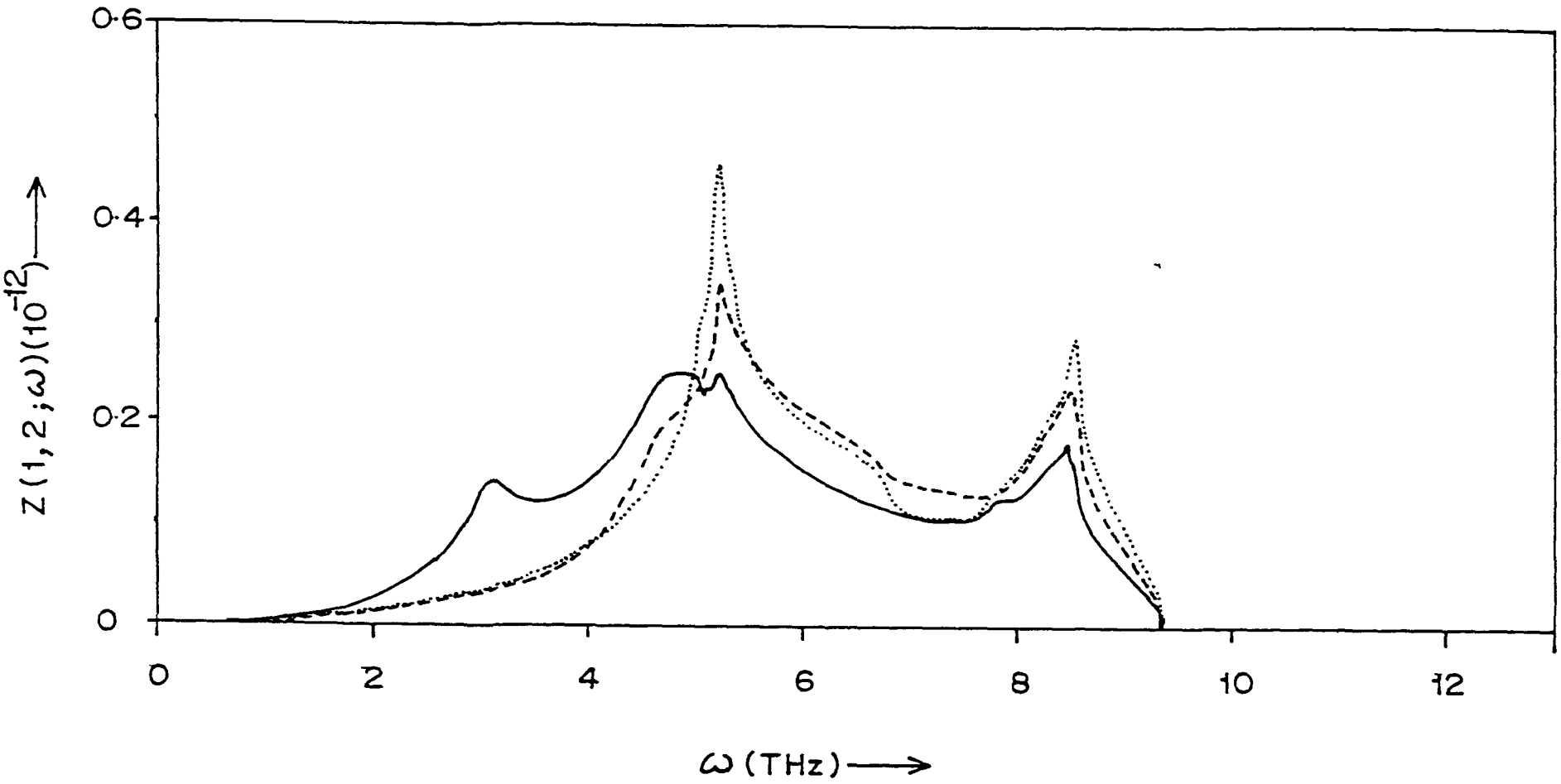

Fig.31 Local density of states of first neighbour (——), second neighbour (- - -) of a vacancy and a host atom (....) in Mo in the case of a relaxed lattice, with ideal phonons calculated from the JW potential.

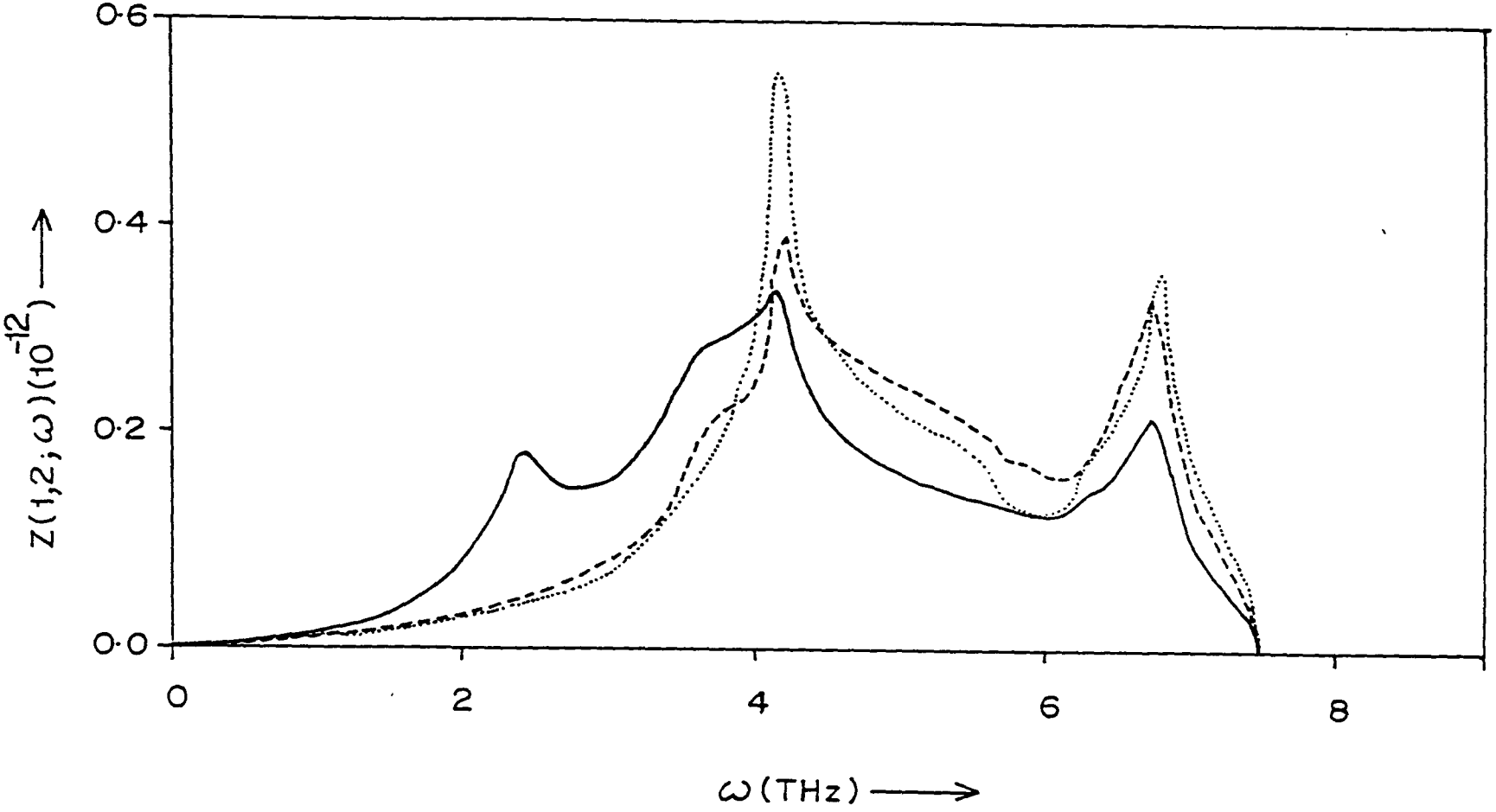

Fig.32 Local density of states of first neighbour (——), second neighbour (- - -) of a vacancy and a host atom (....) in W in the case of a relaxed lattice, with ideal phonons calculated from the JW potential.

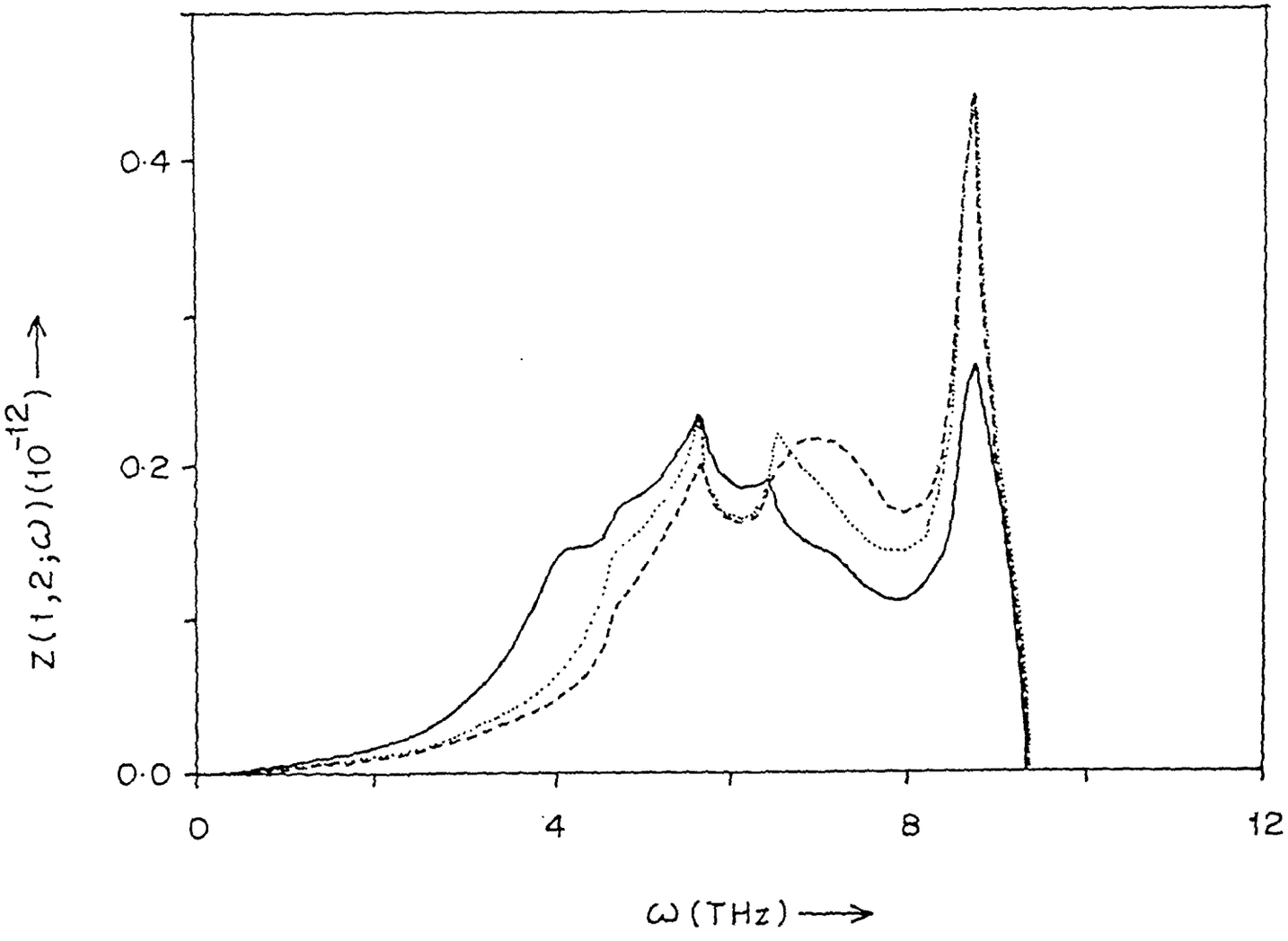

Fig.33 Local density of states of first neighbour (——), second neighbour (- - -) of a vacancy and a host atom (....) in α-Fe in the case of a relaxed lattice, with ideal phonons

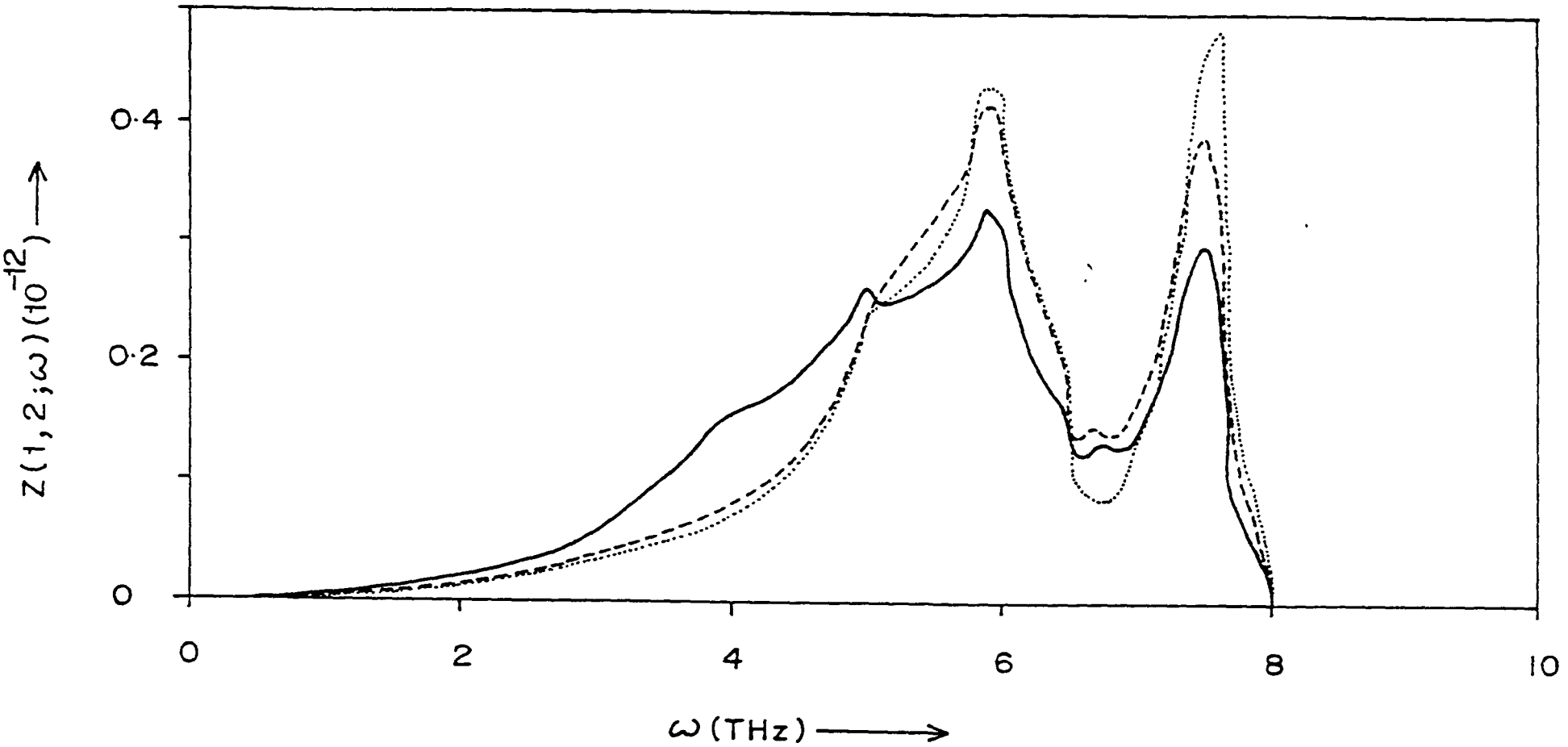

Fig.34 Local density of states of first neighbour (——), second neighbour (- - -) of a vacancy and a host atom (....) in Mo in the case of a relaxed lattice, with ideal phonons taken from ref. [72]

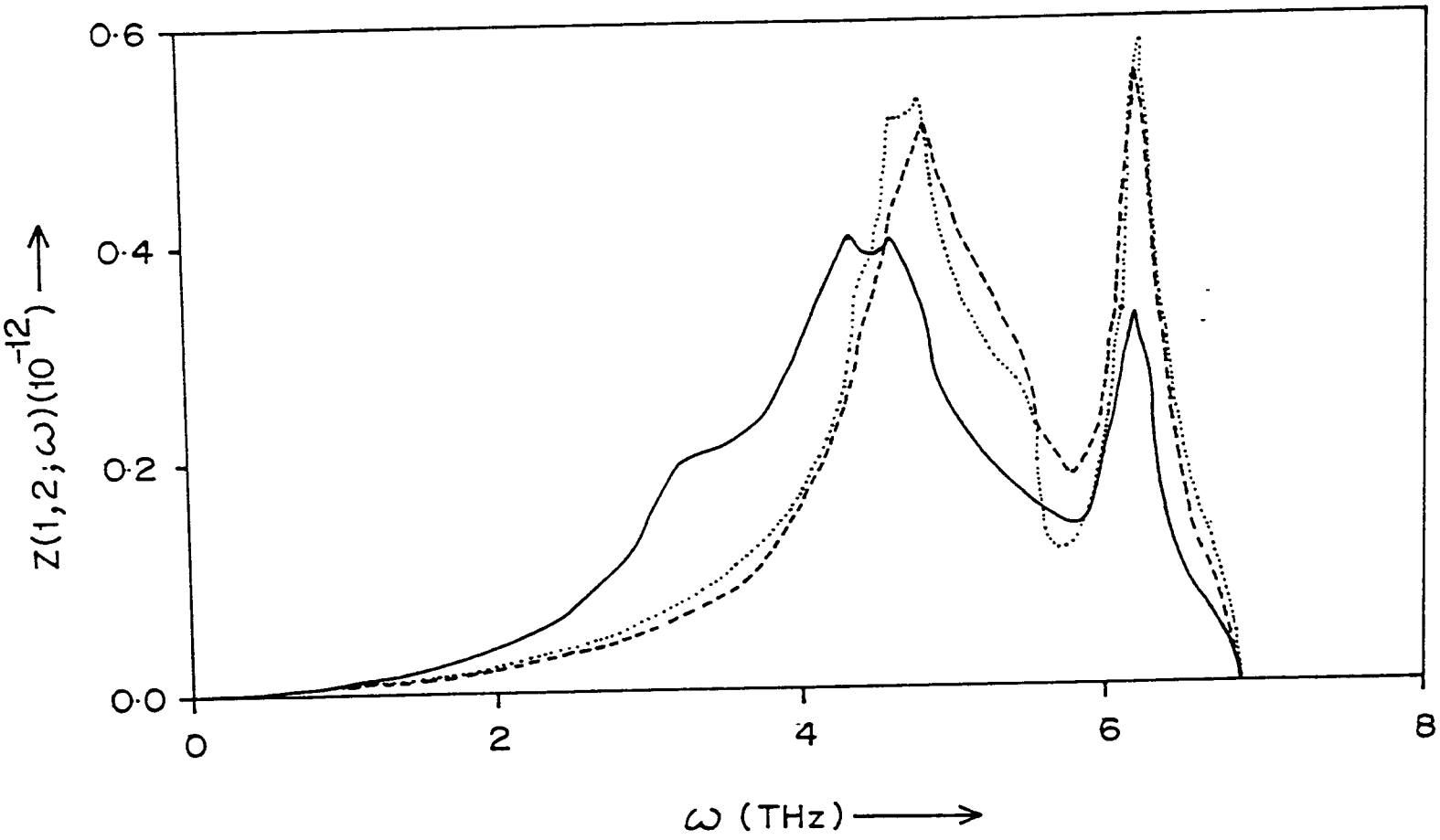

Fig.35 Local density of states of first neighbour (——), second neighbour (- - -) of a vacancy and a host atom (....) in W in the case of a relaxed lattice, with ideal phonons taken from ref. [74]

for the atom. The result is similar to that found by Hatcher *et al* for copper [81]. However, the frequency spectrum of the second neighbour is not much different from that of the host lattice in the case of Mo and W. This shows that the vibrations of only the first neighbours of the vacancy are significantly changed compared to those of the atoms in the host lattice. Contrary to the case of Mo and W, the spectrum of the second neigbours in α-Fe shows a signifigant shift of the spectrum towards the higher frequencies irrespective of the phonons used.

The obtained local density of states is used to calculate the formation entropy S^F_{1V} of the vacancy in all the three metals : α-Fe, Mo and W with both types of phonons used and also for both for the relaxed lattice as well as for the case of unrelaxed lattice. In these calculations both sets of the local spectra have been utilized, so, it is clear that we can present four values of the formation entropy for each metal. For a relaxed lattice, the contribution to S^F_{1V} from image forces in the crystal is also taken into consideration . The image forces yield a negative contribution to S^F_{1V} indicating a homogeneous contraction

of the lattice and hence a general strengthening of the force constants in the lattice. The relaxation volume for α-Fe and Mo are $0.05V_c$ and $0.1V_c$ respectively as quoted by Ehrhart *et al* [129], where V_c is the unit cell volume. For W we take relaxation volume equal to that of Mo, i.e., $0.1V_c$, since the measured value is not available in this case. The contribution from image forces towards the formation entropy are : -0.0909k for α-Fe, -0.1738k for Mo and -0.1342k for W. The final values of the formation entropy are presented in Table XI. From Table XI it is evident that the effect of relaxation is different for different metals: while for Mo and W the formation entropy increases in the relaxed lattice while for α-Fe it is reduced. The increase in formation entropy for Mo and W in the relaxed lattice is understandable, since the most affected atoms are first neighbours and their local spectra shift to lower frequency region where the density of modes in the host lattice is negligible, whereas, the second neighbour spectra are not much changed in these metals. In the case of α-Fe also the first neighbour spectrum shifts to lower frequencies but the second neighbour spectrum shifts to higher frequencies which causes reduction of formation entropy.

Table XI. Obtained vacancy formation entropy S^{F}_{1V} in α-Fe, Mo and W in the unit of k/atom ; (a) using JW potentials consistently and (b) using experimental based phonons.

Phonons used	α-Fe	Mo	W	Remark
a	2.043	1.61	1.921	u
a	1.559	2.25	3.199	r
b	1.646	1.69	2.143	u
b	1.485	1.94	2.446	r

u is for unrelaxed lattice and r for relaxed lattice.

It would be of interest to compare the values of S^F_{1V} obtained in the present work with those obtained by other workers. Burton [137] has reported values from 2.2k to 2.6k for bcc metals based on an empirical relation between formation entropy and lattice relaxation due the vacancy. This relation shows an increase in formation entropy due to inward relaxation of nearest neighbours of a vacancy.The other calculations of formation entropy in bcc metals are by Hatcher *et al* [81] in α-Fe who find a value of 2.1k and in all the three metals by Schober *et al* [138] with a value of about 1.8k. Schober *et al* [138] have considered a cluster of 432 atoms with a vacancy at the centre. Vacancy is modelled by missing force constants to neighbours, thus ignoring the relaxation completely. An examination of Table XI shows that our results for S^F_{1V} for a relaxed lattice are in the same range as obtained by others. As regards experimental measurements of formation entropy, Schwirtlich and Schultz [139] have derived a value 1.5k for Mo on the basis of quenching and recovery experiments. The calculated values are somewhat higher than the quoted experimental results.

We have also utilized the obtained density of states to calculate mean square thermal displacements of first and second neighbours of the vacancy. The mean square thermal displacement of an atom at site l is given by equations (3.56) to (3.58). For the first neighbours the thermal displacements are larger than their respective host atoms while for second neighbour the thermal displacement is almost same as that of the host atoms for Mo and W in both sets of studies as shown in Figs.(36-38 and 39-41). In the case of α-Fe the thermal displacements of the second neighbours are lower than that of the host as shown in Figs. (36,39). The increase in thermal displacement of the first neighbour is the result of general shift of the spectrum to lower frequencies, whereas the decrease in thermal displacements of the second neighbours of α-Fe is accounted forby the shift of the spectrum towards the higher frequencies. At high temperatures the mean square thermal displacement increases linearly with temperature T.

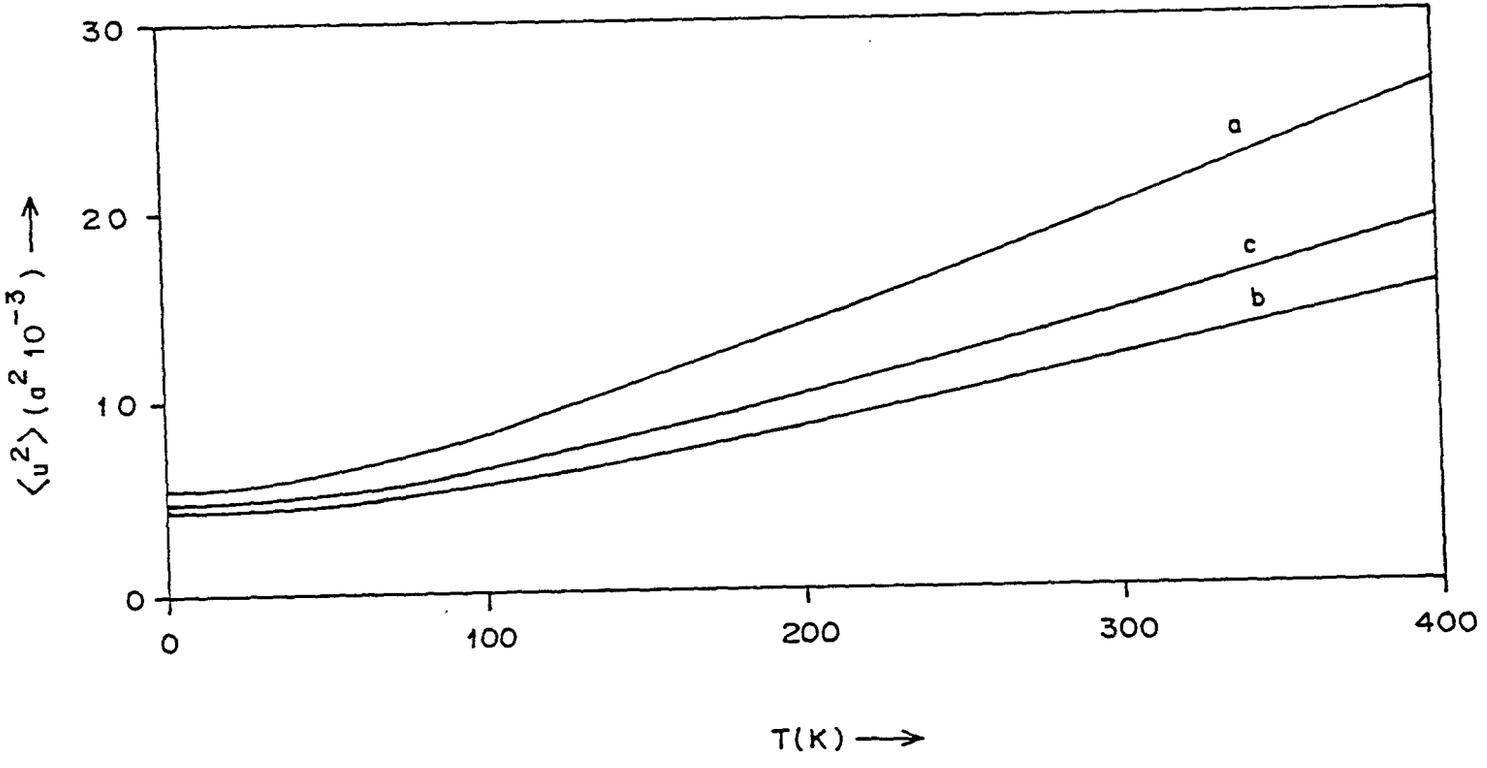

Fig.36 Mean square thermal displacement of first neighbour (a), second neighbour (b) of a vacancy and a host atom (c) in α-Fe in the case of a relaxed lattice, with ideal phonons calculated from the JW potential.

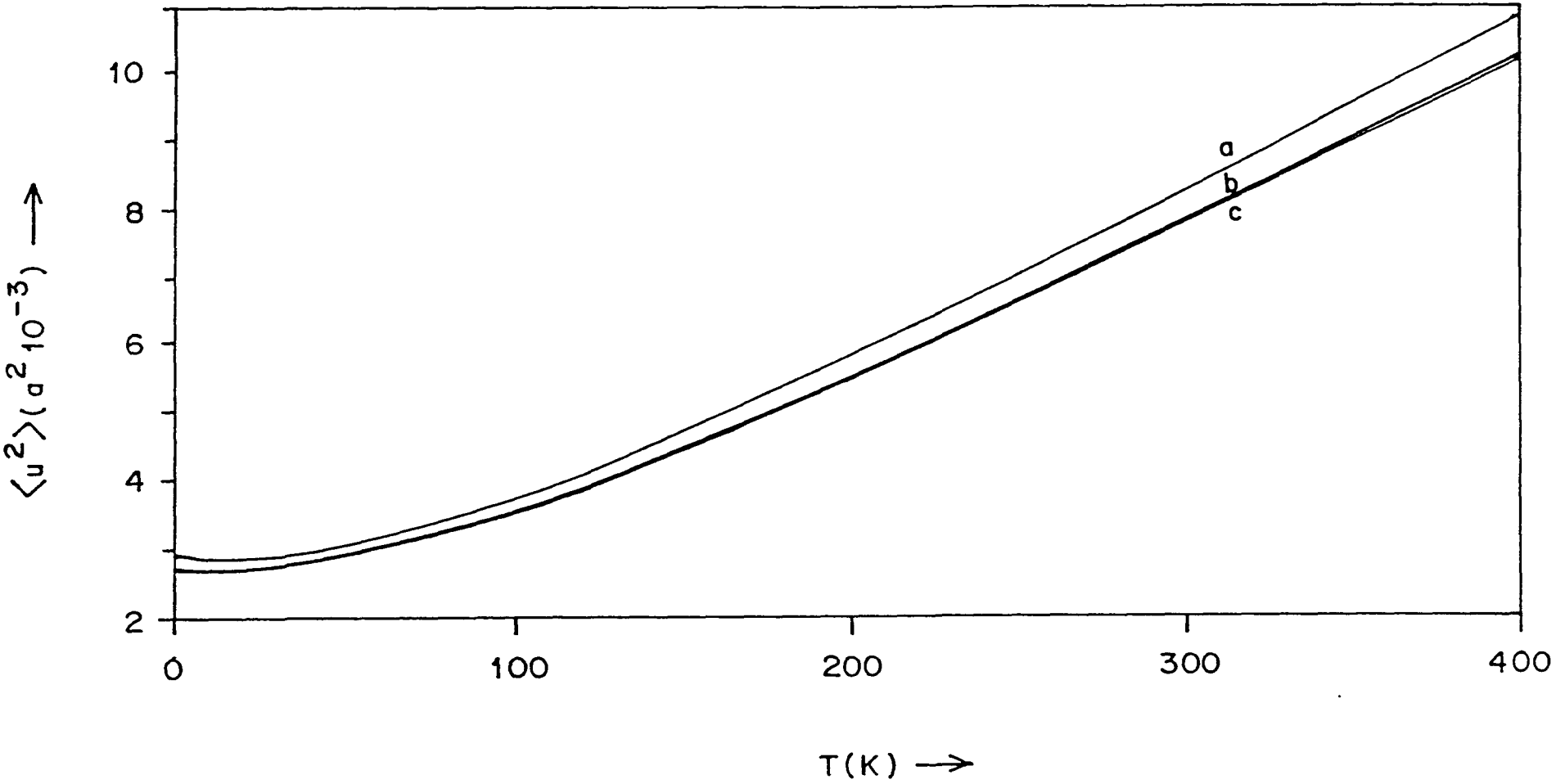

Fig.37 Mean square thermal displacement of first neighbour (a), second neighbour (b) of a vacancy and a host atom (c) in mo in the case of a relaxed lattice, with ideal phonons calculated from the JW potential.

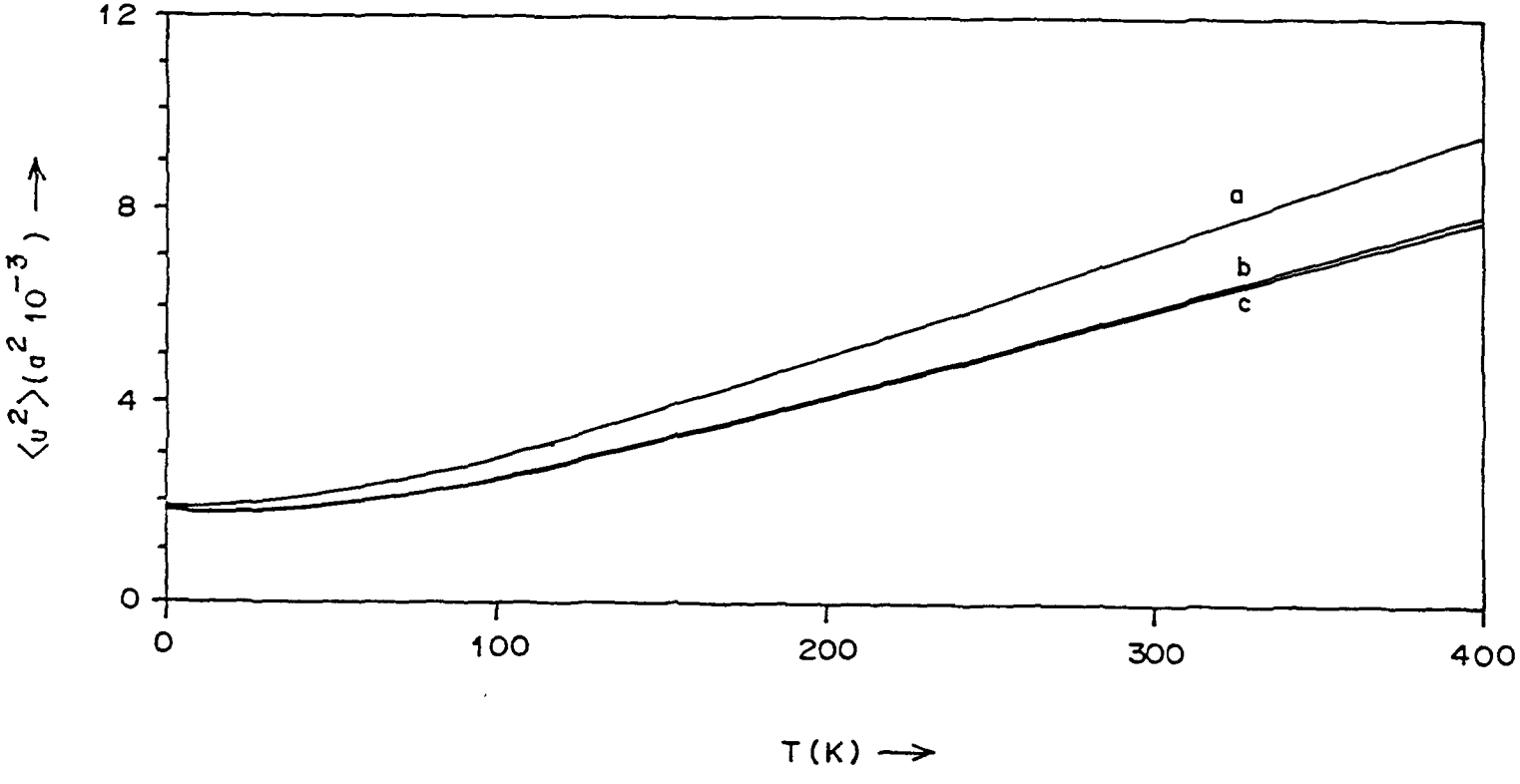

Fig.38 Mean square thermal displacement of first neighbour (a), second neighbour (b) of a vacancy and a host atom (c) in W in the case of a relaxed lattice, with ideal phonons calculated from the JW potential.

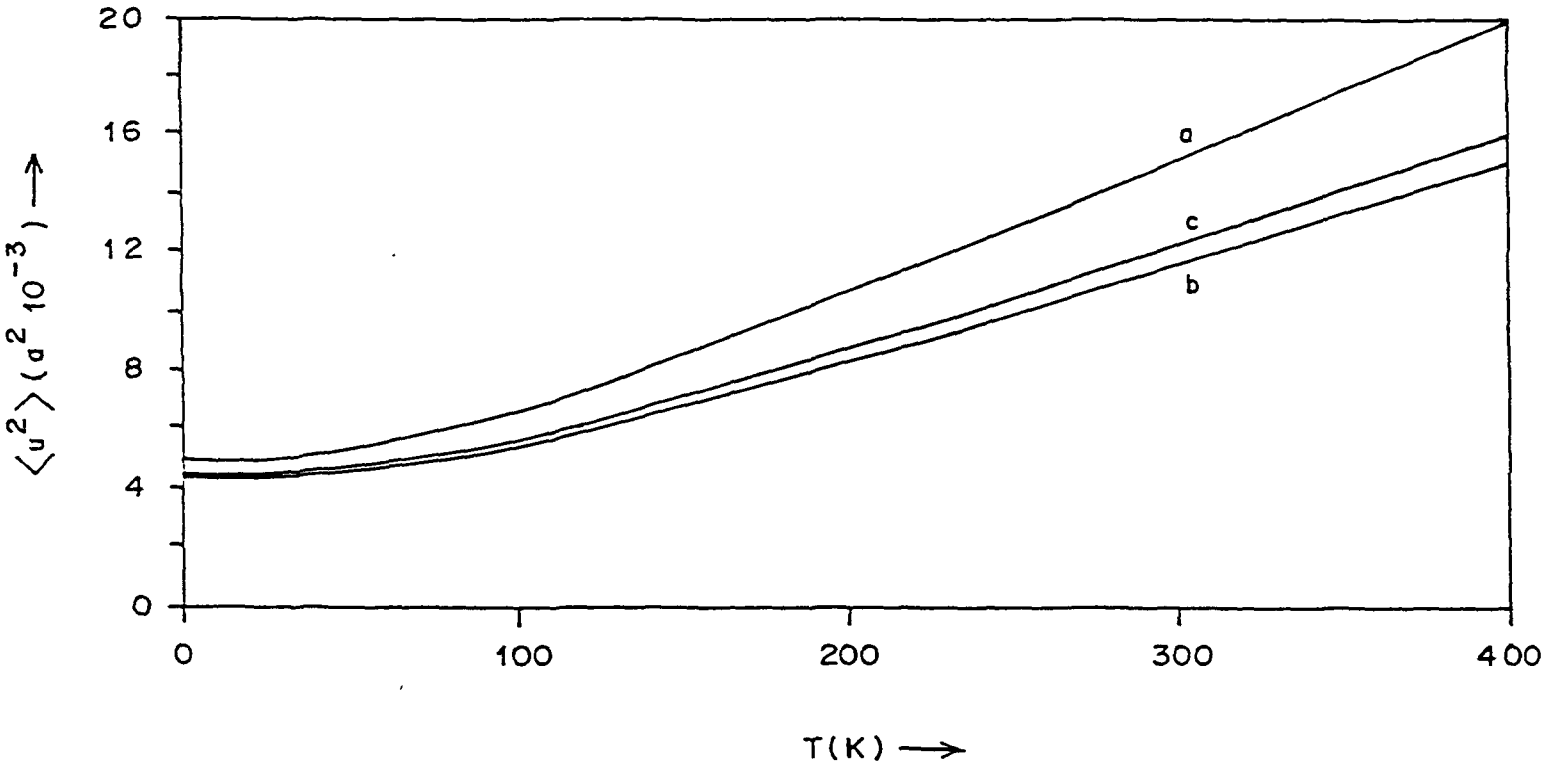

Fig.39 Mean square thermal displacement of first neighbour (a), second neighbour (b) of a vacancy and a host atom (c) in α-Fe in the case of a relaxed lattice, with ideal phonons taken from ref.[73].

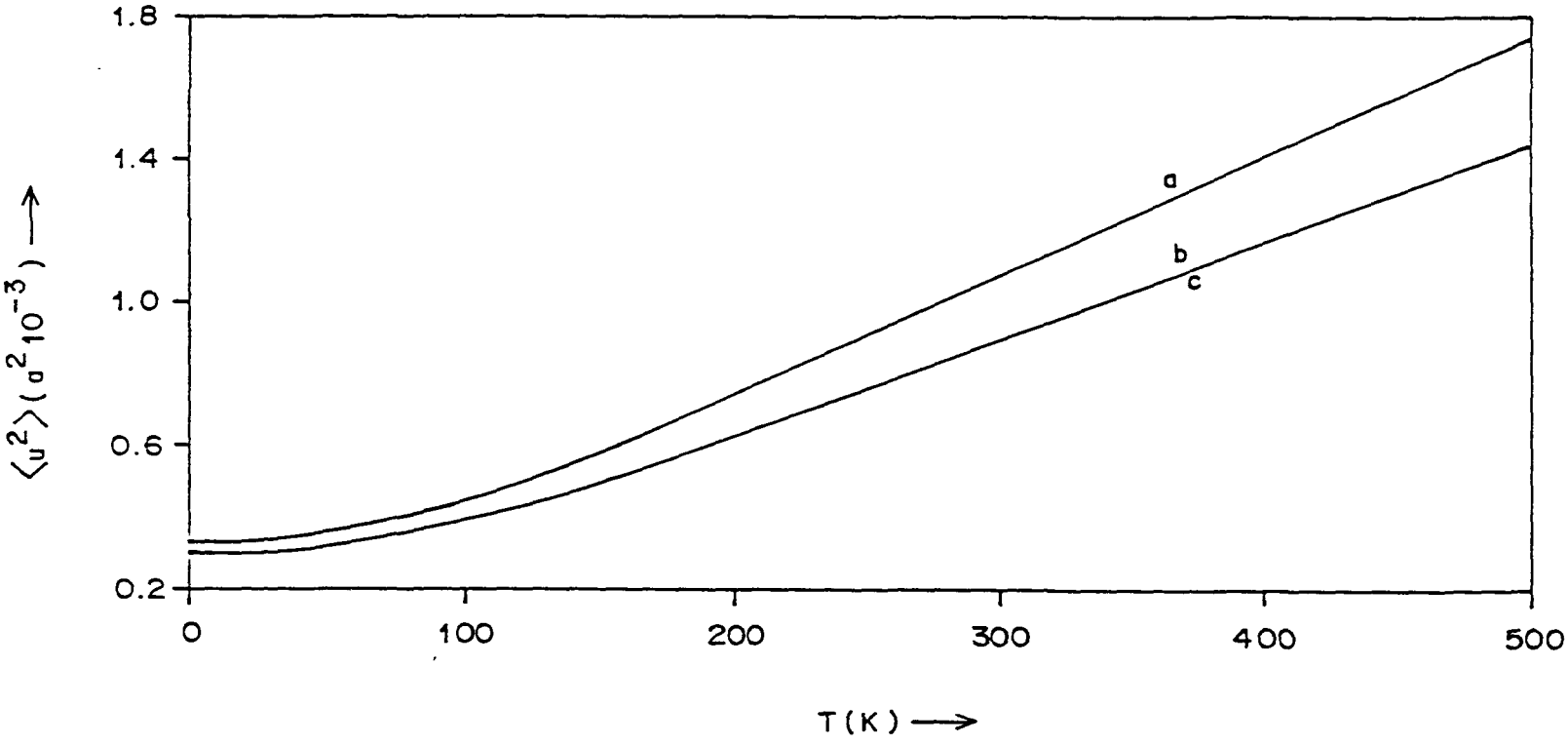

Fig.40 Mean square thermal displacement of first neighbour (a), second neighbour (b) of a vacancy and a host atom (c) in Mo in the case of a relaxed lattice, with ideal phonons taken from ref.[72].

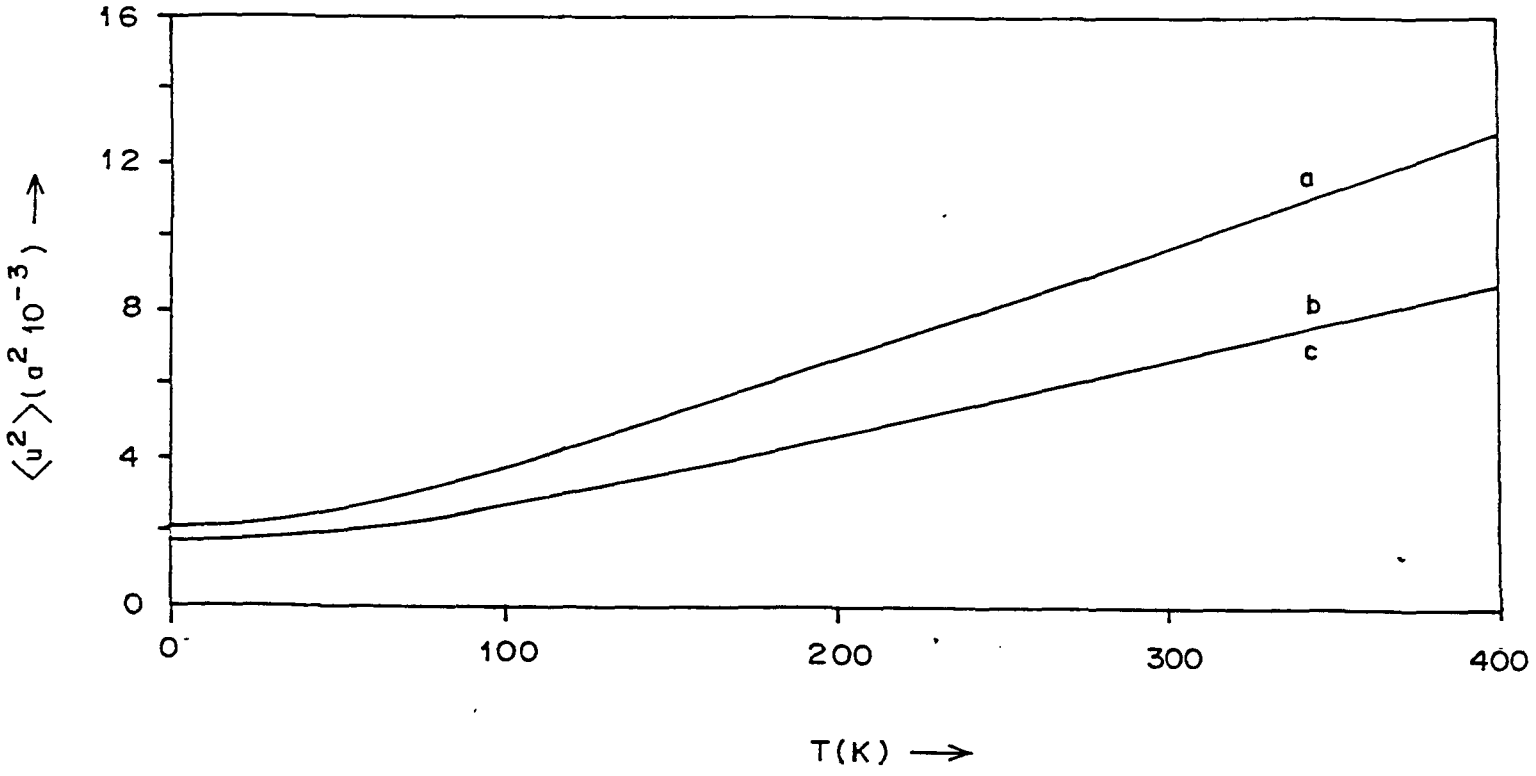

Fig.41 Mean square thermal displacement of first neighbour (a), second neighbour (b) of a vacancy and a host atom (c) in W in the case of a relaxed lattice, with ideal phonons taken from ref.[74].

To summarize, the local density of states of neighbours of the vacancy shows that the vibrations of only the first neighbours are significantly changed compared to a host atom. The obtained value of formation entropy based on local density of states of the neighbours of the vacancy is in close agreement with the value determined using static lattice Green's functions and is in reasonable agreement with the earlier calculations in the literature.

REFERENCES :

[1] A.A. Maradudin, E.W. Montroll, G.H. Weiss,and I.P. Ipatova, *Theory of Lattice Dynamics in the Harmonic Approximation, Solid State Physics, Suppl.3*, Second ed. Academic Press, N.Y. (1971).

[2] P.H. Dederichs, and R. Zeller, in *Point Defects in Metals II*, edited by G.Hohler and E.A. Niekisch, SpringerTracts in Modern Physics Vol.87 (Springer, Berlin, (1980).

[3] R.J. Elliot, J.Krumhansl and P. Leath , *Rev. Mod. Phys*, 46, 465 (1974).

[4] R.M. Nicklow, in *Treatise in Materials Science and Technology*, p.191, Academic Press (1979).

[5] R.F. Wood, *Methods in computational Phys.*, 15,119 (1976)

[6] J.B. Gibson, A.N. Goland, M. Milgram and G.H. Vineyard *Phys. Rev.* 120, 1229 (1960)

[7] A. Seeger, E. Mann and R.V. Jan *J. Phys. Chem. Solids* 23, 639 (1962)

[8] A. Scholz and C. Lehman *Phys. Rev. B* 6, 813 (1972)

[9] J.R. Beeler,Jr., *Radiation Effects Computer Experiments.* North Holland Amsterdam (1983)

[10] P. Ehrart, H.G.Haubold and W. Schilling *Adv. Solid State Phys.* XIV, 87 (1974)

[11] H.G. Haubold, in *Proceedings of the Conference on Fundamental Aspects of Radiation Damage in Metals,* Gatlinburg 1975 (ed. M.T. Robinson and F.W. Young, Jr.) U.S. Department of Commerce, Springfield, Virginia (1976) p.268. 1

[12] P.Ehrahrt, *J. Nucl. Mater.* 69/70, 200 (1978)

[13] O. Bender and P. Ehrahrt, in *Point Defects and Defect Interactions in Metals,* (Ed. by J.I.Takamura, M. Doyama and M.Kiritani) Tokyo University Press (1982) p.639.

[14] V. Spiric, L.E. Rehn, K.H. Robrock and W. Schilling *Phys. Rev.* B, 15, 672 (1977).

[15] K. Ehrensperger, V. Fischer, J. Kerscher and H. Wenzl, *J. Phys. Chem. Solids,* 31, 1855 (1970).

[16] K. Forsch, J. Hemmerich, H. Knoll and G. Lucki *Phys. Stat. Sol.(a),* 23, (1974); H. Knoll, U. Dedek and W. Schilling, *J.Phys. F.* 4, 1095 (1974).

[17] J. Holder, A.V. Granato and L.E. Rehn, *Phys. Rev. Lett.* 32, 1054 (1974); L.E. Rehn, J. Holder, A.V. Granato, R.R. Coltman and R.W. Young, Jr., *Phys. Rev. B* 10, 349 (1974); J. Holder, A.V.Granato and L.E. Rehn *Phys. Rev. B* 10, 363 (1974).

[18] K.H.Robrock and W.Schilling, *J.Phys.F* 6, 303 (1976).

[19] S.Okuda and H. Mizubayashi, in *Point Defects and Defects Interactions in Metals*,(ed.by J.I. Takamura, M. Doyama and M. Kiritani) Tokyo University Press (1982), p.163.

[20] P.Ehrhart, *British Nuclear Energy Society, London*, (1983) p.101.

[21] G.Wallner, H.Franz, R. Rauch, A. Schmalzbauer and J.Peisl, *Materials Science Forum*, 15-18, 907(1987).

[22] W.Chambrone, J.Verdone and P.Moser, in *Proceedings of the Conference on Fundamental Aspects of Radiation Damage in Metals, Gatlinburg* 1975, (ed. by M.T.Robinson and F.W.Young, Jr.) U.S. Department of Commerce, Springfield, Virginia (1976) p.261; V.Hivert, R.Pichon, H.Bilger, P. Bichon, J.Verdone, D.Dautreppe and P. Moser, *J. Phys. Chem. Solids* 31, 1843 (1970).

[23] H.Mizubayashi and S.Okuda, *Rad.Effects* 54, 201 (1981).

[24] M.Weller and J.Diehl, in *Point Defects and Defect Interactions in Metals*, (ed.by J.I. Takamura, M. Doyama and M. Kiritani)Tokyo University Press (1982), p.417.

[25] S.Okuda and H.Mizubayashi, *Crystal Lattice Defects* 4, 75 (1973); Rad. Effects 33, 221 (1977).

[26] J.A. Dicarlo, C.L. Snead Jr. and A.N. Goland, *Phys. Rev.* 178, 1059 (1969); S. Okuda, H.Mizubayashi, *Phys. Rev. B* 13, 4207 (1976); J.R. Townsend, M. Schildcrout and C.Reft, *Phys. Rev. B* 14, 500 (1976).

[27] H.E.Schaefer, D.Butteweg and W.Dander, in *Proceedings of the Conference on Fundamental Aspects of Radiation Damage in Metals, Gatlinburg* 1975, (ed. by M.T. Robinson and F.W.Young, Jr.) U.S. Department of Commerce, Springfield, Virginia (1976) p.463; W.Chambron, J.Verdone and P.Moser, in *Proceedings of the Conference on Fundamental Aspects of Radiation Damage in Metals*, Gatlinburg 1975, (ed. by M.T. Robinson and F.W. Young, Jr.) U.S. Department of Commerce, Springfield, Virginia (1976) p.261; M. Hirscher, B. Schwendemann and H. Kronmuller, *Cryst. Latt. Def. and*

Amorph. Mat. 11, 245 (1985).

[28] S.Okuda, in *Proceedings of the Conference on Fundamental Aspects of Radiation Damage in Metals, Gatlinburg* 1975, (ed. by M.T. Robinson and F.W.Young, Jr.) U.S. Department of Commerce, Springfield, Virginia (1976) p.361.

[29] C. Erginsoy, G.H. Vineyard, and A. Englert, *Phys. Rev.* 133, A595 (1964).

[30] R.A. Johnson, *Phys. Rev.* 134, A1329 (1964).

[31] K.M. Miller, *J. Phys.F* 11, 1175 (1981).

[32] N.W. Guinan, R.N. Stuart, and T.J. Borg, *Phys. Rev.B* 15, 699 (1977).

[33] Y. Taji, T. Iwata, T. Yokata, and M. Fuse, *Phys. Rev.B* 39, 6381 (1989).

[34] M.Wagner, *Phys. Rev.* 131, 1443 (1963); *Phys. Rev.* 133, A750 (1964).

[35] J.A.Krumhansl and J.A.D. Matthews, *Phys. Rev.* 166, 856 (1968); J.A.Krumhansl, in *Localized Excitations in Solids* (ed. by R.F. Wallis) Plenum, N.Y.(1968) p.17.

[36] I.M.Litshitz, *J.Phys. (USSR)* 7, 215, 249 (1943); *J.Phys. (USSR)* 8, 89 (1948).

[37] K.Oda, R. Yamamoto and M. Doyama, *J. Phys. F* , 12, L85 (1982)

[38] R. Haydock, V. Heine and M.J. Kelley, *J. Phys. C*, 2845 (1972); *J. Phys. C.*, 8, 2591 (1975)

[39] M. Imafuku, R. Yamamoto and M. Doyama, in *Point Defects and Defect Interactions in Metals*.(Ed. J.I. Takamura, M. Doyama and M. Kiritani) Tokyo Univ. Press (1982) p. 145

[40] R.A. Johnson and W.D. Wilson *Interatomic Potentials and simulation of lattice defects* ed. P.C. Gehlen, J.R. Beeler and R.I.Jaffee (New York: Plenum, 1971).

[41] R.A. Johnson , *J. Phys. F* 3, 295 (1973).

[42] P.H. Dederichs, C. Lehmann, and A. Scholz, *Phys. Rev. Lett.* 31, 1130 (1973).

[43] P.H. Dederichs, in *Proceedings of the Conference on Fundamental Aspects of Radiation Damage in Metals, Gatlinburg*, 1975 (Edited by M.T. Robinson and F.W. Young Jr.) U.S.Department of Commerce, Springfield, Virginia (1976),p.187.

[44] P.H. Dederichs, C. Lehmann, H.R. Schober, A. Scholz, and R. Zeller, *J.Nucl.Mater.* 69&70, 176 (1978).

[45] P.N. Ram, *Phys. Rev. B*, 43, 6480 (1991).

[46] P.N.Ram, *Radiation Effects and Defects in Solids*, 118, 1 (1991).

[47] P.N. Ram *Phys Rev. B.* 43 6977 (1991).

[48] J.A. Blah, S.S. Pohlong and P.N. Ram, *Phys. Rev. B.* 49, 15055 (1994).

[49] M.S.Daw and M.I.Baskes *Phys. Rev. Lett.* 50 1285 (1983).

[50] M.S.Daw and M.I.Baskes *Phys. Rev. B* 29 6443 (1984).

[51] M.W.Finnis and J.E.Sinclair *Philos. Mag.* A50 45 (1984).

[52] S.M.Foiles, M.I.Baskes and M.S.Daw *Phys. Rev. B* 33 7983 (1986).

[53] R.G.Hoagland, M.S.Daw, S.M.Foiles and M.I.Baskes *J. Mater. Res.* 5 313 (1990).

[54] W. Schilling, *J. Nucl. Mater.* 69/70, 465 (1978).

[55] F.W. Young, Jr., *J.Nucl.Mater.* 69/70, 310 (1978).

[56] H.R. Schober, V.K. Tewary,and P.H. Dederichs, *Z. Phys. B* 21, 225 (1975).

[57] R.F. Wood, and M. Mostoller, *Phys. Rev. Lett.* 35, 45 (1975)

[58] P.N. Ram, *J. Phys.F* 15, 35 (1985).

[59] R. Zeller, and P.H. Dederichs, *Z. Phys.B* 25, 139 (1976).

[60] R. Zeller, *KFA Julich Report*, Jül.1259-FF(1975).

[61] P.N. Ram, and P.H. Dederichs, *Z. Phys.B*, **42**, 57 (1981).

[62] P.N. Ram, *Phys. Rev.B* **37**, 6783 (1988).

[63] P.H. Dederichs, C. Lehmann, and A. Scholz, *Z. Phys.B* **20**, 155 (1975).

[64] R. Urban, P. Ehrhart, W. Schilling, H.R. Schober, and H. Lauter, *Mater. Sci. Forum.* 15-18 243 (1987)

[65] R. Urban, P. Ehrhart, W. Schilling, H.R. Schober, and H. Lauter, *Phys. Status Solidi B* **144**, 287 (1987).

[66] P.N. Ram, and P.H. Dederichs, *Kernforschung sanlage Jülich Report* No. Jül.1725, 1981 (unpublished).

[67] P.N. Ram, *Phys. Rev.B* **30**, 6146 (1984)

[68] K. Boning, G.S. Bauer, H.J. Fenzl, R. Scherm and W. Kaiser, *Phys. Rev. Letts.* 38, 852 (1977).

[69] K. Boning, G.S. Bauer, H.J. Fenzl, R. Scherm and R.M. Nicklow, in *Lattice Dynamics* 1978, (*Proc. Int. Conf. Paris* (1977) (ed. M. Balkanski) Flammarion, Paris

[70] R.M.Nicklow, R.R. Coltman, F.W. Young Jr. and R.F. Wood *Phys. Rev. Letts.* 35, 1444 (1975); R.M.Nicklow, W.P. Crummet and J.M. Williams *Phys. Rev. B*, **20** 5034 (1979).

[71] R.M.Nicklow, G.Gilat, H.J. Smith, Raubenheimer and M.K. Wilkinson *Phys. Rev.* 164 922 (1967).

[72] A.D.B. Woods and S.H. Chen, *Solid State Commun.*, 2, 233 (1964).

[73] V.J. Minkiewicz, G. Shirane and R. Nathans, *Phys. Rev.* 162, 528 (1967).

[74] S.H. Chen and B.N. Brockhouse, *Sol. Sate Comm.*, 2, 73 (1964)

[75] G. Vogl, M. Mansel, and W.Vogl. *J. Phys. F* 4, 2321 (1974)

[76] G. Vogl and M. Mansel, in *proceedings of the Conference on Fundamental Aspects od Radiation Damage in Metals, gatlinburg* 1975, (Edited by M.T. Robinson and F.W. Young,Jr.) U.S.Department of Commerce, Springfield, Virginia (1976),p.349.

[77] J. Marangos, W. Mansel,and G.Vogl, *Rad. Effects* 83, 251 (1984).

[78] J. Marangos, W. Mansel,and D. Wahl, *Materials Science Forum* 15-18, 225 (1987).

[79] P.N. Kenny, A.J. Trott and P.T. Heald, J.Phys.F, 3, 513 (1973).

[80] P.L. Land and B. Goodman, *J. Phys. Chem. Solids*, 28, 113 (1967).

[81] R.D. Hatcher, R. Zeller And P.H. Dederichs, *Phys. Rev. B*, 19, 5083 (1978).

[82] R.Chang and L.J. Graham, *U.S. Natl. Bur. Stand. Spec. Publ.*, 287, 53 (1966).

[83] R.Chang and L.J. Graham, *Phys. Status Solidi*, 18, 99 (1966).

[84] M.I.Baskes and C.F.Melius *Phys. Rev. B* 20 3197 (1979).

[85] W.D. Wilson *Phys. Rev. B* 20, 3197(1979); M.I.Baskes and C.F. Melius and W.D. Wilson, in *Interatomic Potentials and Crystalline Defects*, (ed. by J.K. Lee, Metalurgical Societyo of AIME, New York, 1981)

[86] M.S. Daw and R.D. Hatcher *Sol. Stat. Comm.* 56, 697 (1985).

[87] L. Ninsheng, X. Welan and S.C. Chen *Sol Stat. Comm.* 75, 877 (1990).

[88] M.S. Daw *Surf. Sci. Lett.* 166, 1161 (1986)

[89] G.J. Ackland and V. Vitek, *Phys. Rev. B* 41, 10324 (1990).

[90] M.S.Daw *Phys. Rev. B* 39 7441 (1989) & references contained therein.

[91] M.S. Daw, M.I. Baskes and W.G. Wolfer, in *Proceedings of the Special Symposium on modelling Environmental Effects on Crack Initiation and Propagation*, Toronto, AIME (1985)

[92] J.K.Norskov and N.D.Lang *Phys. Rev. B* 21 2131 (1980).

[93] M.J.Stott and E.Zaremba *Phys. Rev. B* 22 1564 (1980).

[94] R.A.Johnson *Phys. Rev. B* 37 3924 (1988).

[95] D.J.Oh and R.A.Johnson *J. Mater. Res.* 3 471 (1988).

[96] J.H.Rose, J.R.Smith, F.Guinea and J.Ferrante *Phys. Rev. B* 29 2963 (1984).

[97] J.Mei, J.W.Davenport and G.W.Fernando *Phys. Rev. B* 43 4653 (1990).

[98] K.W.Jacobson, J.K.Norskov and M.J.Puska *Phys. Rev. B* 35 7423 (1987).

[99] M.J.Puska, R.M.Nieminen and M.Manninen *Phys. Rev. B* 24 3037 (1981).

[100] A.Banerjea and J.R.Smith *Phys. Rev. B* 37 6632 (1988).

[101] R.A.Johnson and D.J.Oh *J. Mater. Res.* 4 1195 (1989).

[102] S.M.Foiles *Phys. Rev. B* 32 3409 (1986).

[103] D.J.Oh and R.A.Johnson *Atomistic simulation of materials* ed. by V Vitek and D Srolovitz (New York : Plenum, 1989) p 233

[104] M.I.Baskes *Phys. Rev. B* **46** 2727 (1992).

[105] E.Clementi and C.Roetti *At.Data Nucl.Data tables* **14** 177 (1974) ; A.D.McLean and R.S.McLean *At.Data Nucl.Data tables* **26** 197 (1981).

[106] G.Simmons and H.Wang *Single Crystal Elastic Constants and Calculated Aggregate Properties* (Cambridge, Massachusetts: Hand Book, 1971).

[107] R.W.Bullutti *J. Nucl. Mater.* **69/70** 240 (1978).

[108] R.W. Siegel *J. Nucl. Mater.* **69/70**, 117 (1978).

[109] W. Wycisk and M. Feller-Kniepmeier, *J. Nucl. Mater.* **69/70**, 616 (1978).

[110] Y.A. Kraftmakher and P.G. Strelkov, in *Vacancies and Interstitials in Metals*, ed. A. Seeger, D. Schmacher, W. Schilling and J. Diehl (Amsterdam: North Holland) p 59

[111] R. Pasianot, D. Farkas and E.J. Savino *Phys. Rev. B* 43 6952 (1991).

[112] U.Klemradt, B.Drittler, T.Hoshino, R.Zeller and P.H. Dederichs *Phys. Rev. B* **43** 9487 (1991).

[113] W.A.Kamitakahara and B.N.Brockhouse *Phys. Lett.* **29A** 639 (1969).

[114] J.W.Lynn, H.G.Smith and R.M.Nicklow *Phys. Rev. B* **8** 3493 (1973).

[115] R.J.Birgeneau, J.Cordes, G.Dolling and A.B.D.Woods *Phys. Rev.* **136** A1359 (1964).

[116] A.P.Miller and B.N.Brockhouse *Can Jour. Phys.* **49** 704 (1971).

[117] D.H.Dutton and B.N.Brockhouse *Can. Jour. Phys.* **50** 2915 (1972).

[118] C.J.Martin , D.A. O'Connor *Phys. Rev. B* **8** 3493 (1977).

[119] *Metals Reference Book* ed. C.J.Smith (London: Butterworth, 1976) 5th. edition p 186.

[120] W. Bowers and H.B Rosenstock, *J. Chem. Phys.*, **18**, 1056 (1950).

[121] O. Litzmann and P. Rosza, *Proc. Phys. Soc. Lond.*, **85**, 285 (1965).

[122] K. Kunc, *Czech. J. Phys. B*, 15, 883 (1965); J. Mahanty, *Phys. Letts. A*, 29, 583 (1969); M.Sachdev and J. Mahnaty, J.Phys.C, 3, 1225 (1970).

[123] P.H.Dederichs and R. Zeller, *Phys. Rev.B*, 14, 2314 (1976).

[124] H. Wollenberger and T. Monsau *Private Communication* (1980).

[125] H.R. Schober and R.Zeller, *J. Nucl. Mater.*, 69/70, 341 (1978).

[126] G. Gilat, and L.J. Raubenheimer, *Phys. Rev.* 144, 390 (1966).

[127] J.Verdone, P. Perreto, P.Moser, D.Dautreppe and J.Verdier, *CR Acad. Sci.* (France) 260 5209 (1965); H.E.Schaefer, D.Butteweg and W.Dander, in *Fundamental Aspects of Radiation Damage in Metals, Gatlinburg* 1975, (ed. by M.T. Robinson and F.W.Young, Jr.) U.S. Department of Commerce, Springfield, Virginia (1976) p.463.

[128] F.Walz, H. Schreyer and H.Krömuller, *Phys. Status Solidi a*, 43, K81 (1977).

[129] P. Ehrhart, K.H. Robrock and H. Schober, in *Physics of Radiation Damage in Crystals*, (Ed. by R.A. Johnson and A.N. Orlow) Elsevier Pub. Com. Amsterdam. New York (1986) p.3.

[130] H. Jacques and K.H. Robrock, J. Physique 42,C5-723 (1981); *in Point Defects and Defect Interactions in Metals*, (Editted byJ.I.Takamura, M.Doyama and M.Kiritani) Tokyo University Press (1982),p.159.

[131] C.P. Flynn and A.M. Stoneham, *Phys. Rev.* B1, 3966 (1970).

[132] H. Schultz, *Materials Sci. Forum*, 15-18, 727 (1987).

[133] F. Maury, A. Lucasson, P. Moser and Y. Loreaux, *J. Phys. F*, 15, 456 (1985).

[134] H.J. Blyth, F.Dwarschak, R.M. Richardson and F.Walz, *Phys. Stat. Sol a*, 69, K97 (1982).

[135] H.Mizubayashi and S.Okuda, *Phys. Stat. Sol. a*, 29, K35 (1975).

[136] J.A. Blah and P.N. Ram, *Communicated to Phys. Stat. Sol.b.*

[137] J.J. Burton, *Phys.Rev.B*, 5, 2948(1972).

[138] H.R. Schober, W. Petry and J. Trampenau, *J. Phys. Condens Matter*, 4, 9321 (1992).

[139] I.A. Schwirtlich and H. Schultz, *Philos. Mag.* A 42, 601 (1980).

LISTS OF PUBLICATIONS

1. Local density of states of <110>-split interstitials and their neighbours, J.A. Blah, S.S. Pohlong and P.N. Ram, *Phys. Rev. B.* 49, 15055 (1994).

2. Analytic Embedded Atom Method Potentials for FCC metals, S.S. Pohlong and P.N. Ram, *J. Mater. Res.* (Revised).

3. Local density of states of Self interstitials in bcc Metals, S.S. Pohlong and P.N. Ram, *Phys. Rev. B.* (Communicated).

4. Local density of states of first and second neighbours of vacancies in bcc Metals, S.S. Pohlong and P.N. Ram, *J. Phys. C* (Communicated).